

Confocal Raman Microspectroscopy Applications in Cartilage Tissue Engineering



2012

**Confocal Raman Microspectroscopy;
Applications in Cartilage Tissue Engineering**

Aliz Kunstár

2012

Members of the Graduation Committee:

Chairman: Prof. Dr. G. van der Steenhoven (University of Twente)

Promoter: Prof. Dr. C.A. van Blitterswijk (University of Twente)

Co-Promoter: Dr. A.A. van Apeldoorn (University of Twente)

Members:

Dr. G. van Osch (Erasmus Medical Center Rotterdam)

Prof. Dr. J.L. Herek (University of Twente)

Prof. Dr. M. Karperien (University of Twente)

Prof. Dr. J.F.J. Engbersen (University of Twente)

Prof. Dr. F.P.J.G. Lafeber (University Medical Center Utrecht)

Prof. Dr. P.J. Dijkstra (University of Twente / Soochow University, Suzhou, China)

**Confocal Raman Microspectroscopy;
Applications in Cartilage Tissue Engineering**

Aliz Kunstar

PhD thesis, University of Twente, Enschede, The Netherlands

Copyright © Aliz Kunstar, 2012, Enschede, The Netherlands. All rights reserved. Neither this book nor its parts may be reproduced without written permission of the author.

ISBN : 978-90-365-3363-8

DOI nummer : 10.3990/1.9789036533638

The research described in this thesis was supported by the DPTE (Dutch Program for Tissue Engineering) and the Technology Foundation STW:



The publication of this thesis was financially supported by the Anna Fonds te Leiden:

**Anna
Fonds**

Cover design by Dr. Aart A. van Apeldoorn: It illustrates the laser light coming from the laser (back cover page) of the Raman setup, and after the laser light hits a dichroic mirror, it illuminates a molecule (front cover page).

Printed by Ipskamp Drukkers B.V.

CONFOCAL RAMAN MICROSPECTROSCOPY;
APPLICATIONS IN CARTILAGE TISSUE
ENGINEERING

DISSERTATION

to obtain

the degree of doctor at the University of Twente,

on the authority of the rector magnificus,

Prof. Dr. H. Brinksma,

on account of the decision of the graduation committee,

to be publicly defended

on Wednesday, October 31st, 2012, at 12.45

by

Aliz Kunstár

born on September 15th, 1982

in Békéscsaba, Hungary

This dissertation has been approved by:

Promoter: Prof. Dr. Clemens A. van Blitterswijk

Assistant Promoter: Dr. Aart A. van Apeldoorn

Szüleimnek
To my parents



Table of Contents

Chapter 1	Introduction	3
Chapter 2	Raman microspectroscopy: A label-free tool for monitoring chondrocyte dedifferentiation	31
Chapter 3	Raman Microspectroscopy – A Non-Invasive Analysis Tool for Monitoring of Collagen-Containing Extracellular Matrix Formation in a Medium-Throughput Culture System	61
Chapter 4	Label-free Raman monitoring of extracellular matrix formation in 3D PEOT/PBT scaffolds	89
Chapter 5	Recognizing different tissues in human fetal femur cartilage by label-free Raman microspectroscopy	121
Chapter 6	Conclusion and future perspectives	151
	Summary and Samenvatting	157
	List of publications	163
	Curriculum vitae	165
	Acknowledgements	167



Chapter 1

Chapter 1

Introduction

Currently, advanced cartilage tissue engineering generally involves the use of three-dimensional (3D) scaffolds, which can support the growth, proliferation and differentiation of incorporated chondrocytes and/or progenitor cells [1-2].

Studies performed to investigate the composition and quality of tissue engineered cartilage are generally done by using destructive methods like immunohistological, molecular, biochemical or microscopy techniques. Obviously there is an emerging need for non-invasive and non-destructive monitoring methods. These methods would allow for real time monitoring of tissue engineered constructs and study changes in phenotype of the cells involved and changes in extracellular matrix deposition. This thesis aims at studying relevant problems in cartilage tissue engineering by using confocal Raman spectroscopy which is an excellent non-invasive and non-destructive optical tool for high resolution spatially resolved chemical imaging and analysis of tissue engineered samples. Moreover, unlike conventional methods which only give information on the presence of specific compounds, Raman spectroscopy provides a spectroscopic “fingerprint” representing the entire molecular composition of samples of interest. In this Chapter a general introduction is given on cartilage biology, cartilage tissue engineering, the Raman effect, confocal Raman spectroscopy and Raman applications in tissue engineering, more specifically in cartilage tissue engineering.

Articular Cartilage and Cartilage Tissue Engineering

Articular cartilage is a highly specialized connective tissue with the function to provide a low-friction interaction between the bones of a joint and to distribute the load over the surface of joints during movement. Diseased or damaged cartilage has limited ability for regeneration mainly due to the distribution of a low number of cells and the poor innervation of blood vessels into the surrounding extracellular matrix [3-4]. The main features of cartilage are highly determined by its 3D extracellular matrix, which mainly consists of collagen, proteoglycans and water [5-6]. There are three major types of cartilage: hyaline, elastic and fibrocartilage. These different types of cartilage differ from each other in the amount and proportion of the collagen and proteoglycans. In cartilage tissue the majority of collagen is comprised of collagen type II. The microfibrillar nature of the collagen matrix provides the tensile strength and viscoelasticity of this tissue (**Figure 1**). Collagen molecules have a specific structure with three parallel polypeptide strands in a helical conformation combined into a triple helix. Proteoglycans – of which the major type is aggrecan - are involved in binding water molecules, thus providing compressive strength to cartilage [7-8]. Proteoglycans consist of a core protein to which glycosaminoglycan (GAG) side chains are attached [9]. The GAG group in cartilage consists of chondroitin sulphate, dermatan sulphate, heparan sulphate, keratan sulphate and hyaluronic acid. Cartilage extracellular matrix is produced by a surprisingly small number of cells - the chondrocytes (**Figure 1**) compared to the total amount of tissue. Despite their small abundance, chondrocytes are able to produce large amounts of extracellular matrix during cartilage development and are able to maintain this tissue during adult life in healthy conditions [3, 10]. In regard to diffusion of oxygen molecules, since this is the only manner in which chondrocytes can be

supplied with this necessary metabolic molecule, the oxygen tension gradually decreases from the superficial zone towards the deep zone, and in the middle and deep zones of cartilage the oxygen tension is only one-third of that found in well-vascularized tissues [11-12]. Chondrocytes, therefore, have the ability to synthesize and secrete matrix components in a low oxygen tension. The chondrocyte and its pericellular microenvironment are located in the chondron, the primary structural, functional and metabolic unit of articular cartilage [13-14]. One of its function is to protect the chondrocyte from severe deformation under load [15]. The microenvironment of the chondron comprises two integrated parts [14]: the pericellular glycoalyx, which is rich in hyaluronan [16-17], aggrecan [18] and fibronectin [19], and the pericellular capsule, which is composed of fibrillar collagen types II, IX and XI [20-21], microfibrillar collagen type VI [22] and laminin [23].

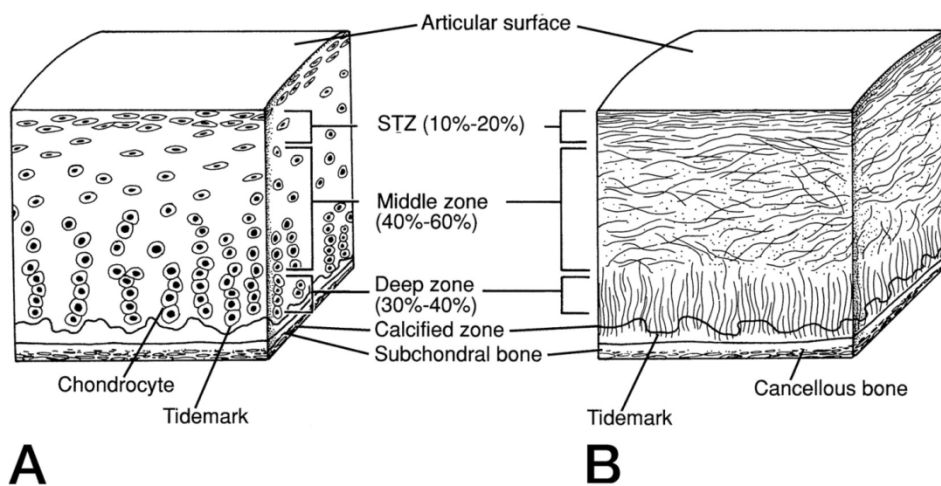


Figure 1. Chondrocyte distribution (A) and collagen distribution (B) in articular cartilage (© 1994 American Academy of Orthopaedic Surgeons. Reprinted from the *Journal of the American Academy of Orthopaedic Surgeons*, Volume 2 (4), pp. 192-201 with permission)

The 3D environment on a micro scale is further known to play an important role in maintaining and supporting cell-matrix interactions during chondrogenesis [24]. Currently, advanced cartilage tissue engineering generally involves the use of 3D scaffolds, these can support the growth, proliferation and differentiation of incorporated chondrocytes and/or progenitor cells while resembling the natural cartilaginous environment [1-2]. After implantation, these constructs should function as and biologically mimic the surrounding tissue as much as possible. A much used source of cells for cartilage regeneration are primary chondrocytes. With regard to chondrocyte implantation, using an autologous cell source is obviously preferred because of the low-risk of immunogenic response associated with allogeneic strategies. Although some allogeneic osteochondral plugs have been shown to exhibit a tolerable immunogenic response [25].

To obtain sufficient numbers of cells for tissue engineering applications chondrocytes are commonly expanded in monolayer culture systems. However isolating chondrocytes from their native environment and expanding them in monolayer cultures leads to a reduction of their chondrocyte phenotype, including a loss in functional tissue formation capacity [26-28]. Loss of the chondrocyte phenotype typically means that cells gain a fibroblastic morphology and secrete type I collagen rather than expressing collagen type II and the aggrecan core protein [29]. This process is known as chondrocyte dedifferentiation and impedes their potential use in cartilage tissue regeneration. Several tactics have been described for optimizing culture conditions to limit chondrocyte dedifferentiation, or to restore the differentiated phenotype. Among them, low oxygen tension as well as 3D culture systems have been, in some cases quite successfully, exploited to preserve better

chondrocyte phenotype, or to promote redifferentiation in culture [30-33]. Using pellet or microaggregate cultures in agarose microwell arrays, the cellular interactions between chondrocytes can be stimulated and maintenance of a spherical morphology is promoted. It has already been shown that there is a relation between cell aggregation and enhanced cartilaginous tissue formation [34-35]. The rationale behind these methods are: (1) that chondrocyte phenotype is stabilized in the aggregate; and (2) that tissue engineered cartilage can be created without supportive carriers, such as polymers or gels in the form of a scaffold [36-37]. In addition, this model is often applied to study chondrogenic differentiation of mesenchymal stem cells (MSCs), which are another potential source of cells for cartilage regeneration and tissue engineering applications in general. The capacity of MSCs to differentiate into tissues of mesenchymal lineages, including bone, cartilage, fat, tendon and muscle, depending on culture conditions and the use of specific growth factors, make these cells ideal candidates for tissue engineering [4]. MSCs are usually isolated from bone marrow, but can also be obtained from adipose tissue or cord blood, and can be multiplied *ex vivo* without loss of phenotype or their multipotency [4, 38-41]. Micromolded non adhesive hydrogels (i.e. agarose), in which an array of well-defined microwells with fixed dimensions are made, have recently become a reproducible and accurate tool to study self-assembly of complex cellular aggregates [42-43].

As it was mentioned before, the use 3D scaffolds in cartilage tissue engineering can support the growth, proliferation and differentiation of incorporated cells. In our laboratory and a number of others have studied the use of a family of block copolymers poly(ethylene oxide terephthalate)-poly(butylene terephthalate) (PEOT/PBT) as a biomaterial for scaffolds and they proved to be highly biocompatible both

in vitro and *in vivo* [44-47] and some compositions have reached clinical application (PolyActive™, IsoTis Orthopaedics S.A.) as dermal substitutes [48] and bone fillers [49-50]. Currently, among scaffold fabrication techniques, rapid prototyping – and within rapid prototyping systems, 3D fiber deposition - appears to be the most promising and widely used fabrication method. This scaffold fabrication technique allows one to tailor the porosity, pore size and shape of scaffolds and the process results in implants which have a completely interconnected pore network and predefined shape [47, 51-52]. It has been demonstrated that scaffolds can be fabricated with such composition and architecture that they can have instructive properties for expanded human chondrocytes to enhance the formation of cartilaginous tissues [2, 53]. Another type of scaffold are hydrogels, which are three dimensional elastic networks with high water content. Hydrogels can mimic hydrated native cartilage tissue and when produced with the right properties can be used as suitable scaffolds for cartilage tissue engineering [1, 54]. One major advantage of hydrogels is that they can be applied as an injectable, which make them highly suitable in clinical applications, since they can be applied via a minimally invasive procedure [55].

Studies performed to investigate the composition and quality of tissue engineered cartilage are in general done by destructive methods such as immunohistological, molecular and/or biochemical techniques. Obviously there is an emerging need for non-invasive and non-destructive monitoring methods, since the quality of tissue engineered constructs can potentially be followed in real-time during culture. Non-invasive methods which allow for the observation of tissue formation and changes in cell phenotype type, based on chemical microscopy, such as confocal Raman spectroscopy are therefore an interesting tool to study

tissue engineered constructs. Using this high resolution microscopy method allows one to not only observe the morphology of cells and tissues, but study their molecular composition in the same time.

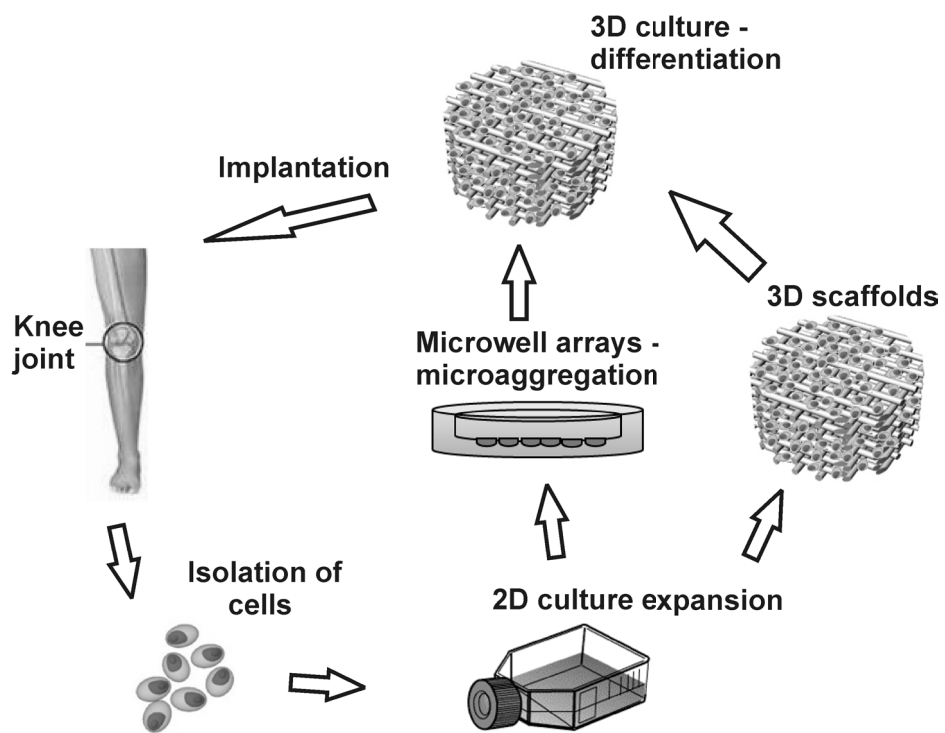


Figure 2. Cartilage tissue engineering approach.

The Raman Effect

The so-called Raman effect was discovered by Sir C. V. Raman and K. S. Krishnan. In 1928 they published a paper on a “New Type of Secondary Radiation” [56]. Raman received the Nobel Prize in physics for his discovery.

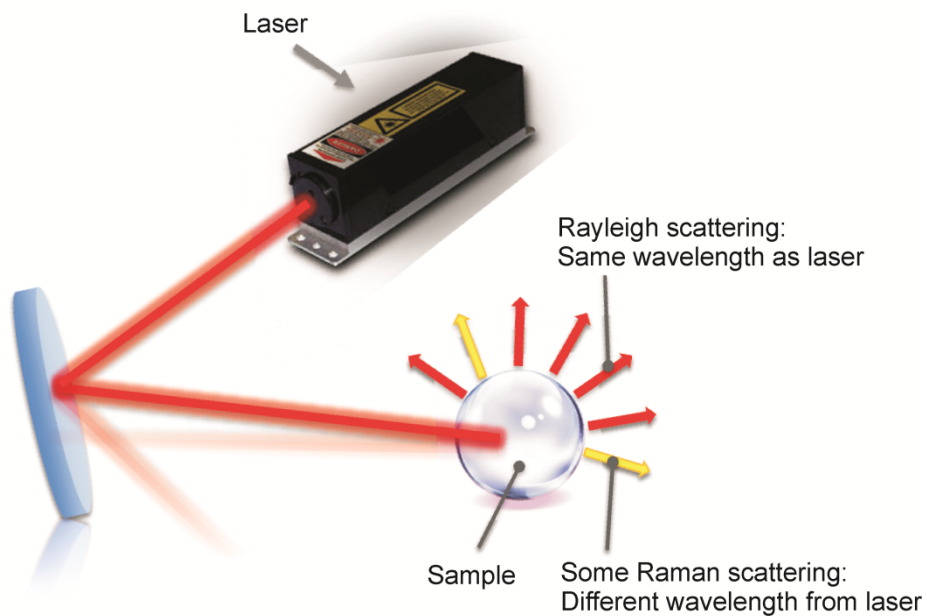


Figure 3. Schematic diagram illustrating the Raman Effect.

Several description of Raman scattering can be found in literature [57-59]. A schematic diagram can be found in **Figure 3** illustrating the Raman Effect. When a monochromatic light source interacts with matter, most of the light is absorbed or transmitted and a small fraction of light is scattered. The light can be scattered elastically (Rayleigh scattering) or

a very small portion of it, inelastically (Raman scattering). In Raman scattering, the emitted photon has a longer (Stokes Raman scattering) or shorter wavelength (anti-Stokes Raman scattering) than that of the initial light source [60]. These wavelength shifts can be collected and are specific for a given functional molecular group or chemical bond and thus a so called Raman “fingerprint” spectrum can be taken from a sample of interest [60].

Raman Spectroscopy and Confocal Raman Microspectroscopy

Raman spectroscopy is a vibrational spectroscopic technique which utilizes the Raman effect to generate molecular fingerprints of samples of interest in order to detect specific wavelength shifts caused by vibrations of chemical bonds. By detecting all photons with shifted wavelengths Raman spectra can be constructed. Several variations of Raman spectroscopy have been developed. One type of Raman spectroscopy is the surface-enhanced Raman scattering (SERS) spectroscopy. In this technique the weak intensity of the Raman signal is enormously amplified by the enhancement of electromagnetic fields induced by the specific surface on which the molecules are adsorbed on. Mostly, patterned gold and silver surfaces [61] or metal nanoparticles [62], distributed on the surface, are used for this method.

Furthermore, it was shown that SERS can be also applied as a novel diagnostic tool for detecting osteoarthritis [63]. Intense spectra of hyaluronic acid, which is a potential osteoarthritis biomarker – could be acquired from synovial fluid by SERS [63].

Coherent anti-Stokes Raman scattering (CARS) spectroscopy is a non-linear variant of Raman spectroscopy. Molecular information can be obtained with high spatial resolution and high speed of imaging when

compared to spontaneous, non-resonant Raman imaging albeit within a narrow bandwidth. In this thesis in Chapter 2, cytoplasmic lipid droplets were investigated in chondrocytes from multiple passages with the ultimate goal to find a Raman marker for dedifferentiation of these cells. In this study spontaneous confocal Raman microspectroscopy and as a complementary technique, CARS microspectroscopy were used. Due to their high CH stretching vibration signal, lipids are comparatively easy to be detected *in vitro* in cells by CARS microscopy at 2845 cm^{-1} [64-66] Furthermore, great advantage of this technique is its capability of 3D imaging [67-68].

A confocal Raman microscope is basically a confocal light microscope coupled with a Raman microscope. A schematic representation of a confocal Raman microscope can be found in **Figure 5**. In this thesis a home-built confocal Raman microspectrometer was used as previously described [69]. Briefly, a Raman microspectrometer utilize a laser as a monochromatic light and excitation source, which is focused on a sample by an objective. The scattered light is collected with the same objective and filtered by a razor-edge filter to suppress reflected laser light and Rayleigh-scattered light. The Raman scattered photons are focused onto a pinhole at the entrance of an imaging spectrograph providing confocality. The spectrograph contains a holographic grating which diverts different wavelengths at different angles. The decomposed wavelengths are then detected on an air-cooled electron-multiplying charge-coupled device (EMCCD) camera, of which the data is then recorded by a computer.

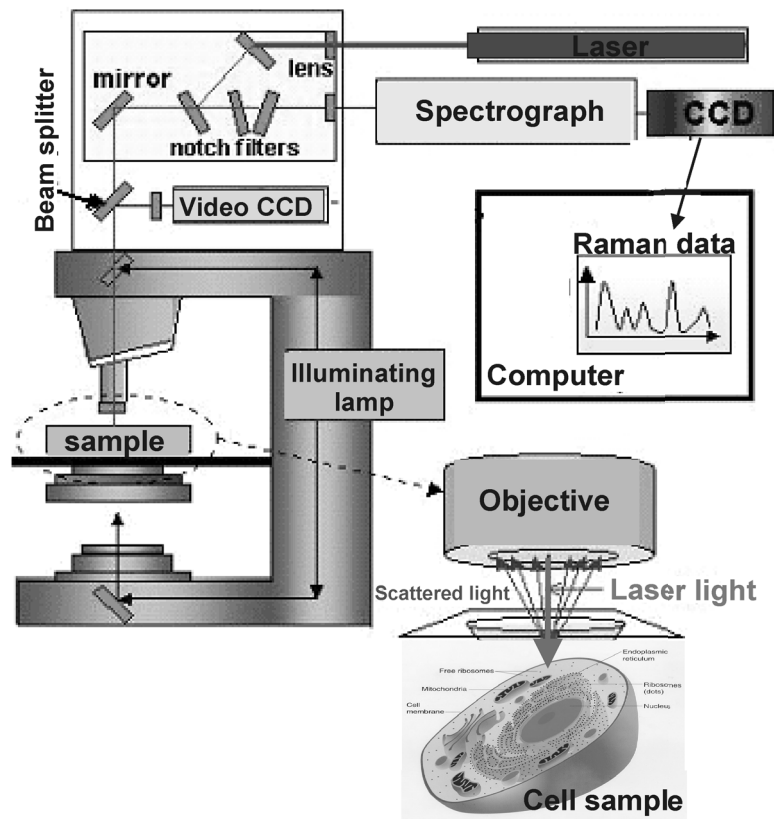


Figure 5. Schematic representation of a confocal Raman microscope. (Original image adopted from <http://www.cwru.edu/med/biochemistry/faculty/carey.html> with permission)

Combining the system with a scanning mirror or scanning sample stage, so called Raman images can be generated. Raman images can be collected in the point-mapping or line illumination mode. An example of Raman imaging of single cells in the point-mapping mode is given in **Figure 6**. Here, the laser is focused onto the sample, the scattered light is registered, and subsequently the focus is moved by a scanning mirror to the next position. A full spectrum is recorded from each position of the

laser beam (**Fig. 6A**). The Raman image of 32 x 32 spectra is acquired using a 60x water immersion objective, an excitation wavelength of 647 nm and an exposure time of 0.5 sec per spectrum. The Raman image is segmented into groups (clusters) by principal component analysis (PCA) and hierarchical cluster analysis (HCA) according to the similarity of spectra. HCA made use of the scores obtained from the PCA to visualize the regions of high spectral similarities. A cluster image with corresponding mean cluster spectra can be constructed (**Fig. 6B**). The clusters can be assigned according to the location and spectral profile. Mean cluster spectra display representative Raman spectra of the nucleus (red spectrum: red cluster) with contributions from DNA and proteins, Raman spectra of the cytoplasm (purple spectrum: purple cluster) with contributions from RNA and proteins and Raman spectra of the calcium fluoride (CaF₂)-substrate and phosphate buffered saline (PBS) solution in which the cells were stored and measured (black spectrum: black cluster). Univariate Raman images (Raman maps) focused on a specific vibrational band of interest can be also constructed from the image-dataset by integrating the band intensity [70]. As an example a Raman image focused on the DNA band at 786 cm⁻¹ is demonstrated in **Figure 6C**. The highest (red) intensity of DNA content is concentrated in the area of the nucleus in the cell. The results demonstrate that detailed information on molecular structure of unlabeled cells can be obtained at subcellular level.

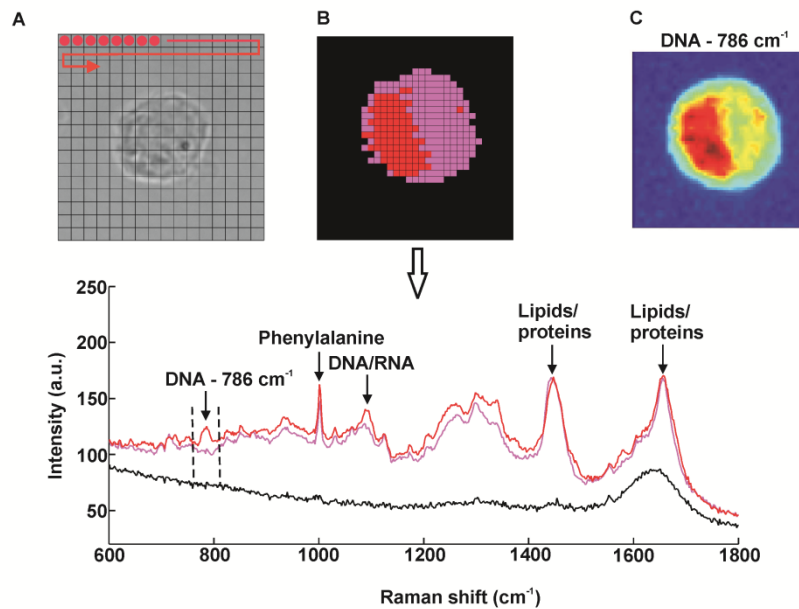


Figure 6. Raman imaging of single cells. **A:** A full spectrum is recorded from each position (red dots) of the laser beam **B:** Raman image after segmentation by cluster analysis (cluster image) with corresponding mean cluster spectra. Mean cluster spectra display representative Raman spectra of the nucleus (red spectrum: red cluster) with contributions from DNA, proteins and lipids, Raman spectra of the cytoplasm (purple spectrum: purple cluster) with contributions from RNA, proteins and lipids and Raman spectra of the calcium fluoride (CaF_2)-substrate and phosphate buffered saline (PBS) solution in which the cells were stored and measured (black spectrum: black cluster). **C:** Raman image focused on the DNA band at 786 cm^{-1} .

In the case of laser line illumination of a sample, the spatial data can be registered on the detector on a line parallel to the entrance slit of the spectrometer, and the spectral information is dispersed perpendicularly [71]. The second spatial dimension of an image is recorded by scanning in the direction perpendicular to that line [71]. This type of imaging is faster when compared to point-mapping mode, however the confocality

is reduced along the slit, therefore the resolution decreases along the line.

In general, the acquisition of images – instead of acquisition of a single spectra with point measurement - offers advantages in tissue studies because a larger area can be scanned in the inhomogeneous tissue samples. For example Raman mapping in combination with multivariate data analysis has been successfully applied for analysis of cartilage sections [72].

HCA can be performed applying Wards clustering method based on Euclidean inter-point distances [73]. The result of HCA can be represented in a dendrogram, as it can be seen in **Figure 6 in Chapter 5**, which shows the cluster linking of spectra from different zones of the human fetal femur. The smaller the variance-weighted distance between the cluster centers is, the more they resemble each other.

Raman data is usually displayed as a plot of Raman scattering intensity as a function of wavelength [74]. At the x-axis the Raman shift is displayed in wavenumbers [74]. Wavenumber is the reciprocal of wavelength in centimeters. One wavenumber is equal to a unit of energy E (Formula 1). The x-axis in Raman spectra displays the difference between excitation and Raman wavelength (Formula 2).

$$E = h \nu = \frac{h c}{\lambda} = h c \omega \quad (\text{Formula 1})$$

h = Planck's constant, ν = frequency of light, c = speed of light, λ = wavelength of light, ω = wavenumber of light

$$\text{Raman shift} = \frac{1}{\lambda_0} - \frac{1}{\lambda_{\text{Raman}}} \quad (\text{cm}^{-1})$$

(Formula 2)

λ_0 = excitation wavelength, λ_{Raman} = Raman wavelength.

Cell and tissue imaging and Raman applications in tissue engineering

As opposed to conventional methods, such as histology and immunohistochemistry, which only provides information regarding the presence of specific compounds, Raman spectroscopy creates a “fingerprint” representing the entire molecular composition of the investigated sample. For inorganic samples a wide range of laser excitation wavelengths can be used [75-77]. It has been demonstrated that a careful selection of suitable laser wavelength and laser intensity eliminates the possibility of cell damage [78-79]. Therefore Raman microscopy for biological specimens generally utilizes near-infrared (NIR) lasers. Since Puppels et al. have shown the feasibility of the system to study single living cells and chromosomes [80-82], this technique has been widely used for single cell imaging applications. High-resolution Raman spectral studies were performed and successfully applied to study cell-cycle [83-84], cell death due to apoptosis or necrosis [85], proliferation and differentiation of cells [86-87], including chondrocyte response to bioactive scaffolds [88]. Evaluating these differences in health and status of cells provided basis for continued research into cellular behavior in tissue engineering.

Overall Raman microscopy has several advantages. It is a label-free and non-destructive technique, which does not require special sample

preparation, such as dehydration (water does not generally interfere with Raman spectral analysis) and fixation. Furthermore by using the high resolution capabilities of this system samples can be analyzed on a submicrometer scale.

Because of its applicability for non-destructive sensing and fast imaging [89], Raman spectroscopy has also been widely used for *in vivo* measurements [90]. Such applications will often require the use of small and flexible fiber-optic probes, in which the signal is detected at a distance from the point or points where light is injected into the system [91]. Such system can be used for depth-resolved subsurface optical spectroscopy in highly scattering (turbid) systems, such as tablets, polymers, and human or animal tissue [91]. Fiber-optic Raman systems have already been used for monitoring joint tissues *in vivo* [92] such as for assessing progress of bone graft incorporation in bone reconstruction and repair transcutaneously [93]. Other researchers have reported *in vivo* measurements from the bladder and prostate [94], oesophagus [95], skin [96] cervix [97-98], and arteries [99].

Beside non-resonant Raman microscopy there are other vibrational spectroscopic techniques, such as CARS – which has already been described in the previous **Raman spectroscopy and Confocal Raman Microspectroscopy** section - and Fourier-transform infrared spectroscopy (FTIR) that are also widely used and successfully applied for cell and tissue imaging. FTIR and non-resonant Raman spectroscopic techniques are complementary in that the Raman imaging affords superior spatial and spectral resolution ($\sim 1 \mu\text{m}$ and 1 cm^{-1} , respectively) and spectral discrimination, whereas the infrared technique produces data about 100 times faster and with a much better signal-to-noise ratio (S/N), but lower spatial and spectral resolution ($\sim 12 \mu\text{m}$ and 4 cm^{-1} , respectively) [83, 100-101].

Raman microspectroscopy of cartilage and applications in cartilage tissue engineering - Scope of the thesis

Monitoring the production levels of essential ECM components is one of the key methods used to determine tissue quality in tissue engineered constructs. Chondrocyte response to bioactive scaffolds has already been monitored by obtaining Raman signal from the extracellular matrix deposited onto the scaffold and by assessing Raman bands indicative for collagen in the spectral region between 1200 cm^{-1} and 1800 cm^{-1} [88]. Raman spectroscopic studies of native cartilage were also mainly focused on direct analysis of ECM components. Raman analysis has been performed on analysis of collagen in the sclera, articular cartilage and subchondral bone of wild-type and transgenic mice harboring structural truncations in the introduced collagen type II transgene [102]. Furthermore chemical imaging was carried out employing Raman imaging combined with uni- and multivariate data analysis on articular cartilage sections. Variations between different regions of the extracellular matrix were detected and semiquantitative mapping of the biochemical constituents - in agreement with average composition found in the literature - was possible by performing sophisticated multivariate data analysis [72]. These results showed that Raman imaging in combination with multivariate data analysis has an excellent potential as a tool, complementary to other imaging techniques, for studying biochemical and morphological changes during cartilage degradation in aging or diseased cartilage [72]. Articular cartilage has been more extensively investigated by FTIR spectroscopy. It has been demonstrated in literature that FTIR imaging is useful in quantitatively assessing pathology-related changes in the composition and distribution of primary macromolecular extracellular matrix components of human osteoarthritic cartilage [103]. Additionally for molecules with a unique

spectral signature, such as chondroitin sulfate, the FTIR technique coupled with multivariate analysis can define a unique spatial distribution [104]. However, for some applications, the lack of specificity of this technique for different types of proteins may be a limitation [104].

Current protocols for autologous chondrocyte implantation require culture expansion of chondrocytes to obtain sufficient cells for implantation. Culture expansion of chondrocytes is associated with chondrocyte dedifferentiation. In this thesis in **Chapter 2** use of label-free Raman microspectroscopy to monitor chondrocyte dedifferentiation has been explored with the ultimate aim of developing a non-invasive assay for assessing the quality of expanded chondrocytes for cartilage repair.

In **Chapter 3 and 4** chondrocyte response in 3D culture systems was investigated by *in vitro* monitoring of extracellular matrix formation in a medium-throughput pellet culture system with soft-lithography, agarose microwell arrays (in Chapter 3) and in 3D scaffolds in (Chapter 4). Furthermore in **Chapter 4**, the aim was, beside to determine tissue quality in large tissue engineered constructs in a label-free manner, to detect possible differences in matrix formation of single cell- and microaggregate-seeded scaffolds. In **Chapter 5** the main focus was to determine whether confocal Raman microspectroscopy is able to effectively discriminate between different cartilaginous zones of a developing diarthrodial joint and to identify the molecular differences between the (pre)articular cartilage and the different zones of the growth plate cartilage. Together, this knowledge will contribute to our understanding on how to generate a specific sort of cartilage for future tissue engineering and clinical purposes.

REFERENCES

1. Jin, R., et al., *Enzymatically-crosslinked injectable hydrogels based on biomimetic dextran-hyaluronic acid conjugates for cartilage tissue engineering*. *Biomaterials*, 2010. **31**(11): p. 3103-13.
2. Malda, J., et al., *The effect of PEGT/PBT scaffold architecture on the composition of tissue engineered cartilage*. *Biomaterials*, 2005. **26**(1): p. 63-72.
3. Mankin, H.J., *The response of articular cartilage to mechanical injury*. *J Bone Joint Surg Am*, 1982. **64**(3): p. 460-6.
4. Dudics, V., et al., *Chondrogenic potential of mesenchymal stem cells from patients with rheumatoid arthritis and osteoarthritis: measurements in a microculture system*. *Cells Tissues Organs*, 2009. **189**(5): p. 307-16.
5. Zhang, Z., et al., *Hyaline cartilage engineered by chondrocytes in pellet culture: histological, immunohistochemical and ultrastructural analysis in comparison with cartilage explants*. *J Anat*, 2004. **205**(3): p. 229-37.
6. Kuettner, K.E., *Biochemistry of articular cartilage in health and disease*. *Clin Biochem*, 1992. **25**(3): p. 155-63.
7. Hardingham, T., B.C. Heng, and P. Gribbon, *New approaches to the investigation of hyaluronan networks*. *Biochemical Society Transactions*, 1999. **27**(2): p. 124-127.
8. Poole, A.R., et al., *Composition and structure of articular cartilage - A template for tissue repair*. *Clinical Orthopaedics and Related Research*, 2001(391): p. S26-S33.
9. Forriol, F. and F. Shapiro, *Bone development: interaction of molecular components and biophysical forces*. *Clin Orthop Relat Res*, 2005(432): p. 14-33.
10. Martin, J.A. and J.A. Buckwalter, *The role of chondrocyte-matrix interactions in maintaining and repairing articular cartilage*. *Biorheology*, 2000. **37**(1-2): p. 129-40.
11. Brighton, C.T. and Heppenst.Rb, *Oxygen Tension in Zones of Epiphyseal Plate, Metaphysis and Diaphysis - in-Vitro and in-Vivo Study in Rats and Rabbits*. *Journal of Bone and Joint Surgery-American Volume*, 1971. **A 53**(4): p. 719-&.
12. Otte, P., *Basic Cell-Metabolism of Articular-Cartilage - Manometric Studies*. *Zeitschrift Fur Rheumatologie*, 1991. **50**(5): p. 304-312.
13. Poole, C.A., *Articular cartilage chondrons: form, function and failure*. *J Anat*, 1997. **191 (Pt 1)**: p. 1-13.

14. Hing, W.A., A.F. Sherwin, and C.A. Poole, *The influence of the pericellular microenvironment on the chondrocyte response to osmotic challenge*. Osteoarthritis Cartilage, 2002. **10**(4): p. 297-307.
15. Poole, C.A., M.H. Flint, and B.W. Beaumont, *Chondrons Extracted from Canine Tibial Cartilage - Preliminary-Report on Their Isolation and Structure*. Journal of Orthopaedic Research, 1988. **6**(3): p. 408-419.
16. Mason, R.M., *Recent advances in the biochemistry of hyaluronic acid in cartilage*. Prog Clin Biol Res, 1981. **54**: p. 87-112.
17. Poole, C.A., T.T. Glant, and J.R. Schofield, *Chondrons from articular cartilage. (IV). Immunolocalization of proteoglycan epitopes in isolated canine tibial chondrons*. J Histochem Cytochem, 1991. **39**(9): p. 1175-87.
18. Winter, G.M., et al., *Identification of distinct metabolic pools of aggrecan and their relationship to type VI collagen in the chondrons of mature bovine articular cartilage explants*. Connective Tissue Research, 1998. **37**(3-4): p. 277-+.
19. Glant, T.T., et al., *Appearance and Persistence of Fibronectin in Cartilage - Specific Interaction of Fibronectin with Collagen Type-II*. Histochemistry, 1985. **82**(2): p. 149-158.
20. Poole, C.A., et al., *Immunolocalization of type IX collagen in normal and spontaneously osteoarthritic canine tibial cartilage and isolated chondrons*. Osteoarthritis and Cartilage, 1997. **5**(3): p. 191-204.
21. Wotton, S.F., et al., *The Application of Scanning Confocal Microscopy in Cartilage Research*. Histochemical Journal, 1991. **23**(7): p. 328-335.
22. Poole, C.A., *Chondrons - the Chondrocyte and Its Pericellular Microenvironment*. Articular Cartilage and Osteoarthritis, 1992: p. 201-220.
23. Durr, J., et al., *Identification and immunolocalization of laminin in cartilage*. Exp Cell Res, 1996. **222**(1): p. 225-33.
24. Zhang, Z.J., et al., *Hyaline cartilage engineered by chondrocytes in pellet culture: histological, immunohistochemical and ultrastructural analysis in comparison with cartilage explants*. Journal of Anatomy, 2004. **205**(3): p. 229-237.
25. Revell, C.M. and K.A. Athanasiou, *Success Rates and Immunologic Responses of Autogenic, Allogenic, and Xenogenic Treatments to Repair Articular Cartilage Defects*. Tissue Engineering Part B-Reviews, 2009. **15**(1): p. 1-15.
26. Stewart, M.C., et al., *Phenotypic stability of articular chondrocytes in vitro: The effects of culture models, bone morphogenetic protein 2, and serum supplementation*. Journal of Bone and Mineral Research, 2000. **15**(1): p. 166-174.

27. Thirion, S. and F. Berenbaum, *Culture and phenotyping of chondrocytes in primary culture*. Methods Mol Med, 2004. **100**: p. 1-14.
28. Binette, F., et al., *Expression of a stable articular cartilage phenotype without evidence of hypertrophy by adult human articular chondrocytes in vitro*. Journal of Orthopaedic Research, 1998. **16**(2): p. 207-216.
29. Schnabel, M., et al., *Dedifferentiation-associated changes in morphology and gene expression in primary human articular chondrocytes in cell culture*. Osteoarthritis Cartilage, 2002. **10**(1): p. 62-70.
30. Domm, C., et al., *Redifferentiation of dedifferentiated bovine articular chondrocytes in alginate culture under low oxygen tension*. Osteoarthritis Cartilage, 2002. **10**(1): p. 13-22.
31. Murphy, C.L. and A. Sambanis, *Effect of oxygen tension and alginate encapsulation on restoration of the differentiated phenotype of passaged chondrocytes*. Tissue Eng, 2001. **7**(6): p. 791-803.
32. Pfander, D., et al., *HIF-1alpha controls extracellular matrix synthesis by epiphyseal chondrocytes*. J Cell Sci, 2003. **116**(Pt 9): p. 1819-26.
33. Strobel, S., et al., *Anabolic and catabolic responses of human articular chondrocytes to varying oxygen percentages*. Arthritis Res Ther, 2010. **12**(2): p. R34.
34. Duke, P.J., E.L. Daane, and D. Montufar-Solis, *Studies of chondrogenesis in rotating systems*. J Cell Biochem, 1993. **51**(3): p. 274-82.
35. Naumann, A., et al., *Tissue engineering of autologous cartilage grafts in three-dimensional in vitro macroaggregate culture system*. Tissue Eng, 2004. **10**(11-12): p. 1695-706.
36. Temenoff, J.S. and A.G. Mikos, *Review: tissue engineering for regeneration of articular cartilage*. Biomaterials, 2000. **21**(5): p. 431-40.
37. Vunjak-Novakovic, G., et al., *Bioreactor cultivation conditions modulate the composition and mechanical properties of tissue-engineered cartilage*. J Orthop Res, 1999. **17**(1): p. 130-8.
38. Barry, F.P. and J.M. Murphy, *Mesenchymal stem cells: clinical applications and biological characterization*. Int J Biochem Cell Biol, 2004. **36**(4): p. 568-84.
39. Johnstone, B., et al., *In vitro chondrogenesis of bone marrow-derived mesenchymal progenitor cells*. Experimental Cell Research, 1998. **238**(1): p. 265-272.
40. Krampera, M., et al., *Regenerative and immunomodulatory potential of mesenchymal stem cells*. Curr Opin Pharmacol, 2006. **6**(4): p. 435-41.

41. Pittenger, M.F., et al., *Multilineage potential of adult human mesenchymal stem cells*. *Science*, 1999. **284**(5411): p. 143-147.
42. Napolitano, A.P., et al., *Dynamics of the self-assembly of complex cellular aggregates on micromolded nonadhesive hydrogels*. *Tissue Engineering*, 2007. **13**(8): p. 2087-2094.
43. Rivron, N.C., et al., *Tissue assembly and organization: developmental mechanisms in microfabricated tissues*. *Biomaterials*, 2009. **30**(28): p. 4851-8.
44. Beumer, G.J., C.A. van Blitterswijk, and M. Ponec, *Biocompatibility of a biodegradable matrix used as a skin substitute: an in vivo evaluation*. *J Biomed Mater Res*, 1994. **28**(5): p. 545-52.
45. Bakker, D., et al., *Effect of implantation site on phagocyte/polymer interaction and fibrous capsule formation*. *Biomaterials*, 1988. **9**(1): p. 14-23.
46. Beumer, G.J., C.A. van Blitterswijk, and M. Ponec, *Degradative behaviour of polymeric matrices in (sub)dermal and muscle tissue of the rat: a quantitative study*. *Biomaterials*, 1994. **15**(7): p. 551-9.
47. Moroni, L., et al., *Design of biphasic polymeric 3-dimensional fiber deposited scaffolds for cartilage tissue engineering applications*. *Tissue Eng*, 2007. **13**(2): p. 361-71.
48. Mensik, I., et al., *Effectiveness and Safety of the PEGT/PBT Copolymer Scaffold as Dermal Substitute in Scar Reconstruction Wounds (Feasibility Trial)*. *Cell Tissue Bank*, 2002. **3**(4): p. 245-53.
49. Meijer, G.J., et al., *Polyactive as a bone-filler in a beagle dog model*. *Int J Oral Maxillofac Surg*, 1996. **25**(3): p. 210-16.
50. Du, C., et al., *Bone growth in biomimetic apatite coated porous Polyactive((R)) 1000PEGT70PBT30 implants*. *Biomaterials*, 2002. **23**(23): p. 4649-4656.
51. Malda, J., et al., *The effect of PEGT/PBT scaffold architecture on oxygen gradients in tissue engineered cartilaginous constructs*. *Biomaterials*, 2004. **25**(26): p. 5773-80.
52. Sachlos, E. and J.T. Czernuszka, *Making tissue engineering scaffolds work. Review: the application of solid freeform fabrication technology to the production of tissue engineering scaffolds*. *Eur Cell Mater*, 2003. **5**: p. 29-39; discussion 39-40.
53. Miot, S., et al., *Effects of scaffold composition and architecture on human nasal chondrocyte redifferentiation and cartilaginous matrix deposition*. *Biomaterials*, 2005. **26**(15): p. 2479-2489.
54. Moreira Teixeira, L.S., et al., *The effect of platelet lysate supplementation of a dextran-based hydrogel on cartilage formation*. *Biomaterials*, 2012. **33**(14): p. 3651-61.

55. Moreira Teixeira, L.S., et al., *Self-attaching and cell-attracting in-situ forming dextran-tyramine conjugates hydrogels for arthroscopic cartilage repair*. *Biomaterials*, 2012. **33**(11): p. 3164-74.
56. Raman, C.V. and K.S. Krishnan, *A new type of secondary radiation (Reprinted from Nature, vol 121, pg 501-502, 1928)*. *Current Science*, 1998. **74**(4): p. 381-381.
57. Bhagavantam, S., *Scattering of light and the Raman effect*. 1940, Waltair India: Andhra University. x, 333 p.
58. Long, D.A., *The Raman effect : a unified treatment of the theory of Raman scattering by molecules*. 2002, Chichester ; New York: Wiley. xxiv, 597 p.
59. Pelletier, M.J., *Analytical applications of Raman spectroscopy*. 1999, Osney Mead, Oxford ; Malden, MA: Blackwell Science. vii, 478 p.
60. van Apeldoorn, A.A., et al., *Parallel high-resolution confocal Raman SEM analysis of inorganic and organic bone matrix constituents*. *J R Soc Interface*, 2005. **2**(2): p. 39-45.
61. Fleischm.M, P.J. Hendra, and Mcquilla.Aj, *Raman-Spectra of Pyridine Adsorbed at a Silver Electrode*. *Chemical Physics Letters*, 1974. **26**(2): p. 163-166.
62. Mock, J.J., et al., *Shape effects in plasmon resonance of individual colloidal silver nanoparticles*. *Journal of Chemical Physics*, 2002. **116**(15): p. 6755-6759.
63. Mandair, G.S., et al., *Detection of potential osteoarthritis biomarkers using surface-enhanced Raman spectroscopy in the near-infrared - art. no. 60930H*. *Biomedical Vibrational Spectroscopy III: Advances in Research and Industry*, 2006. **6093**: p. H930-H930.
64. Hellerer, T., A.M.K. Enejder, and A. Zumbusch, *Spectral focusing: High spectral resolution spectroscopy with broad-bandwidth laser pulses*. *Applied Physics Letters*, 2004. **85**(1): p. 25-27.
65. Nan, X., J.X. Cheng, and X.S. Xie, *Vibrational imaging of lipid droplets in live fibroblast cells with coherent anti-Stokes Raman scattering microscopy*. *J Lipid Res*, 2003. **44**(11): p. 2202-8.
66. Evans, C.L., et al., *Chemical imaging of tissue in vivo with video-rate coherent anti-Stokes Raman scattering microscopy*. *Proc Natl Acad Sci U S A*, 2005. **102**(46): p. 16807-12.
67. Cheng, J.X., A. Volkmer, and X.S. Xie, *Theoretical and experimental characterization of coherent anti-Stokes Raman scattering microscopy*. *Journal of the Optical Society of America B-Optical Physics*, 2002. **19**(6): p. 1363-1375.
68. Jurna, M., et al., *Noncritical phase-matched lithium triborate optical parametric oscillator for high resolution coherent anti-Stokes Raman*

- scattering spectroscopy and microscopy. *Applied Physics Letters*, 2006. **89**(25).
69. van Manen, H.J., A. Lenferink, and C. Otto, *Noninvasive imaging of protein metabolic labeling in single human cells using stable isotopes and Raman microscopy*. *Anal Chem*, 2008. **80**(24): p. 9576-82.
70. Uzunbajakava, N., et al., *Nonresonant confocal Raman imaging of DNA and protein distribution in apoptotic cells*. *Biophys J*, 2003. **84**(6): p. 3968-81.
71. Krafft, C., B. Dietzek, and J. Popp, *Raman and CARS microspectroscopy of cells and tissues*. *Analyst*, 2009. **134**(6): p. 1046-57.
72. Bonifacio, A., et al., *Chemical imaging of articular cartilage sections with Raman mapping, employing uni- and multi-variate methods for data analysis*. *Analyst*, 2010. **135**(12): p. 3193-3204.
73. Hervada-Sala, C. and E. Jarauta-Bragulat, *A program to perform Ward's clustering method on several regionalized variables*. *Computers & Geosciences*, 2004. **30**(8): p. 881-886.
74. vanApeldoorn, A.A., *Confocal Raman Microscopy; Applications in Tissue Engineering*. 2005, University of Twente: Enschede, the Netherlands. p. 19.
75. Jehlicka, J., O. Urban, and J. Pokorny, *Raman spectroscopy of carbon and solid bitumens in sedimentary and metamorphic rocks*. *Spectrochimica Acta Part a-Molecular and Biomolecular Spectroscopy*, 2003. **59**(10): p. 2341-2352.
76. Jirasek, A.I., et al., *Characterization of monomer/crosslinker consumption and polymer formation observed in FT-Raman spectra of irradiated polyacrylamide gels*. *Phys Med Biol*, 2001. **46**(1): p. 151-65.
77. Liem, N.Q., N.T. Thanh, and P. Colomban, *Reliability of Raman microspectroscopy in analysing ancient ceramics: the case of ancient Vietnamese porcelain and celadon glazes*. *Journal of Raman Spectroscopy*, 2002. **33**(4): p. 287-294.
78. Notingher, I., et al., *In situ characterisation of living cells by Raman spectroscopy*. *Spectroscopy*, 2002. **16**(2): p. 43-51.
79. Puppels, G.J., et al., *Laser irradiation and Raman spectroscopy of single living cells and chromosomes: Sample degradation occurs with 514.5 nm but not with 660 nm laser light*. *Experimental Cell Research*, 1991. **195**(2): p. 361-367.
80. Puppels, G.J., et al., *Studying Single Living Cells and Chromosomes by Confocal Raman Microspectroscopy*. *Nature*, 1990. **347**(6290): p. 301-303.

81. Puppels, G.J., et al., *Carotenoids Located in Human Lymphocyte Subpopulations and Natural-Killer-Cells by Raman Microspectroscopy*. Cytometry, 1993. **14**(3): p. 251-256.
82. Puppels, G.J., et al., *Raman Microspectroscopic Approach to the Study of Human Granulocytes*. Biophysical Journal, 1991. **60**(5): p. 1046-1056.
83. Matthaus, C., et al., *Raman and infrared microspectral imaging of mitotic cells*. Applied Spectroscopy, 2006. **60**(1): p. 1-8.
84. Notingher, I., et al., *Spectroscopic study of human lung epithelial cells (A549) in culture: Living cells versus dead cells*. Biopolymers, 2003. **72**(4): p. 230-240.
85. Verrier, S., et al., *In situ monitoring of cell death using Raman microspectroscopy*. Biopolymers, 2004. **74**(1-2): p. 157-162.
86. Notingher, I., et al., *In situ non-invasive spectral discrimination between bone cell phenotypes used in tissue engineering*. J Cell Biochem, 2004. **92**(6): p. 1180-92.
87. Notingher, L., et al., *In situ spectroscopic study of nucleic acids in differentiating embryonic stem cells*. Vibrational Spectroscopy, 2004. **35**(1-2): p. 199-203.
88. Jones, J., et al., *In situ monitoring of chondrocyte response to bioactive scaffolds using Raman spectroscopy*. Key Engineering Materials, 2005. **284-286**: p. 623-626.
89. Krafft, C., et al., *Mapping of single cells by near infrared Raman microspectroscopy*. Vib Spectrosc, 2003. **32**: p. 75-83.
90. Bakker Schut, T.C., et al., *In vivo detection of dysplastic tissue by Raman spectroscopy*. Anal Chem, 2000. **72**(24): p. 6010-8.
91. Schulmerich, M.V., et al., *Subsurface and transcutaneous Raman Spectroscopy and mapping using concentric illumination rings and collection with a circular fiber-optic array*. Applied Spectroscopy, 2007. **61**(7): p. 671-678.
92. Matousek, P., et al., *Noninvasive Raman Spectroscopy of human tissue in vivo*. Applied Spectroscopy, 2006. **60**(7): p. 758-763.
93. Okagbare, P.I., et al., *Transcutaneous Raman spectroscopy for assessing progress of bone graft incorporation in bone reconstruction and repair*. Photonic Therapeutics and Diagnostics Vii, 2011. **7883**.
94. Crow, P., et al., *Fibre-optic raman spectrsocopy: The prospects for in vivo diagnosis of bladder and prostate cancer*. Journal of Urology, 2004. **171**(4): p. 68-68.
95. Shim, M.G., et al., *In vivo near-infrared Raman spectroscopy: Demonstration of feasibility during clinical gastrointestinal endoscopy*. Photochemistry and Photobiology, 2000. **72**(1): p. 146-150.

96. Hata, T.R., et al., *Non-invasive Raman spectroscopic detection of carotenoids in human skin*. Journal of Investigative Dermatology, 2000. **115**(3): p. 441-448.
97. Mahadevan-Jansen, A., et al., *Development of a fiber optic probe to measure NIR Raman spectra of cervical tissue in vivo*. Photochemistry and Photobiology, 1998. **68**(3): p. 427-431.
98. Utzinger, U., et al., *Near-infrared Raman spectroscopy for in vivo detection of cervical precancers*. Applied Spectroscopy, 2001. **55**(8): p. 955-959.
99. Buschman, H.P., et al., *In vivo determination of the molecular composition of artery wall by intravascular Raman spectroscopy*. Analytical Chemistry, 2000. **72**(16): p. 3771-3775.
100. Boskey, A. and N.P. Camacho, *FT-IR imaging of native and tissue-engineered bone and cartilage*. Biomaterials, 2007. **28**(15): p. 2465-2478.
101. Kazanci, M., et al., *Bone osteonal tissues by Raman spectral mapping: Orientation-composition*. Journal of Structural Biology, 2006. **156**(3): p. 489-496.
102. Dehring, K.A., et al., *Correlating changes in collagen secondary structure with aging and defective type II collagen by Raman spectroscopy*. Appl Spectrosc, 2006. **60**(4): p. 366-72.
103. David-Vaudey, E., et al., *Fourier Transform Infrared Imaging of focal lesions in human osteoarthritic cartilage*. Eur Cell Mater, 2005. **10**: p. 51-60; discussion 60.
104. Potter, K., et al., *Imaging of collagen and proteoglycan in cartilage sections using Fourier transform infrared spectral imaging*. Arthritis and Rheumatism, 2001. **44**(4): p. 846-855.

Chapter 2

Raman microspectroscopy: A label-free tool for monitoring chondrocyte dedifferentiation

*Aliz Kunstar¹, Erik T. Garbacik⁴, Tim W. G. M. Spitters^{1,2},
Herman L. Offerhaus⁴, Cees Otto³, Clemens A. van Blitterswijk¹,
Marcel Karperien^{1,2}, Aart A. van Apeldoorn^{1,2}*

¹Department of Tissue Regeneration, ²Present address: Department of Developmental Bioengineering, ³Department of Medical Cell Biophysics of MIRA – Institute for Biomedical Technology and Technical Medicine, University of Twente, Drienerlolaan 5, 7522 NB Enschede, The Netherlands

⁴Optical Sciences Group, MESA+ Institute for Nanotechnology, University of Twente, Drienerlolaan 5, 7522 NB Enschede, the Netherlands

ABSTRACT: Current protocols for autologous chondrocyte implantation require culture expansion of chondrocytes to obtain sufficient number of cells for implantation. Culture expansion of chondrocytes is associated with chondrocyte dedifferentiation, a gradual process in which the cells lose their chondrocyte characteristics, lose their capacity to produce cartilaginous matrix and acquire fibroblast like features. Non-invasive methods for measuring the quality of culture expanded cell populations for implantation are not present. In this study we have explored the use of confocal label-free Raman microspectroscopy to monitor chondrocyte dedifferentiation.

Bovine primary chondrocytes directly after isolation (Passage=0) and after culture expansion (P=2 and P=4) were analyzed by real-time quantitative polymerase chain reaction (qPCR) for chondrogenic differentiation markers and by confocal label-free Raman microspectroscopy. Single human primary chondrocytes directly after isolation (P=0) and after culture expansion at normoxia and hypoxia (P=2 and P=4) and chondrocytes within human cartilage tissue at normoxia and hypoxia were analyzed by confocal label-free Raman microspectroscopy and by coherent anti-Stokes Raman scattering (CARS) microscopy.

Decreased mRNA expression of collagen type II and gained fibroblast-like appearance of chondrocytes with increased passage number, observed in this study, are in line with gradual dedifferentiation of chondrocytes during culture expansion in 2D. The Raman band at 2924 cm^{-1} signifying lipids was found as a universal marker for dedifferentiation of chondrocytes. It was also shown by confocal Raman and CARS microscopy that culturing at hypoxic conditions was not sufficient for retaining lipid droplets in expanded human chondrocytes. However band-area ratios for lipid content demonstrated that

chondrocytes, within their endogenous cartilage matrix and cultured at hypoxic conditions, retained their lipid content, unlike the ones cultured at normoxia. This demonstrates the importance of both oxygen concentration and interaction with the extracellular matrix in retaining the lipid droplets of chondrocytes. Overall it can be concluded that in this study a label-free assay for assessing the quality of expanded chondrocytes has been developed.

INTRODUCTION

Cartilage is a skeletal tissue largely consisting of extracellular matrix produced by a relative small number of cells - the chondrocytes. Despite their low abundance, chondrocytes are able to produce large amounts of extracellular matrix during cartilage development and are able to maintain this tissue during adult life in healthy conditions [1-2]. Oxygen tension gradually decreases from the superficial zone towards the deep zone of the cartilage and in the middle and deep zones is only one-third of that found in well-vascularized tissues [3-4]. Chondrocytes, therefore, have the ability to synthesize and secrete matrix components in an avascular environment. A possible source of cells for cartilage regeneration is the autologous chondrocytes. With regard to chondrocyte implantation, using autologous cell source is preferred because of the risk of immunogenic response associated with allogeneic strategies [5]. Autologous chondrocyte implantation (ACI) is a two-step procedure [6-7]. First, healthy cartilage tissue is removed from a non-weight bearing area, then it is sent to the laboratory. To obtain sufficient number, these chondrocytes are expanded in 2D monolayer culture systems. However isolating chondrocytes from their native ECM, from a hypoxic environment, and expanding them in 2D monolayer cultures in

relatively high oxygen level leads to a reduction of their chondrogenic phenotype, including a loss of functional tissue forming capability and loss of aggrecan and collagen type II synthesis to the profit of collagen type I and type III synthesis. [8-9]. This process is known as chondrocyte dedifferentiation and hampers their use in cartilage tissue regeneration. Several approaches have been described for optimizing culture conditions to limit chondrocyte dedifferentiation or to restore the differentiated phenotype. Among them, low oxygen tension as well as 3D culture has been successfully used to preserve better chondrocyte phenotype or promote redifferentiation in culture [10-13] .

Current techniques, available for measuring the quality of culture expanded cell populations for implantation, are invasive or destructive, requiring cell lysis and/or the use of molecular probes or fluorophores for labeling specific proteins and studying gene expression. In this study we have explored the use of confocal non-resonant Raman and CARS microscopy to monitor chondrocyte dedifferentiation, with the ultimate goal to develop a label-free assay for assessing the quality of expanded chondrocytes for cartilage repair. Raman microspectroscopy allows label-free collection of data over a wide spectrum of nutrients, extracellular matrix and cellular components at high spatial resolution [14]. The greatest advantage of Raman microspectroscopy is that it does not require any labeling or special sample preparation. Raman measurement can be performed on live cells as it has been shown that no cell damage is induced if the near infrared region is selected for excitation wavelengths during single cell Raman imaging [15-16]. This vibrational spectroscopic technique employs an inelastic scattering effect (the Raman effect) to generate a molecular fingerprint of samples of interest by detecting particular wavelength shifts triggered by the vibrations of covalent bonds. Since the first application of Raman

spectroscopy on single living cells and chromosomes [17], this technique has been widely used for biological and single cell imaging applications. High-resolution Raman spectral studies were performed and successfully applied to study cell-cycle [18-19], cell death due to apoptosis or necrosis [20], proliferation and differentiation of cells [21-22], including chondrocyte responses to bioactive scaffolds [23]. With CARS microscopy, molecular information can be obtained with high spatial resolution and high speed of imaging when compared to spontaneous, non-resonant Raman imaging albeit within a narrow bandwidth. However, this procedure requires considerable higher laser power and longer exposures of samples for the generation of the coherent signal than are used during non-resonant Raman measurements.

MATERIALS AND METHODS

Isolation of bovine and human chondrocytes and cell culture.

Primary bovine chondrocytes were isolated from articular cartilage pieces derived from the femoral-patellar groove of a 10-month-old calf by digestion with 420 Units/ml collagenase type II as previously described [24] (Worthington Biochemical, Lakewood, NJ). Primary chondrocytes were isolated from articular cartilage after informed consent and medical ethical committee approval for the use of human donor material from three human donors undergoing knee replacement surgery - aged between 60 and 80 years old - by digestion with 420 Units/ml collagenase type II. The freshly isolated, passage 0 (P0) - chondrocytes were expanded on tissue culture plastic (T-flask; Nunc; Thermo Fischer Scientific, Roskilde, Denmark) in chondrocyte medium (CM): Dulbecco's Modified Eagle's Medium (DMEM; Gibco, Carlsbad,

CA) containing 10 v/v % fetal bovine serum (FBS; South American Origin; Biowhittaker, Lonza, Verviers, Belgium), 100 Units/mL penicillin G (Invitrogen, Carlsbad, CA), 100 µg/mL streptomycin (Invitrogen), 0.1 mM non-essential amino acids (Sigma, St. Louis, MO), 0.4 mM proline (Sigma, St. Louis, MO), and 0.2 mM L-ascorbic-acid-2-phosphate (Sigma, St. Louis, MO) at 37 °C, 5% CO₂ at normoxic (ambient air) or hypoxic conditions (2.5 % oxygen concentration). In parallel, articular cartilage cubes (3 cubes per donor) were fixed in 10% formalin overnight at 4 °C directly after isolation (t₀), as a control representing untreated articular cartilage, or after 7 days of culture period at normoxia or after 7 days of culture period at hypoxia.

Sample preparation for Raman measurements. In order to promote cell adhesion, UV grade calcium fluoride (CaF₂) slides (Crystran Ltd., UK) were coated with proteins by incubation in FBS for 2 hours at 37 °C. After incubation, the coated slides were washed with phosphate buffered saline (PBS) solution and P0, P2 or P4 chondrocyte samples were seeded on them in CM and incubated for 2 hours. Coating promoted and enhanced cellular adhesion on the slides. To prepare for Raman measurements, slides were then washed with PBS, fixed in 10% formalin for 10 minutes and washed with PBS again.

The fixed human cartilage cubes (t₀, cultured for 7 days at normoxia and cultured for 7 days at hypoxia) were washed with PBS, embedded in cryomatrix (Cryomatrix, Shandon), frozen to -49 °C, sectioned at 20 µm intervals at -19 °C using a cryotome (Shandon 77210160, Shandon) and placed on CaF₂ slides. For CARS measurements cyosections were placed on SuperFrost Plus adhesion slides (Menzel-Gläser, Germany).

Confocal Raman Microscopy. Fifteen randomly chosen chondrocytes were scanned from each passage (single chondrocyte samples) or at fixed time points (cartilage samples) per condition per donor (human samples) on a home-built confocal Raman microspectrometer as previously described [25]. Briefly, a Krypton ion laser (Coherent, Innova 90K, Santa Clara, CA) with an emission wavelength of 647.1 nm was used as excitation source. A water immersion 63x/1.0NA objective (Zeiss W-plan Aplanachromat, Carl Zeiss MicroImaging GmbH, Göttingen, Germany) was used to illuminate the cell samples and a 40x/0.75 NA objective (Olympus UIS2, UPlanFLN, Olympus, Hamburg, Europe) as used to illuminate the cartilage samples. The scattered light was collected by the same objective in epi-detection mode and filtered by a razor-edge filter (Semrock, Rochester, NY, USA) to suppress reflected laser light and Rayleigh-scattered light, and focused onto a confocal pinhole of 15 μm diameter at the entrance of a spectrograph (HR460; Jobin-Yvon, Paris, France). The spectrograph dispersed the Raman-scattered photons on an air-cooled electron-multiplying charge-coupled device (EMCCD) camera (Newton DU-970N, Andor Technology, Belfast, Northern Ireland). The system provided a spectral resolution of 1.85 to 2.85 $\text{cm}^{-1}/\text{pixel}$ over the wavenumber range from -20 to 3670 cm^{-1} . Confocal Raman scans were made from the samples by recording a full spectrum from each position of the laser beam guided by the displacement of the scanning mirror in the area of interest on the samples (SM, MG325D and G120D, General Scanning, Bedford, USA). Each Raman scans were resulted in 1024 spectra. Measurements on cell samples were performed over an area of 20 x 20 μm with a spectral resolution of 310 nm per scan, an accumulation time of 0.5 s/step and an excitation power of 35 mW. Measurements on cartilage cryosections

were performed over an area of 30 x 30 μm with an accumulation time of 1 s/step and an excitation power of 35mW.

Toluene, a Raman calibration standard - with well-described peak frequencies (521, 785, 1004, 1624, 2921 and 3054 cm^{-1}) - was used for wavenumber calibration of the spectra.

Raman data analysis. Preprocessing of the data was performed as described previously [26-28]. The spectra were preprocessed by: (1) removing cosmic ray events; (2) subtracting the camera-offset noise (dark current); and (3) calibrating the wave number axis. The well-known band-positions were used to relate wavenumbers to pixels. The frequency-dependent optical detection efficiency of the setup was corrected using a tungsten halogen light source (Avalight-HAL; Avantes BV, Eerbeek, The Netherlands) with a known emission spectrum. The detector-induced etaloning effect was compensated by this procedure. After data correction, the spectra of the Raman scans were averaged to generate mean spectra for samples from each passage (single chondrocyte samples) or at fixed time points (cartilage samples) per condition.

Semi-quantitative univariate data analysis was performed by selecting specific vibrational bands in the mean spectra from each passage (single chondrocyte samples) or at fixed time points (cartilage samples) per condition, and integrating each band after local baseline subtraction. Subsequently, band-area ratios were obtained from the band of interest, such as the lipid band, over the integrated band of the nitrogen stretch-mode at 2328 cm^{-1} as an intensity standard. The calculations were made

using normalized band area ratios, not absolute values, so the system allows for a relative comparison of lipid formation within the total study. Singular value decomposition (SVD) was applied to the hyperspectral data cubes to reduce the uncorrelated noise resulting in the raw 3D data matrix after converting them to 2D matrix. The SVD-treated data was analyzed by multivariate data analysis procedures. In multivariate analysis, both principal component analysis and hierarchical cluster analysis were performed on the datasets, and cluster images were made to separate the spectra of cells from the spectra of substrate or ECM. All data manipulations were performed using routines written in MATLAB 7.4 (The Math Works Inc., Natick, MA).

Coherent anti-Stokes Raman scattering (CARS) microscopy. Fixed cell and cartilage samples were measured with a custom-built CARS setup as previously described [29-30]. The setup consisted of a frequency-doubled Coherent Paladin Nd: YVO₄ laser pumping an APE Levante Emerald optical parametric oscillator (OPO). In this setup, the laser fundamental beam (1064 nm, 80 MHz, ~10 ps) is used as the Stokes wavelength, whereas the signal beam from the OPO (nominally used at 816.7 nm) is used degenerately as both the pump and probe. The beams are scanned over the sample by galvano mirrors (Olympus FluoView 300 scan unit on an IX71 frame) and focused by a 60x/1.2NA water immersion objective lens (Olympus UPLSAPO) into the sample. Both beams have a power of several tens of mWs at the sample. The generated CARS signal was collected in the forward direction (F-CARS) by a 0.55NA long-working distance objective, spectrally filtered to remove the strong pump/probe beam, and detected with a photomultiplier tube (Hamamatsu R3896). Backscattered CARS (B-

CARS) signals were collected by the focusing objective, reflected from a dichroic beamsplitter, further isolated with bandpass spectral filters, and detected on a separate PMT (Hamamatsu R3896). The OPO signal was tuned to 816.7 nm to access the 2845 cm^{-1} band corresponding to the CH_2 asymmetric stretch found predominantly in lipids. All images are 512×512 pixels, acquired in 3.2 seconds/frame with average of 3 frames (9.6 seconds/image) and cover an area of $150\text{ }\mu\text{m} \times 150\text{ }\mu\text{m}$ with $\sim 400\text{ nm}$ lateral resolution. The natural confocality of CARS allowed 3D images to be obtained by stacking multiple slices along the z-axis (z-stack images) with $\sim 1\text{ }\mu\text{m}$ axial resolution. Each slice was recorded in 0.99 seconds/frame with average of 2 frames (1.98 seconds/slice), over an area of 256×256 pixels and with $0.2\text{ }\mu\text{m}$ axial step size. Differential interference contrast (DIC) and transmission (at 817 nm) micrographs of the samples were also collected.

Metabolism. In order to determine glucose consumption rate during cell culture, the concentration of glucose in the medium was measured. Cell culture medium samples (1mL) were taken before refreshment. Glucose was measured with the Vitros DT 60 II and the corresponding slides (Ortho-Clinical Diagnostics, U.S.A.). Glucose consumption rate has been depicted as the amount of glucose consumed per cell per day.

RNA isolation and real-time quantitative polymerase chain reaction (qPCR) analysis. Total RNA was extracted from bovine chondrocytes of multiple passages using the RNeasy Mini Kit according to the manufacturer's instructions (Qiagen Pty Ltd, Hilden, Germany). cDNA was synthesized from $1\text{ }\mu\text{g}$ RNA, using random hexamers (Sigma, St.

Louis, MO), 5x First Strand Buffer (Invitrogen, Carlsbad, CA), 0.1M dithiothreitol and 20mM deoxyribonucleotide triphosphates (dNTPs), 40 units of RNAsin Ribonuclease Inhibitor (Promega Corp, Madison, WI) and 200 units of SuperScript II reverse transcriptase (Invitrogen, Carlsbad, CA) according to the manufacturer's instructions. qPCR was performed for glyceraldehyde 3-phosphate dehydrogenase as an internal control (*GAPDH*, Forward - 5' GCCATCACTGCCACCCAGAA 3' and Reverse - 5' GCGGCAGGTCAGATCCACAA 3'), Collagen type II (*COL2A1*, Forward - 5' ATCAACGGTGGCTTCCACT 3' and Reverse - 5' TTCGTGCAGCCATCCTTCAG 3') and Collagen type I (*COL1A1*, Forward - 5' GCGGCTACGACTTGAGCTTC 3', Reverse - 5' CACGGTCACGGACCACATTG 3') on cDNA samples using the iQ SYBR Green Supermix (Bio-Rad, Hercules, CA). Thermocycling was carried out on a MyiQ2 Two-Color Real-Time PCR Detection System (Bio-Rad, Hercules, CA), under the following conditions: denaturation for 5 min at 95 °C, followed by 45 cycles consisting of 15s at 95°C, 15s 60°C and 30s at 72°C. For each reaction, a melting curve was generated to test for occurrence of primer dimer formation or false priming. The mRNA expression levels relative to GAPDH were calculated using the comparative C_t method.

Histology. 8-µm thick cryosections from cartilage tissue samples, that were made consecutive to sections used for non-resonant Raman and CARS analysis, were stained with Safranin-O (Sigma, St. Louis, MO) for visualization of sGAGs and with haematoxylin (Sigma, St. Louis, MO) for visualization of the cell nuclei.

Statistical analysis. The results are presented as mean \pm standard deviation (SD). Experimental data were analyzed for statistical significance using a student t-test. Statistical significance was set to p-value < 0.05 (*).

RESULTS AND DISCUSSION

To identify Raman markers associated with chondrocyte dedifferentiation, Raman-scans of bovine primary chondrocytes directly after isolation (P=0) and after culture expansion (P=2 and P=4) were recorded. Bright field micrographs showed that the measured chondrocytes lost their initial spherical shape and gained spindle-shaped fibroblast-like appearance with increased passage number (**Fig. 1A**). Additionally quantitative PCR analysis, performed for chondrocyte differentiation markers, showed significant down-regulation of collagen type II mRNA and a gradual increase in collagen type I mRNA expression with increased passage number (**Fig. 1B**). These changes in morphology and mRNA expression are in line with gradual dedifferentiation of chondrocytes during culture expansion in 2D [31]. Subsequently, as a result of cluster analysis, cluster images with corresponding mean cluster spectra were obtained from each Raman-scan per cell. As an example a cluster image with the corresponding mean cluster spectra of a P0 chondrocyte can be seen in **Figure 1C**.

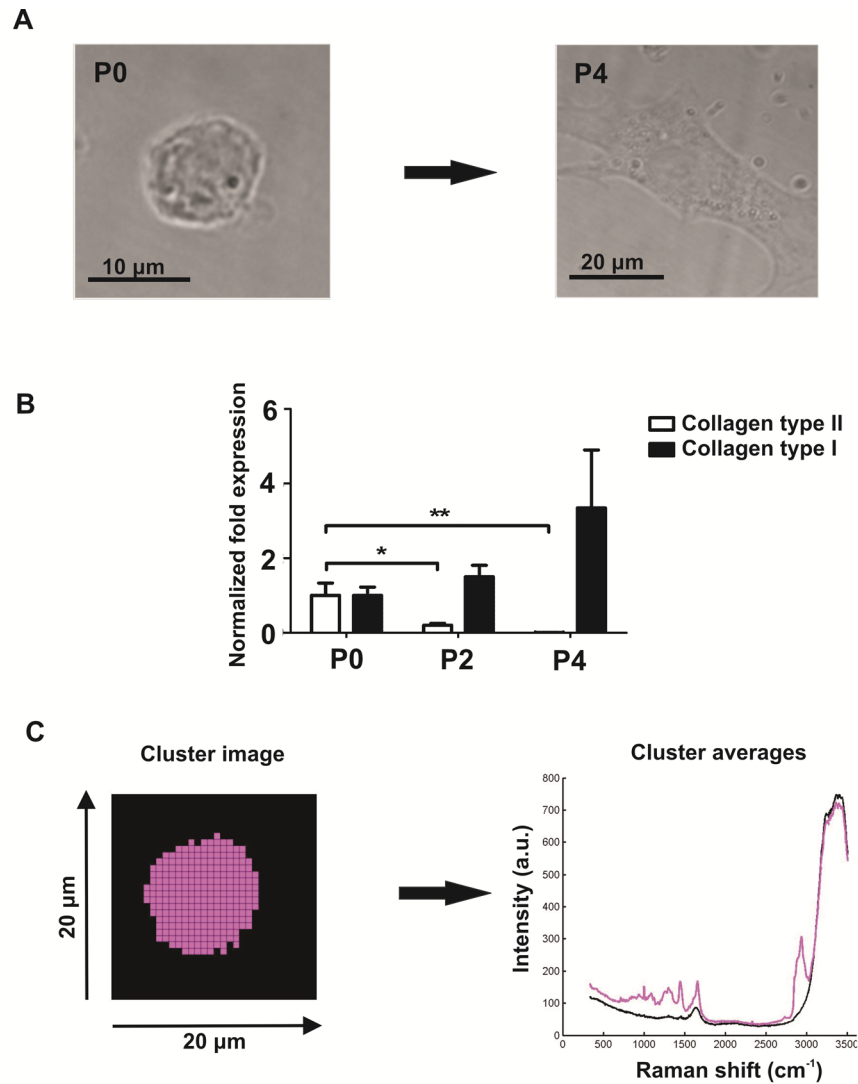


Figure 1. Morphological, gene expression and cluster analysis of bovine chondrocytes. **A:** Bright field micrographs showed that the measured chondrocytes lost their initial spherical and gained spindle-shaped fibroblast-like appearance with increased passage number **B:** Additionally quantitative PCR analysis, performed for chondrogenic differentiation markers, showed significant decrease in collagen type II mRNA expression and a gradual increase in collagen type I mRNA expression with increased

passage number **C**: Cluster image with the corresponding Raman cluster averages of a bovine P0 chondrocyte. Hierarchical clustering separated Raman spectra of the cell (purple squares) from that of the CaF₂ substrate (black squares). The scanned area has the size of 20 x 20 μm and 32 x 32 pixels. Each pixel (square) in the image has a size of 625 x 625 nm. The purple line (purple spectrum) depicts the average spectra of the purple squares. The black line (black spectrum) denotes the average spectra of the black squares.

The hierarchical clustering separated Raman spectra of the cell (purple squares) from that of the CaF₂ substrate (black squares). The purple line (purple spectrum) depicts the average spectra of the purple squares (cell). The black line (black spectrum) denotes the average spectra of the black squares (substrate). Cluster spectra corresponding to cells at each passage (P0, P2, and P4) were averaged, creating one spectrum representative of all cells (**Fig. 2A**). Raman bands of the mean spectra – such as bands of phenylalanine (C-C aromatic ring) at 1001 cm⁻¹ [32], lipids/proteins (CH₂ bending mode) at 1448 cm⁻¹ [33], amide I at 1657 cm⁻¹ [34] and lipids (CH stretch of lipids) at 2924 cm⁻¹ [35] - were identified and assigned. We found that the Raman band at 2924 cm⁻¹ specific for lipids showed a decrease in intensity with increased passage number. Semi-quantitative univariate data analysis was performed to calculate normalized band-area ratios to quantify changes in intensities of these Raman bands in different passages. Normalized band-area ratios for lipid content of chondrocytes showed a significant decrease from P0 to P4 (**Fig. 2B**). Based on the band-area ratios P2 cells resemble better P0 cells than P4 cells. Raman images of chondrocytes - using this lipid band – also showed a decrease in intensity with increased passage number (**Fig. 2C**). It should be pointed out that the highest intensity (red) of the lipid content in the images of the P0

chondrocyte is 20 times higher compared to the images of expanded P2 chondrocytes.

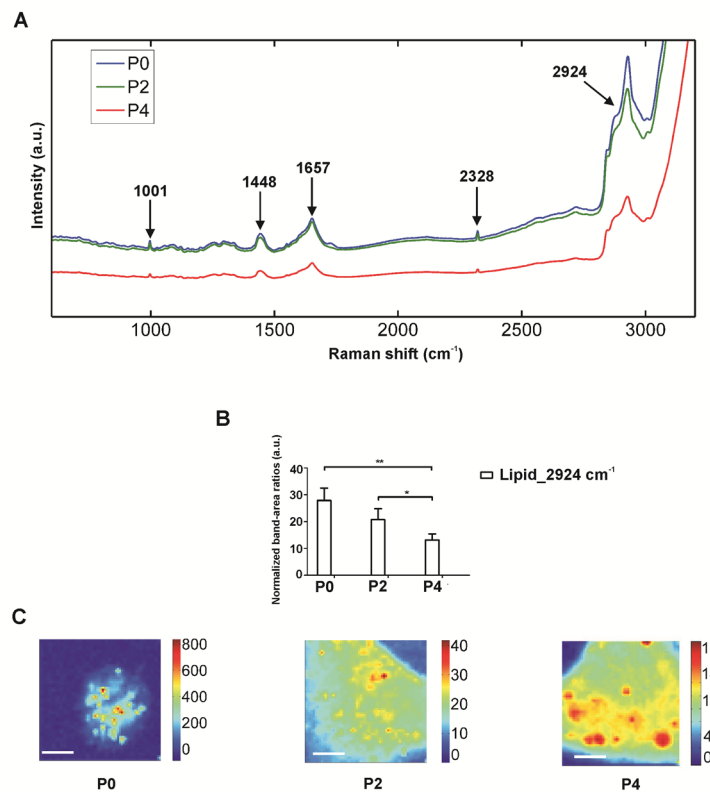


Figure 2. Mean cell-cluster spectra and lipid band-area ratios of bovine chondrocytes from P0, P2 and P4. **A:** Mean cell-cluster spectra of bovine chondrocytes acquired directly after isolation (P0) and after culture expansion (P2 and P4) in the region from 600 cm⁻¹ to 3200 cm⁻¹. Raman band at 2924 cm⁻¹ specific for lipids showed a decrease in intensity with increased passage number. Spectra were vertically displaced for clarity. **B:** Normalized band-area ratios for lipid content of chondrocytes showed a significant decrease from P0 to P4 ($p=0.0076$) and from P2 to P4 ($p=0.0488$). The normalized band-area ratio acquired from the ratio of the lipid band to the band of nitrogen at 2328 cm⁻¹ as intensity standard. All bands were integrated after baseline subtraction. **C:** Raman images of chondrocytes - using this lipid band - also showed a decrease in intensity in the expanded (P2 and P4) chondrocytes compared to P0 chondrocytes. It should be noted that the highest (red) intensity of the lipid content in the image of the P0

chondrocyte is 20 times higher when compared in the images of expanded P2 chondrocytes. Scale bars equal to 5 μm .

Cytoplasmic lipid droplets are considered to be normal and permanently present inclusions in chondrocytes in the cartilage [36-37]. Chondrocytes do not lie close to blood vessels and inclusion of lipid droplets is most probably an adaptive phenomenon related to their hypoxic environment. Possibly these lipid droplets function as a readily accessible storage for energy driving metabolic processes or storage of chemical building blocks for matrix synthesis in the cells [37]. Therefore culture expansion of chondrocytes in 2D monolayer cultures in relatively high oxygen tension could lead to loss of these lipid droplets, which may explain the decreased lipid content of the expanded (P2 and P4) chondrocytes observed by Raman microscopy in our study.

To test whether culture expansion of chondrocytes in hypoxic conditions would preserve the presence of lipid droplets, Raman-scans of human primary chondrocytes directly after isolation (P=0) and after culture expansion (P=2 and P=4), cultured under normoxic and hypoxic conditions, were recorded. Transmission and DIC light microscopy showed that chondrocytes had lost their initial spherical and gained spindle-shaped fibroblast-like appearance with increased passage number (**Fig. 3A**), as it was observed in the case of expanded bovine chondrocytes, both at normoxia and hypoxia. Furthermore increased glucose consumption rates of cells, which cultured at hypoxia, were detected when compared to glucose consumption rates of cells cultured at normoxia in all passages (**Fig. 3B**). It has been shown by others that subjection of chondrocytes to a hypoxic environment causes an increase

in glucose utilization and proportionally elevated level of lactate synthesis [38].

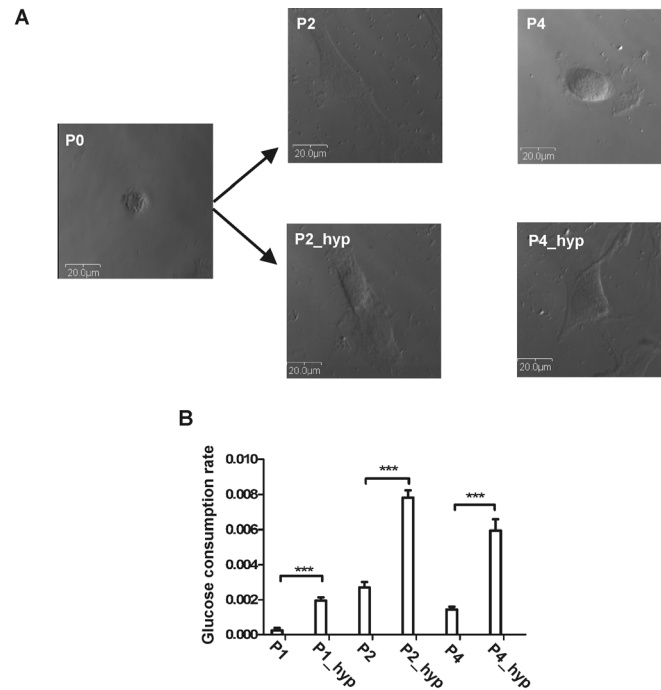


Figure 3. Morphological analysis and metabolism of expanded human chondrocytes. **A:** Transmission (P0) and DIC (P2, P4, P2_hyp, P4_hyp) light microscopy showed that chondrocytes had lost their initial spherical and gained spindle-shaped fibroblast-like appearance with increased passage number both at normoxia (P2, P4) and hypoxia (P2_hyp, P4_hyp). Images were made with a 10x objective and scale bars equal 20 μm. **B:** Increased glucose consumption rates of cells, which cultured at hypoxia, were detected when compared to glucose consumption rates of cells cultured at normoxia in all passages ($p < 0.001$). Glucose consumption rate has been depicted as the amount of glucose consumed per cell per day.

Raman spectra of cells from the Raman-scans were separated from Raman spectra of the CaF₂ substrate as described before. The separated mean cell-cluster spectra from each passage and condition (normoxia or hypoxia) are demonstrated in **Figure 4A**. The Raman band of lipids at 2924 cm⁻¹ showed a decrease in intensity with increased passage number, as it was observed in the case of expanded bovine chondrocytes, both at normoxic and hypoxic culture conditions. Normalized band area ratios for lipid content from 3 donors were averaged in each passage and culture condition and it significantly decreased from P0 to P2 and from P0 to P4 in both normoxic and hypoxic culture conditions (**Figure 4B**). Raman spectroscopy did not reveal a difference between culture expansions in hypoxic or in normoxic conditions, demonstrating that hypoxia is not a driving factor in loss of lipid droplets.

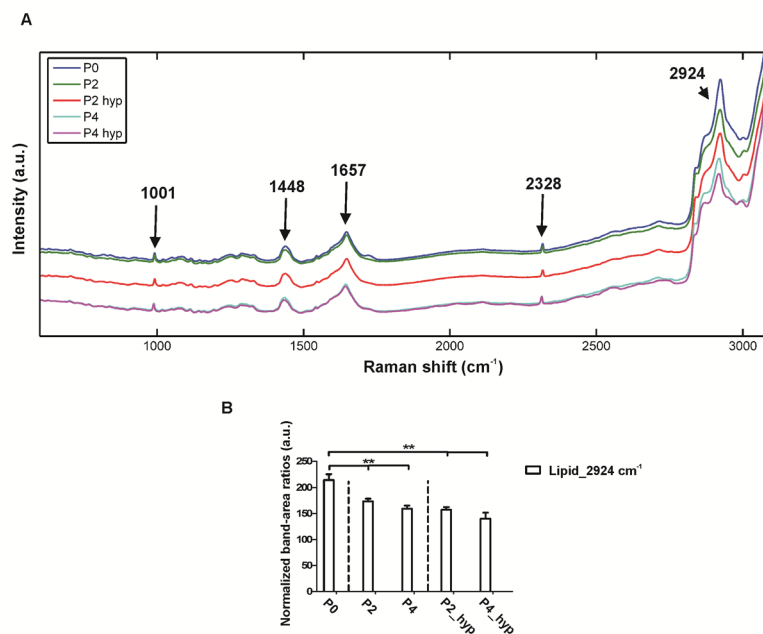


Figure 4. Mean cell-cluster spectra and lipid band-area ratios of human chondrocytes from P0, P2 and P4 cultured at normoxia or hypoxia. **A:** Mean cell-cluster spectra of human chondrocytes directly after isolation (P0) and after culture expansion at normoxia (P2; P4) or hypoxia (P2_hyp; P4_hyp) in the region from 600 cm^{-1} to 3200 cm^{-1} . The Raman band at 2924 cm^{-1} specific for lipids showed a decreased intensity with increased passage number both at normoxia and hypoxia. **B:** Normalized band-area ratios for lipid content from 3 donors were averaged in each passage and conditions and it significantly decreased from P0 to P2 (normoxia: $p=0.0037$; hypoxia: $p=0.0011$) and from P0 to P4 (normoxia: $p=0.0013$; hypoxia: $p=0.0012$) in both culture conditions.

Subsequently, samples of culture expanded chondrocytes were analyzed by CARS microscopy. This technique is capable of 3D chemical imaging with sub-micrometer resolution [39-40]. In this study CARS measurements were focused on the band at 2845 cm^{-1} (CH_2 asymmetric stretch of lipids), which is widely used for imaging of lipids by CARS [41]. We observed that in F-CARS - transmission composite images (**Fig. 5A-a**) and F-CARS z-stack images (**Fig. 5A-b**) of freshly isolated, P0 chondrocytes lipid droplets were clearly visible in the cytoplasm. Subsequently, we showed that lipid droplets were unobservable (**Fig. 5B and C - b**) or considerably reduced (**Fig. 5D and E - b**) in expanded chondrocytes at both hypoxic and normoxic conditions, thus confirming the observations made by non-resonant Raman measurements.

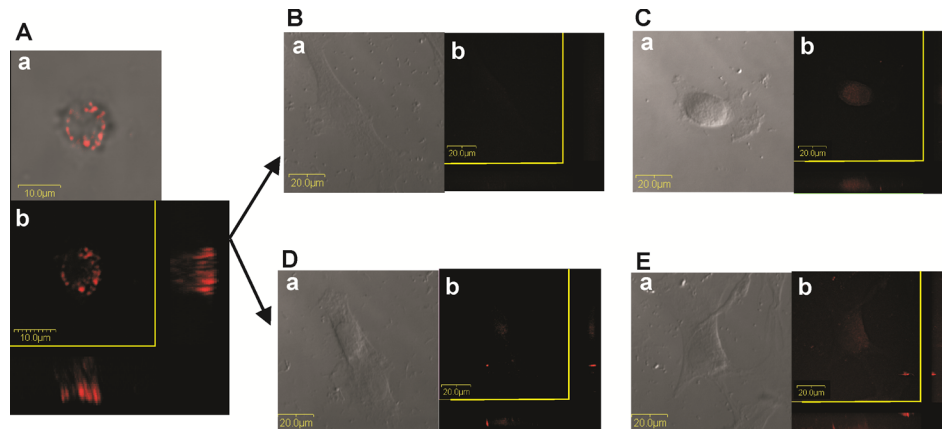


Figure 5. CARS, DIC (**B, C, D, E - a**) and transmission images of P0, P2 and P4 human chondrocytes cultured at normoxia or hypoxia. Measurements were focused on the band at 2845 cm^{-1} specific for lipids. **A - a:** In merged CARS-transmission image and **A - b:** forward-scattered CARS z-stack image of P0 chondrocytes lipid droplets are clearly visible in the cytoplasm. Images were made with a 10x objective and scale bars equal 10 μm . **B, C - b:** We observed that lipid droplets completely disappeared and/or **D, E - b:** the number of lipid droplets had considerably reduced in expanded chondrocytes under both hypoxic and normoxic conditions. Images were made with a 4x objective and scale bars equal 20 μm .

Based on these results it appears that chondrocytes lost their storage of cytoplasmic lipid droplets resulting from isolation from their native 3D matrix and subsequent expansion in 2D monolayer cultures rather than from a change from normoxic to hypoxic conditions. There can be an alternative explanation for the loss of lipid droplets that it was caused by culture expansion in medium, rich in glucose, serum, aminoacids etc. Thus alternative energy sources were readily available and there was no need to have an internal storage since other energy sources were abundant.

To test the role of 3D environment in retaining lipid droplets, Raman measurements were performed on chondrocytes in their natural 3D matrix, in the cartilage. Raman-scans were made from cryosections of

tissue samples, which were freshly fixed (t0) or cultured for 7 days at hypoxia (7d_hyp) or 7 days at normoxia (7d_norm). As a control histochemical analysis was also performed on cryosections from the cartilage tissue samples. Safranin-O staining showed sulfated glycosaminoglycan content while cell nuclei were counterstained using haematoxylin at all time points and both in normoxic and hypoxic cultured cartilage tissue samples (t0, 7d_hyp, 7d_norm) (**Fig. 6A**).

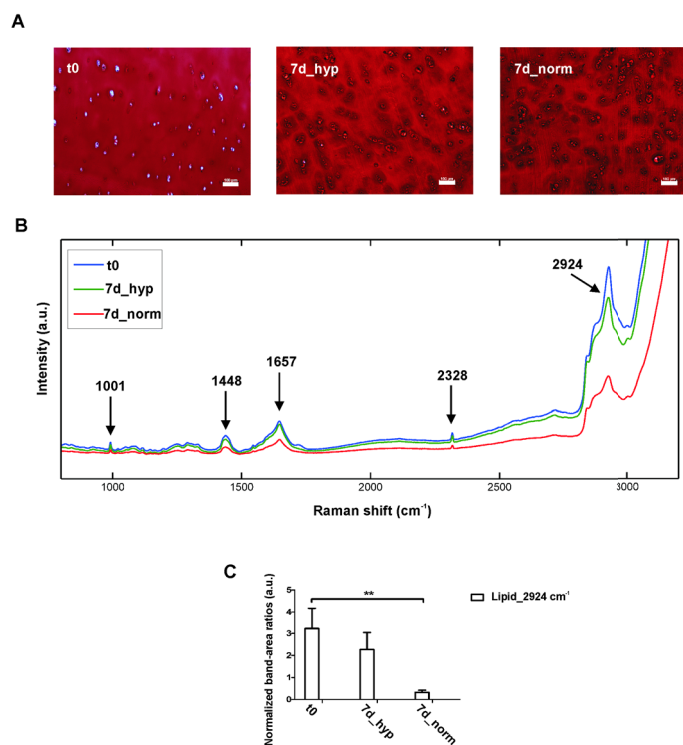


Figure 6. Histochemical and Raman analysis of chondrocytes in cartilage tissue samples. **A:** Histochemical analysis of cryosections from cartilage tissue samples which were freshly fixed (t0) or cultured for 7 days at hypoxia (7d_hyp) or at normoxia (7d_norm). Safranin-O staining showed sulfated glycosaminoglycan content while cell nuclei were counterstained using haematoxylin. Images were made with a 10x objective and scale bars equal 100 μm . **B:** Mean cell-cluster spectra acquired from cryosections of

human cartilage tissue samples which were freshly fixed (t0) or cultured for 7 days at hypoxia (7d_hyp) or at normoxia (7d_norm). **C:** We observed that band-area ratio for lipid content had not significantly changed after 7 days of culture at hypoxic conditions, but had significantly decreased at normoxic culture conditions ($p=0.006$).

Cluster images with corresponding cluster averages were obtained from each Raman-scan of each sample. We separated Raman spectra of cells from spectra of their extracellular matrix by hierarchical clustering. Cluster spectra corresponding to individual cells in each condition (t0, 7d_h, 7d_n) were averaged, creating one spectrum representative of all cells of each condition (**Fig. 6B**). Normalized band-area ratios for lipid content were calculated using these spectra. We observed that lipid content had not significantly changed after 7 days of hypoxic culture, but had significantly decreased at normoxic culture conditions (**Fig. 6C**). These results indicate that both oxygen concentration and interaction with the 3D extracellular matrix together play an important role for chondrocytes to retain their lipid droplets. The presence of lipid droplets in chondrocytes in freshly fixed cartilage tissue sections (t0) was confirmed by CARS measurements. Lipid droplets were observed in the chondrocytes in all the zones, so in the superficial (**Fig. 7A**), middle (**Fig. 7B**) and deep (**Fig. 7C**) zones of cartilage, which agrees with the findings previously described by other investigators [42]. The brightening of the droplets in the F-CARS images relative to the B-CARS images as a function of depth indicates that the droplets may be increasing in size deeper in the cartilage. This finding can be explained by the gradual decrease of oxygen tension in the middle and deep zones of cartilage compared to the superficial zone.

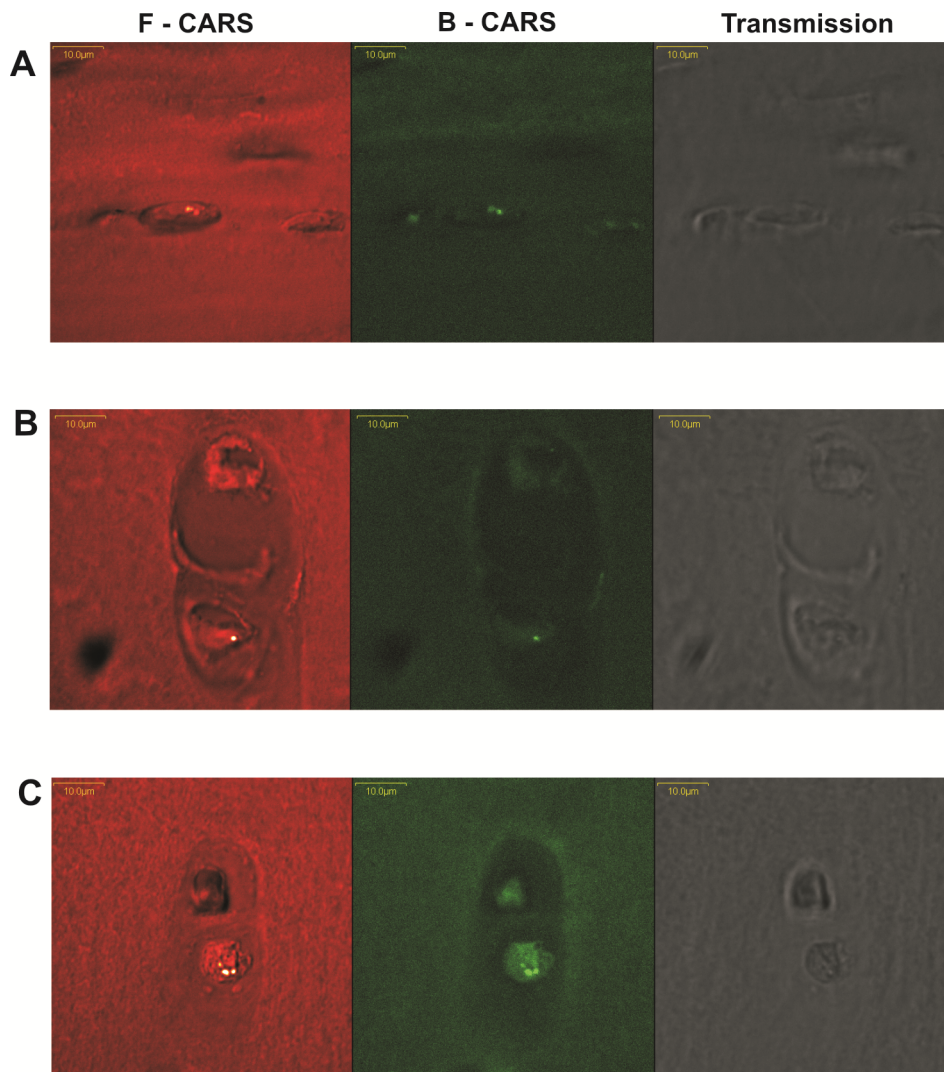


Figure 7. Forward (F – CARS) and backscattered CARS (B – CARS) and transmission images of chondrocytes in freshly fixed (t0) human cartilage tissue samples. Lipid droplets could be observed in the chondrocytes in the superficial (**A**), middle (**B**) and deep (**C**) zones of the cartilage. Images were made with a 10x objective and scale bars equal 10 μm.

CONCLUSIONS

Decrease in mRNA expression of collagen type II and gained fibroblast-like appearance with increased passage number are in line with gradual dedifferentiation of chondrocytes during culture expansion in 2D. The Raman band at 2924 cm^{-1} signifying lipids was found as a universal marker for dedifferentiation of chondrocytes. It was also shown by confocal Raman and CARS microscopy that culturing at hypoxic conditions was not sufficient for retaining lipid droplets in expanded human chondrocytes. However band-area ratios for lipid content demonstrated that chondrocytes in cartilage tissue, cultured at hypoxic conditions, retained their lipid content, unlike the ones cultured at normoxia. These results indicate that both oxygen concentration and interaction with the 3D extracellular matrix together play an important role for chondrocytes to retain their lipid droplets. Overall it can be concluded that in this study a label-free assay for assessing the quality of expanded chondrocytes has been developed.

Interestingly, several studies on articular cartilage have indicated the possible role for extensive lipid accumulation in the onset of chondrocyte degeneration [43-45]. Therefore label-free monitoring of lipid content of chondrocytes within cartilage tissue using non-resonant Raman and CARS spectroscopy can be a valuable future investigative and diagnostic tool for degenerative cartilage diseases.

ACKNOWLEDGEMENT

The authors gratefully acknowledge the support of the Dutch Program for Tissue Engineering (DPTE) through the Grant number TGT. 6737 and the support of a VICI grant to Prof. Jennifer Herek. We thank Coherent for the Paladin laser and APE Berlin for the Levante Emerald OPO.

REFERENCES

1. Martin, J.A. and J.A. Buckwalter, *The role of chondrocyte-matrix interactions in maintaining and repairing articular cartilage*. Biorheology, 2000. **37**(1-2): p. 129-40.
2. Mankin, H.J., *The response of articular cartilage to mechanical injury*. J Bone Joint Surg Am, 1982. **64**(3): p. 460-6.
3. Brighton, C.T. and Heppenst.Rb, *Oxygen Tension in Zones of Epiphyseal Plate, Metaphysis and Diaphysis - in-Vitro and in-Vivo Study in Rats and Rabbits*. Journal of Bone and Joint Surgery-American Volume, 1971. **A 53**(4): p. 719-&.
4. Otte, P., *Basic Cell-Metabolism of Articular-Cartilage - Manometric Studies*. Zeitschrift Fur Rheumatologie, 1991. **50**(5): p. 304-312.
5. Revell, C.M. and K.A. Athanasiou, *Success Rates and Immunologic Responses of Autogenic, Allogenic, and Xenogenic Treatments to Repair Articular Cartilage Defects*. Tissue Engineering Part B-Reviews, 2009. **15**(1): p. 1-15.
6. Brittberg, M., et al., *Treatment of deep cartilage defects in the knee with autologous chondrocyte transplantation*. N Engl J Med, 1994. **331**(14): p. 889-95.
7. Knutsen, G., et al., *Autologous chondrocyte implantation compared with microfracture in the knee. A randomized trial*. J Bone Joint Surg Am, 2004. **86-A**(3): p. 455-64.
8. Stewart, M.C., et al., *Phenotypic stability of articular chondrocytes in vitro: The effects of culture models, bone morphogenetic protein 2, and serum supplementation*. Journal of Bone and Mineral Research, 2000. **15**(1): p. 166-174.
9. Thirion, S. and F. Berenbaum, *Culture and phenotyping of chondrocytes in primary culture*. Methods Mol Med, 2004. **100**: p. 1-14.

10. Domm, C., et al., *Redifferentiation of dedifferentiated bovine articular chondrocytes in alginate culture under low oxygen tension*. Osteoarthritis Cartilage, 2002. **10**(1): p. 13-22.
11. Murphy, C.L. and A. Sambanis, *Effect of oxygen tension and alginate encapsulation on restoration of the differentiated phenotype of passaged chondrocytes*. Tissue Eng, 2001. **7**(6): p. 791-803.
12. Pfander, D., et al., *HIF-1alpha controls extracellular matrix synthesis by epiphyseal chondrocytes*. J Cell Sci, 2003. **116**(Pt 9): p. 1819-26.
13. Strobel, S., et al., *Anabolic and catabolic responses of human articular chondrocytes to varying oxygen percentages*. Arthritis Res Ther, 2010. **12**(2): p. R34.
14. Kazanci, M., et al., *Bone osteonal tissues by Raman spectral mapping: Orientation-composition*. Journal of Structural Biology, 2006. **156**(3): p. 489-496.
15. Notingher, I., et al., *In situ characterisation of living cells by Raman spectroscopy*. Spectroscopy-an International Journal, 2002. **16**(2): p. 43-51.
16. Puppels, G.J., et al., *Laser irradiation and Raman spectroscopy of single living cells and chromosomes: sample degradation occurs with 514.5 nm but not with 660 nm laser light*. Exp Cell Res, 1991. **195**(2): p. 361-7.
17. Puppels, G.J., et al., *Studying Single Living Cells and Chromosomes by Confocal Raman Microspectroscopy*. Nature, 1990. **347**(6290): p. 301-303.
18. Matthaus, C., et al., *Raman and infrared microspectral imaging of mitotic cells*. Applied Spectroscopy, 2006. **60**(1): p. 1-8.
19. Notingher, I., et al., *Spectroscopic study of human lung epithelial cells (A549) in culture: Living cells versus dead cells*. Biopolymers, 2003. **72**(4): p. 230-240.
20. Verrier, S., et al., *In situ monitoring of cell death using Raman microspectroscopy*. Biopolymers, 2004. **74**(1-2): p. 157-162.
21. Notingher, I., et al., *In situ non-invasive spectral discrimination between bone cell phenotypes used in tissue engineering*. J Cell Biochem, 2004. **92**(6): p. 1180-92.
22. Notingher, L., et al., *In situ spectroscopic study of nucleic acids in differentiating embryonic stem cells*. Vibrational Spectroscopy, 2004. **35**(1-2): p. 199-203.
23. Jones, J., et al., *In situ monitoring of chondrocyte response to bioactive scaffolds using Raman spectroscopy*. Key Engineering Materials, 2005. **284-286**: p. 623-626.

24. Jin, R., et al., *Injectable chitosan-based hydrogels for cartilage tissue engineering*. *Biomaterials*, 2009. **30**(13): p. 2544-51.
25. van Manen, H.J., A. Lenferink, and C. Otto, *Noninvasive imaging of protein metabolic labeling in single human cells using stable isotopes and Raman microscopy*. *Anal Chem*, 2008. **80**(24): p. 9576-82.
26. Uzunbajakava, N., et al., *Nonresonant confocal Raman imaging of DNA and protein distribution in apoptotic cells*. *Biophys J*, 2003. **84**(6): p. 3968-81.
27. van Manen, H.J., et al., *Intracellular chemical imaging of heme-containing enzymes involved in innate immunity using resonance Raman microscopy*. *Journal of Physical Chemistry B*, 2004. **108**(48): p. 18762-18771.
28. Pully, V.V., et al., *Hybrid Rayleigh-, Raman and TPE fluorescence spectral confocal microscopy of living cells*. *Journal of Raman Spectroscopy*.
29. Garbacik, E.T., et al., *Background-free nonlinear microspectroscopy with vibrational molecular interferometry*. *Phys Rev Lett*, 2011. **107**(25): p. 253902.
30. Windbergs, M., et al., *Chemical imaging of oral solid dosage forms and changes upon dissolution using coherent anti-Stokes Raman scattering microscopy*. *Anal Chem*, 2009. **81**(6): p. 2085-91.
31. Elima, K. and E. Vuorio, *Expression of mRNAs for collagens and other matrix components in dedifferentiating and redifferentiating human chondrocytes in culture*. *Febs Letters*, 1989. **258**(2): p. 195-8.
32. O Faolain, E., et al., *A study examining the effects of tissue processing on human tissue sections using vibrational spectroscopy*. *Vibrational Spectroscopy*, 2005. **38**(1-2): p. 121-127.
33. Frank, C.J., R.L. McCreery, and D.C.B. Redd, *Raman-Spectroscopy of Normal and Diseased Human Breast Tissues*. *Analytical Chemistry*, 1995. **67**(5): p. 777-783.
34. Krafft, C., et al., *Near infrared Raman spectra of human brain lipids*. *Spectrochimica Acta Part a-Molecular and Biomolecular Spectroscopy*, 2005. **61**(7): p. 1529-1535.
35. Koljenovic, S., et al., *Detection of meningioma in dura mater by Raman spectroscopy*. *Anal Chem*, 2005. **77**(24): p. 7958-65.
36. Bonner, W.M., et al., *Changes in the lipids of human articular cartilage with age*. *Arthritis Rheum*, 1975. **18**(5): p. 461-73.
37. Collins, D.H., F.N. Ghadially, and G. Meachim, *Intra-Cellular Lipids of Cartilage*. *Ann Rheum Dis*, 1965. **24**: p. 123-35.

38. Rajpurohit, R., et al., *Adaptation of chondrocytes to low oxygen tension: Relationship between hypoxia and cellular metabolism*. Journal of Cellular Physiology, 1996. **168**(2): p. 424-432.
39. Cheng, J.X., A. Volkmer, and X.S. Xie, *Theoretical and experimental characterization of coherent anti-Stokes Raman scattering microscopy*. Journal of the Optical Society of America B-Optical Physics, 2002. **19**(6): p. 1363-1375.
40. Jurna, M., et al., *Noncritical phase-matched lithium triborate optical parametric oscillator for high resolution coherent anti-Stokes Raman scattering spectroscopy and microscopy*. Applied Physics Letters, 2006. **89**(25).
41. Nan, X., J.X. Cheng, and X.S. Xie, *Vibrational imaging of lipid droplets in live fibroblast cells with coherent anti-Stokes Raman scattering microscopy*. J Lipid Res, 2003. **44**(11): p. 2202-8.
42. Stockwell, R.A., *The lipid and glycogen content of rabbit articular hyaline and non-articular hyaline cartilage*. J Anat, 1967. **102**(Pt 1): p. 87-94.
43. Bonucci, E., M. Cuicchio, and L.C. Dearden, *Investigations of Aging in Costal and Tracheal Cartilage of Rats*. Zeitschrift Fur Zellforschung Und Mikroskopische Anatomie, 1974. **147**(4): p. 505-527.
44. Carlson, C.S., et al., *The ultrastructure of osteochondrosis of the articular-epiphyseal cartilage complex in growing swine*. Calcif Tissue Int, 1986. **38**(1): p. 44-51.
45. Lippiello, L., T. Walsh, and M. Fienhold, *The Association of Lipid Abnormalities with Tissue Pathology in Human Osteoarthritic Articular-Cartilage*. Metabolism-Clinical and Experimental, 1991. **40**(6): p. 571-576.

Chapter 3

Raman Microspectroscopy – A Non-Invasive Analysis Tool for Monitoring Of Collagen- Containing Extracellular Matrix Formation in a Medium-Throughput Culture System

*Aliz Kunstar¹, Cees Otto², Marcel Karperien^{1,2},
Clemens A. van Blitterswijk¹, Aart A. van Apeldoorn^{1,2}*

¹Department of Tissue Regeneration, ²Present address: Department of Developmental Bioengineering, ³Department of Medical Cell Biophysics of MIRA – Institute for Biomedical Technology and Technical Medicine, University of Twente, Drienerlolaan 5, 7522 NB Enschede, The Netherlands

ABSTRACT: The three-dimensional (3D) environment is known to play an important role in promoting cell-matrix interactions. We have investigated the possibility of using Raman microspectroscopy – which has the great advantage of non-invasive sensing - for in vitro monitoring of extracellular matrix formation in a medium-throughput pellet (3D) culture system with soft-lithography, agarose microwell arrays.

Chondrocytes were seeded in the agarose microwells in basic (BM) or chondrocyte medium (CM). After 3, 7 and 14 days of culture period samples were analyzed for extracellular matrix formation by Raman microspectroscopy, histology and immunofluorescence.

Extracellular matrix formation in the CM cultured samples was detected by histology, immunofluorescence and also non-invasively by Raman microspectroscopy. The Raman band of collagen found at 937 cm^{-1} can be used as a Raman marker for collagen-containing extracellular matrix formation over time in the chondrocyte pellets.

This culture system can be implemented as a medium-throughput platform for Raman applications and screening microtissue formation, since with these agarose microwell arrays relatively large numbers of cell pellets could be screened in a short time 'in situ', without having to transfer the pellets onto microscopic slides. Moreover in this manner the culture system is suitable for long-term, real-time live-cell measurements.

INTRODUCTION

Many powerful techniques are available to monitor the ECM formation over time in 3D culture systems. However, all these techniques are invasive, requiring cell lysis, fixation and/or the use of molecular probes or exogenous fluorophores.

We have investigated the possibility of using Raman microspectroscopy to monitor non-invasively the production of collagen-containing extracellular matrix *in vitro*. In this study chondrocytes and a medium-throughput pellet culture system with agarose microwell arrays were used to evaluate the ECM formation.

Raman microspectroscopy allows the collection of data over a wide spectrum of nutrient, ECM and cellular components of tissue engineered samples at high spatial resolution [1]. This vibrational spectroscopic technique employs an inelastic scattering effect (the Raman effect) to generate the molecular fingerprints of specific samples and to detect specific wavelength shifts caused by the vibrations of chemical bonds. The greatest advantage of Raman microspectroscopy is its non-invasive character [2]: it does not require any staining or special sample preparation. It has been shown that no cell damage is induced if suitable laser wavelengths and powers are used [3-4]. Since the first application of Raman spectroscopy on cells [5], this technique has been widely used for biological applications. High-resolution Raman spectral studies were performed and successfully applied to study cell-cycle [6-7], cell death [8], differentiation of cells [9-10] and chondrocyte response to bioactive scaffolds [11] in a non-invasive manner. Other researchers have reported *in vivo* measurements from the bladder and prostate [12], oesophagus [13], skin [14], cervix [15-16], arteries [17] and bone [18].

In cartilage tissue engineering the monitoring of ECM products, such as collagen, glycosaminoglycans (GAG), etc are used to determine the tissue quality in tissue engineering. To obtain sufficient number of cells for tissue engineering applications chondrocytes are commonly expanded in 2D monolayer culture systems. However, this method of culturing is known to reduce the chondrocyte phenotype of primary chondrocytes with a resulting loss in their capability to form functional tissue [19-20]. The main features of cartilage are also closely related to its 3D matrix of collagen and proteoglycans that are generally lost in monolayer cultures. The 3D environment is known to play an important role in promoting cell-matrix interactions during chondrogenesis [21].

The increasing amount of ECM formation of chondrocytes in pellets over time leads to chemical and structural changes at the molecular level. In this study, a hypothesis was tested that these changes at the molecular level also change the vibrational spectra and Raman microspectroscopy can be used to detect these non-invasively. The results reported in this chapter show the feasibility of the Raman band specific for collagen found at 937 cm^{-1} to detect the increasing amount of collagen formation in chondrocyte pellets over time - already at day 3 of culture - in a non-invasive manner.

The micromolded non-adhesive hydrogel (agarose gel) with soft-lithography microwell arrays are widely used and have already been applied to study self-assembly of complex cellular aggregates [22-23]. Moreover, this pellet culture system with microwell arrays can also be applied as a medium-throughput platform for Raman applications and screening microtissue formation. The medium-throughput characteristic of the culture system means that with these agarose microwell arrays relatively large numbers of cell pellets could be screened in a short time 'in situ' without having to transfer the pellets onto microscopic slides for

Raman measurements. With other words, using these agarose microwell arrays a medium-throughput screening of the samples was possible.

MATERIALS AND METHODS

Casting of agarose microwell arrays. The agarose microwell arrays were prepared with a soft-lithography technique. Polydimethylsiloxane (PDMS) negative molds were used to routinely cast the arrays, with microwells with a diameter of 200 μm , in 3% agarose gel as described earlier [22]. Ultrapure[®] Agarose (Invitrogen, Carlsbad, CA) was dissolved by heating in sterile PBS (Gibco, Carlsbad, CA) to 3%. Seven mL of the dissolved agarose was pipetted into each wells of a 6-well tissue culture plate where the molds were previously placed (one mold/well) and centrifuged briefly to remove air bubbles. After setting at 4 °C for 30 minutes, the solidified gels with the microwell arrays were removed from the wells and separated from the mold using a spatula. A cylindrical puncher was used to cut out the microwell arrays to fit in a 12-well plate.

Isolation of bovine chondrocytes and cell culture. Primary bovine chondrocytes were isolated from articular cartilage derived from the femoral-patellar groove of a 10-month-old calf by digestion with 420 units/ml collagenase type II as previously described [24] (Worthington Biochemical, Lakewood, NJ). The freshly isolated – passage 0 (P0) - chondrocytes were subcultured in CM: Dulbecco's Modified Eagle's Medium (DMEM; Gibco, Carlsbad, CA) containing 10 v/v % fetal bovine serum (FBS; South American Origin; Biowhittaker, Lonza, Verviers, Belgium), 10 mM HEPES, penicillin G (100 units/mL; Invitrogen, Carlsbad, CA), streptomycin (100 $\mu\text{g}/\text{mL}$; Invitrogen), 0.1 mM

nonessential amino acids (Sigma, St. Louis, MO), 0.4 mM proline (Sigma, St. Louis, MO), and 0.2 mM L-ascorbic-acid-2-phosphate (Sigma, St. Louis, MO) at 37 °C under a humidified atmosphere of 5% CO₂.

After being cultured on tissue culture plastic (T-flask; Nunc; Thermo Fischer Scientific, Roskilde, Denmark), the chondrocytes (P1) were seeded on the previously prepared agarose microwell arrays in control BM or in CM and spontaneously formed a pellet at the bottom of the microwells after 12 hours. The BM contained DMEM supplemented with 10 v/v % FBS, penicillin G and streptomycin. After 3, 7 and 14 days of culture period, samples were analyzed by histology, immunofluorescence and Raman microspectroscopy.

Histology. After Raman measurements, samples were embedded in paraffin, sectioned at 5- μ m intervals, and stained with Safranin-O (Sigma, St. Louis, MO) for visualization of sulfated GAGs (sGAG). This staining was also combined with Weigert's haematoxylin (Sigma, St. Louis, MO) and Fast Green staining (Sigma, St. Louis, MO) for the nuclei and cytoplasm respectively.

Immunofluorescence. Immunofluorescent staining was performed on the deparaffinized 5- μ m sections of the samples cultured in CM for 14 days. Collagen type 2 (COL2A1) monoclonal antibody (Purified mouse immunoglobulin IgG1, clone 3HH1-F9, Abnova, 1:100, diluted in PBS/BSA 1%) as primary antibody and Alexa Fluor 488-Goat anti-Mouse IgG1 (g1) (Invitrogen, Molecular Probes, 1:1000, diluted in PBS/BSA 1%) as a secondary antibody were used. The samples were also counterstained with 4',6-diamidino-2-phenylindole (DAPI; Sigma, St.

Louis, MO). Samples were analyzed by using BD Pathway 435 Confocal bioimager (Becton Dickinson Biosciences, USA).

Confocal Raman Microscopy. Raman measurements were performed using a home-built confocal Raman spectrometer as described earlier [25]. Briefly, a Krypton ion laser (Coherent, Innova 90K, Santa Clara, CA) with an emission wavelength of 647.1 nm was used as the excitation source. A water immersion 63x/1.0 NA objective (Zeiss W-plan Apochromat, Carl Zeiss MicroImaging GmbH, Göttingen, Germany) was used to illuminate the sample as well as to collect the Raman-scattered photons in the epi-detection mode. The scattered light was filtered by a razor-edge filter (Semrock, Rochester, NY, USA) to suppress reflected laser light and Rayleigh-scattered light, and focused onto a pinhole of 15 μm diameter at the entrance of an imaging spectrograph/monochromator (HR460; Jobin-Yvon, Paris, France), which contained a blazed holographic grating with 600 grooves/mm. The spectrograph dispersed the Raman-scattered photons on an air-cooled electron-multiplying charge-coupled device (EMCCD: Newton DU-970N, Andor Technology, Belfast, Northern Ireland). The system provided a spectral resolution of 1.85 to 2.85 cm^{-1} /pixel over the wavenumber range from -20 to 3670 cm^{-1} . Raman spectra were acquired in the so-called “spectral scanning mode”. In this measurement mode, a single full spectrum was obtained by raster scanning the laser beam with a laser power of 35mW over an area of 20 μm x 20 μm in 30s. The samples were scanned by using a scanning mirror system (SM, MG325D and G120D, General Scanning, Bedford, USA). The chondrocyte pellets were directly illuminated with the laser from the top and the scattered light was also collected with the same objective. Since the pellets were not encapsulated with agarose – they were just seeded in the agarose

microwells after the microwells were casted – the agarose-material of the microwell did not interfere with the measurements.

Raman measurements were carried out both on living (non-fixed) and fixed chondrocyte pellets in situ in the microwells. First the samples were washed with PBS (Gibco) (no fixation) and Raman spectra were acquired from 3 randomly chosen chondrocyte pellets samples from each condition and time point. After the short Raman measurements on the living chondrocyte pellets, samples were fixed in 2% paraformaldehyde, washed with PBS and Raman spectra were acquired from 10 randomly chosen, fixed pellets to collect statistically significant amount of Raman data for analysis.

As a reference, the Raman spectrum of pure collagen type II from bovine nasal septum (Sigma, St. Louis, MO) was also obtained with a dry objective (Olympus Nederland B.V; Zoeterwoude, Netherlands; 40x, 0.75 NA), 10s accumulation time and 35mW laser power.

A spectrum from the substrate of the samples (agarose) was also taken - over the empty part of the agarose microwell - in the same focal plane as the focal plane in which the spectrum of a chondrocyte pellet was acquired.

Toluene, a Raman calibration standard - with accurately known peak frequencies (521, 785, 1004, 1624, 2921 and 3054 cm^{-1}) - was used for wavenumber calibration of the spectra.

Raman data analysis. The preprocessing of the data was performed as described previously [26-28]. The spectra were preprocessed by: (1) removing cosmic ray events; (2) subtracting the camera offset noise (dark current); and (3) calibrating the wave number axis. The well known band-positions were used to relate wavenumbers to pixels. The frequency-dependent optical detection efficiency of the setup was

corrected using a tungsten halogen light source (Avalight-HAL; Avantes BV, Eerbeek, The Netherlands) with a known emission spectrum. The detector-induced etaloning effect was compensated by this procedure. After data correction, the 10 spectra from the pellets from each medium (BM or CM) on respective measurement days were averaged. Semi-quantitative univariate data analysis was performed by selecting specific vibrational bands of collagen in the averaged spectra from each medium condition and time point, and integrating each band after local baseline subtraction. Subsequently, band-area ratios were obtained from the collagen band over the integrated band of the nitrogen stretch-mode at 2328 cm^{-1} as an intensity standard. The calculations were made using normalized band-area ratios, not absolute values, so the system is rather semi-quantitative than quantitative monitoring of the collagen formation. Since we monitored the extracellular matrix formation in time using the same culture conditions, evaluating absolute values would not change the outcome of this paper.

All data manipulations were performed using routines written in MATLAB 7.4 (The Math Works Inc., Natick, MA).

Statistical analysis. The results are presented as mean \pm standard deviation (SD). Experimental data were analyzed for statistical significance using a student t-test. Statistical significance was set to p-value < 0.05 (*).

RESULTS

Histology. Bright-field micrographs of the chondrocyte pellets in the agarose microwells (**Fig. 1A**) and measurements of pellet dimensions (**Fig. 2**) showed that the pellets incubated in CM grew extensively in size

over time. Moreover, the Safranin-O staining of the samples demonstrated abundant sGAG production over time in CM (**Fig. 1B**). It should be noted that larger amounts of sGAGs were formed between day 7 and day 14 of culture than between day 3 and day 7 of culture. In contrast, the pellets cultured in BM did not grow in size and showed only a small amount of sGAG formation (**Fig. 1C, 1D and 2**).

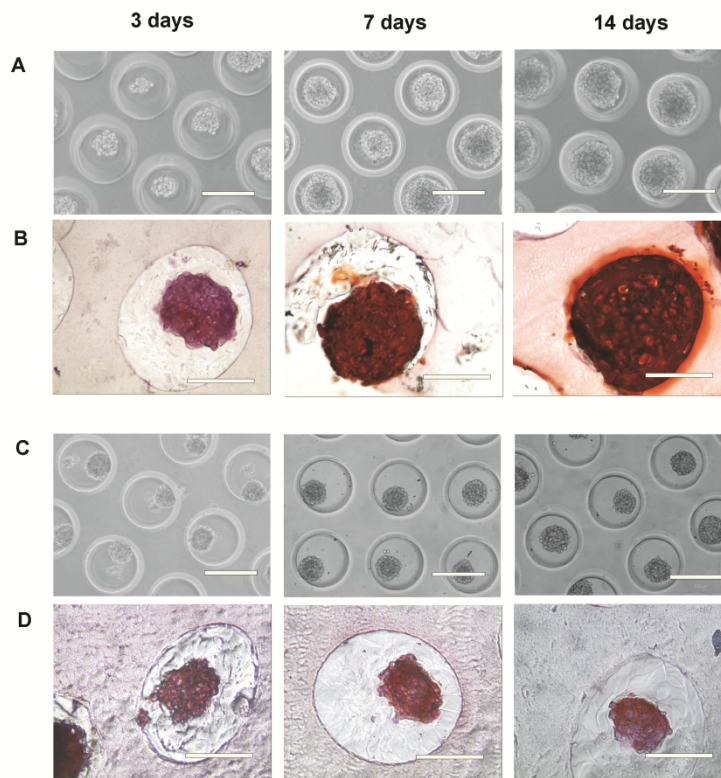


Figure 1: A, B: Chondrocyte pellets cultured in CM. **A:** Bright-field micrographs (20X) and **B:** histological images of Safranin O staining (sGAG production, 40X) of the chondrocyte pellets showing the influence of CM after 3 days, 7 days and 14 days of culture. **C, D:** Chondrocyte pellets cultured in BM. **C:** Bright-field micrographs (20X) and **D:** histological images of Safranin O staining (sGAG production, 40X) of the chondrocyte pellets cultured in BM after 3 days, 7 days and 14 days of culture. Safranin-O staining of

the samples demonstrated abundant sGAG production over time in CM. A, C: Scale bars equal 200 μm . B, D: Scale bars equal 100 μm .

Immunofluorescence. The chondrocyte pellets cultured for 14 days in CM were labeled with DAPI and collagen type 2 antibodies. Samples from day 14 showed strong fluorescence with both DAPI (**Fig. 3A and 3B** - blue fluorescence) and collagen type 2 antibody (**Fig. 3A and 3B** - green fluorescence).

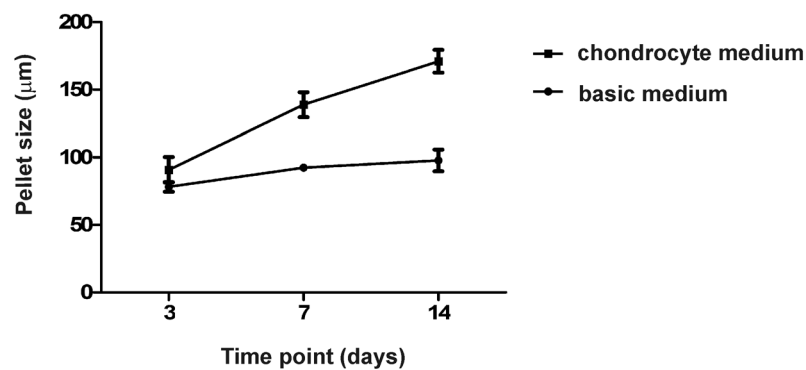


Figure 2: Size of the chondrocyte pellets cultured in CM or BM for 3 days, 7 days and 14 days of culture. The samples cultured in CM grew extensively in size over time.

Confocal Raman microscopy and Raman data analysis. Average Raman spectra ($n=10$) of fixed chondrocyte pellets cultured in BM or CM were acquired by confocal Raman microspectroscopy after 3, 7 and 14 days of culture period (**Fig. 4 a-f**). All spectra showed well-known bands corresponding to phenylalanine [29], lipids/proteins [30] and

amide-I [31] respectively (**Table 1** - see band assignments and wavelengths). A notable difference between these spectra at 937 cm^{-1} had also occurred. This band at 937 cm^{-1} is specific for collagen (proline/hydroxyproline/C-C skeletal of the collagen backbone) [32].

As a reference, the Raman spectrum of collagen type II – the major type of collagen in cartilage - from bovine nasal septum was also obtained shown in **Figure 4 g**. This reference spectrum showed the band at 937 cm^{-1} similar to the spectra of the chondrocyte pellets as shown in **Figure 4 a-f**.

ASSIGNMENT	WAVELENGTH in cm^{-1} (ref.)
Collagen	937 (32)
Phenyl-alanine	1002 (29)
Lipids/Proteins	1442 (30)
Amide I	1630-1680 (31)
Nitrogen	2328 (33)

Table 1. Assignments and wavelength for Raman peaks.

The results of the semi-quantitative univariate data analysis are shown in **Figure 5** with the normalized band-area ratios for the band signifying collagen at 937 cm^{-1} . The results shown in **Figure 5** based on the average spectra of chondrocyte pellets cultured in BM or CM after 3, 7 and 14 days of culture period. The normalized band-area ratio for collagen content significantly increased during the 14-day culture in CM. The collagen band could already be detected after 3 days of culturing and the contribution of collagen to the Raman spectra further increased from day 3 to day 7 and from day 7 to day 14 of the culture.

Raman microspectroscopy is a very sensitive technique and can easily be hindered by background scattering of the measured samples. Therefore a Raman spectrum from the agarose-substrate of a chondrocyte pellet (**Fig. 6B [b]**) was also obtained and did not show any interfering bands at 937 cm^{-1} (**Fig. 6B [a]**).

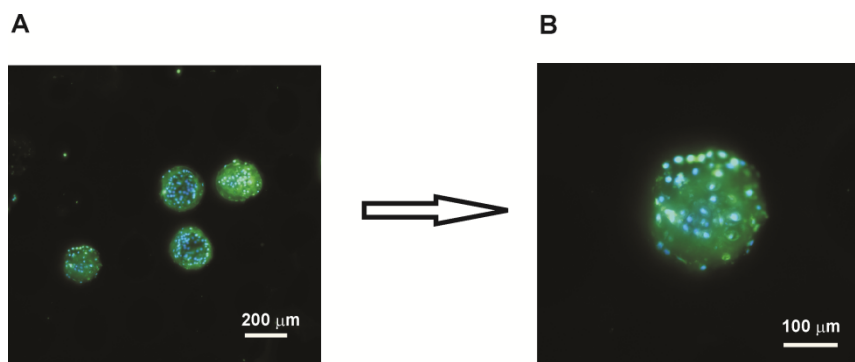


Figure 3: Immunofluorescent staining of chondrocyte pellets. **A, B:** Images of chondrocyte pellets cultured for 14 days in CM and labeled with collagen type 2 antibody (green fluorescence) and DAPI (blue fluorescence). **A:** Montage image of chondrocyte pellets.

In addition Raman measurements were carried out both on living and fixed samples - cultured under the influence of CM for 14 days – in situ in the microwells to verify that the fixation process did not alter the Raman spectra of the samples. In the average Raman spectrum of the fixed chondrocyte pellets ($n=10$, **Fig. 7b**) no major changes could be observed compared to the average spectrum of the living chondrocytes ($n=3$, **Fig. 7a**).

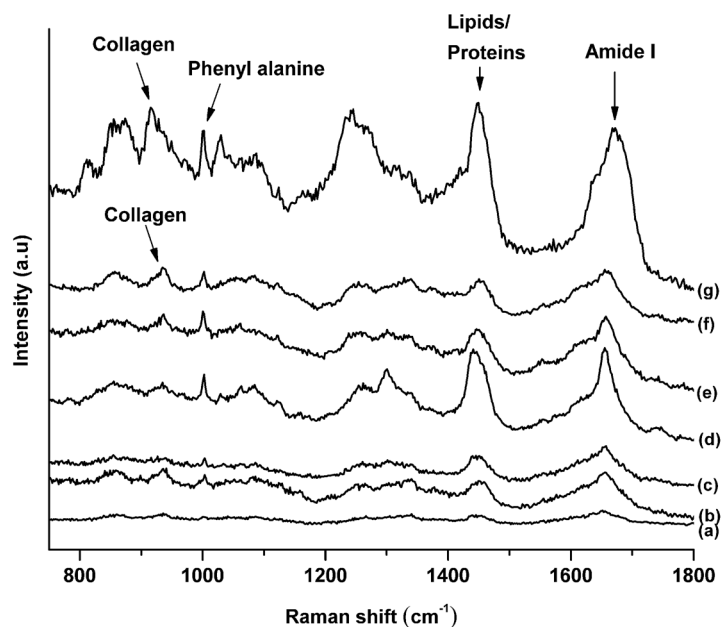


Figure 4: (a-f): Average Raman spectra of fixed chondrocyte pellets in the range of 500 – 1800 cm^{-1} . Each spectrum corresponds to average of 10 randomly chosen chondrocyte pellets cultured under the influence of BM or CM for 3 days, 7 days and 14 days. The spectra were vertically displaced for clarity: (a) 3 days BM, (b) 7 days BM, (c) 14 days BM, (d) 3 days CM, (e) 7 days CM, (f) 14 days CM. (g): Raman spectrum of collagen type II from bovine nasal septum. Increasing band area of collagen at 937 cm^{-1} over time in the samples cultured in CM can be observed (d, e, f).

DISCUSSION

The aim of this study was to find specific Raman markers for the observation of chondrocyte response in pellet culture system by obtaining Raman signal from the ECM deposited by the chondrocytes. The results reported here showed the feasibility of Raman spectroscopy to detect collagen formation of chondrocyte pellets - already at day 3 of culture - in a non-invasive manner. The method described in our study is fundamentally different from the more conventional way of culturing, where pellets are formed in 10 ml-centrifuge tubes, or in the wells of a 96-well (round-bottomed) tissue culture plate and the pellets need to be transferred onto microscope slides for Raman measurements. Moreover the cell pellets from any interested cell type can be constrained in a 'fixed' position at the bottom of each microwell allowing for confocal measurements.

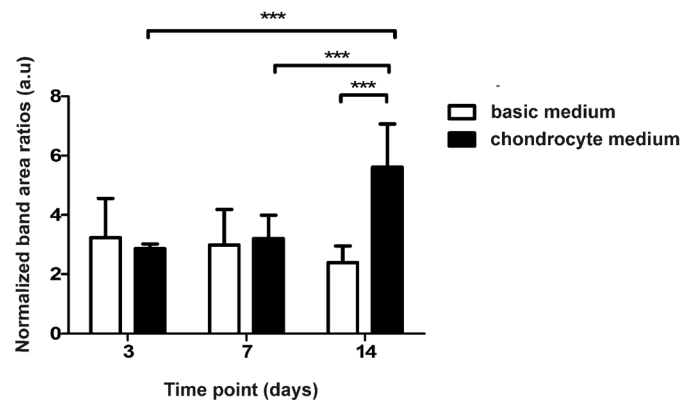


Figure 5: Semi-quantitative univariate data analysis shows normalized integrated band area ratios of the collagen band for the spectra shown in Figure 5 (a-f) of the chondrocyte pellets cultured in BM (white bars) or CM (black bar) for 3 days, 7 days and 14 days (bar=standard deviation; 3 day CM vs. 14 day CM: $p=0.0031$, 7 day CM versus 14 day CM: $p=0.0118$, 14d BM versus 14d CM: $p=0.0017$). The normalized band area

ratio acquired from the ratio of the collagen band to the band of nitrogen. All bands are integrated after baseline subtraction. The normalized band area ratio for collagen content had been significantly increased during the 14-day culture period in CM.

Bright-field micrographs of the chondrocyte pellets in the agarose microwells (**Fig. 1A**) and measurements of the pellet dimensions (**Fig. 2**) showed that pellets incubated in CM had grown extensively in size over time. Moreover, the Safranin-O staining of the samples demonstrated an abundant sGAG production already at 7 days of culture in CM (**Fig. 1B**). In contrast, the pellets cultured in BM did not grow in size and showed only minor amounts of GAG formation (**Fig. 1C, 1D and 2**) most likely due to the fact that the BM did not contain any inductive factors, which could otherwise support extracellular matrix formation.

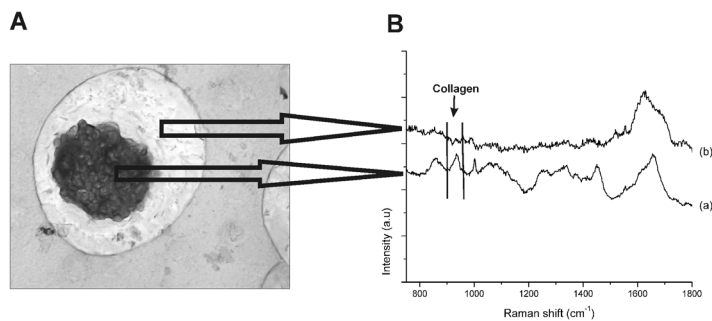


Figure 6: **A:** White light micrograph of a chondrocyte pellet residing in the agarose microwell (20X). **B (a):** Raman spectrum of a chondrocyte pellet in the agarose microwell and **(b):** Raman spectrum of the agarose microwell (agarose-substrate) which was taken over the empty part of the microwell in the same focal plane as the spectrum of the chondrocyte pellet was acquired (background spectrum of the chondrocyte pellet). Raman spectra from the agarose-substrate of chondrocyte pellets did not show any interfering bands at 937 cm⁻¹.

Collagen type II protein expression was also observed in the chondrocyte pellets - cultured for 14 days in CM – (**Fig. 3A and 3B**) by immunofluorescence. Although the initial aim of this study was not to identify the production of collagen specifically, but to evaluate the production of extracellular matrix components. However we were able to show the change of collagen production during culture in the medium-throughput pellet culture system used in this study by Raman spectroscopy and immunofluorescence, and sGAG production by histology. The average spectra of the fixed (**Fig. 4 a-f**) samples from each medium and time point showed well-known bands corresponding to phenylalanine, lipids/proteins and amide-I respectively and the bands for collagen at 937 cm^{-1} (**Table 1** – band assignments).

To compare the intensities in the Raman spectra from different pellets on different days, we used the N_2 -stretch mode at 2328 cm^{-1} as an intensity standard for normalization [33]. The Raman signal from N_2 originates from N_2 in the ambient air in the optical beam path, therefore it was a constant factor always presented in our measurements.

The normalized band-area ratios for collagen content significantly increased during the 14-day culture in CM (**Fig. 5**). Immunofluorescence confirmed the data obtained by Raman spectroscopy indicating a specific collagen matrix deposition (**Fig. 3**). Moreover, the collagen band could already be detected after 3 days of culture and the contribution of collagen to the Raman spectra further increased from day 3 to day 7 and from day 7 to day 14 of the culture. The significant increase between day 7 and day 14 culture can be explained by the fact that the chondrocytes started to produce more collagen matrix after 7 days of culture. **Figure 1B** also shows that larger amounts of sGAGs were formed between day 7 and day 14 of culture than between day 3 and day 7 of culture.

Proline is known to be an essential amino acid in the production of collagen. Together with hydroxyproline and glycine, proline is the major constituent of the functional collagen molecule, also in collagen type II. Ascorbic acid can influence the collagen production of chondrocytes by modulating steady-state procollagen mRNA levels [34], as well as through posttranslational processing of procollagen [35]. The increasing amount of collagen could be the effect of proline and ascorbic acid added to the medium, since specific differentiation growth factors, such as TGF β -3 was not used in this study. This was also what confirmed by the fact that the pellets cultured in BM for 14 days showed a significantly lower amount of collagen compared to the collagen content in samples cultured in CM for 14 days (**Fig. 5**). The collagen deposition in the pellets cultured in the BM can possibly explained by the fact that direct cell-cell contact in the 3D pellet culture system was sufficient to induce matrix production in the cells without the addition of extra inductive factors.

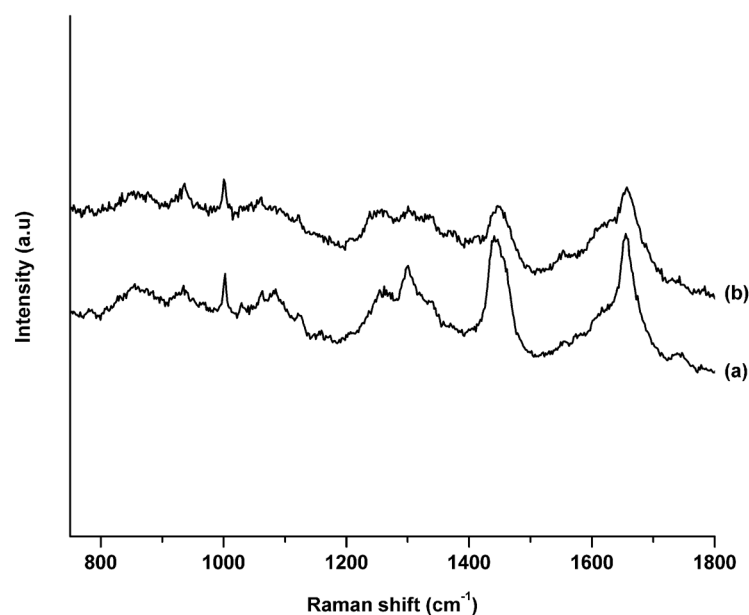


Figure 7: Living versus fixed chondrocyte pellets. **(a):** Average Raman spectrum of a living chondrocyte pellets (n=3) and **(b)** average Raman spectrum of fixed chondrocyte pellets (n=10) cultured under the influence of CM for 14 days. In the average Raman spectrum of the fixed chondrocyte pellets no major changes could be observed compared to the average spectrum of the living chondrocytes.

Raman microspectroscopy is a very sensitive technique and can easily be hindered by background scattering of the measured samples. Therefore a Raman spectrum from the agarose-substrate of a chondrocyte pellet (**Fig. 6B [b]**) was also obtained and it did not show any interfering bands at 937 cm⁻¹ (**Fig. 6B [a]**).

In addition the average Raman spectrum of fixed chondrocyte pellets (n=10, **Figure 7b**) showed no major changes compared to the average spectrum of the non-fixed samples (n=3, **Figure 7a**), indicating that the use of fixative – in this case 2% paraformaldehyde - had no major

influence on the obtained Raman spectra. Therefore the univariate data analysis and the statistical calculations could be safely made from the Raman data of the fixed pellets without interfering with the outcome of this study.

CONCLUSIONS

This study has demonstrated the feasibility of Raman spectroscopy to detect collagen-containing extracellular matrix formation in pellet culture systems in a non-invasive manner for future tissue engineering purposes. In this study chondrocytes and a pellet (3D) culture system with agarose microwell arrays were used to evaluate the extracellular matrix formation.

This agarose microwell system can be implemented as a medium-throughput platform for Raman applications and screening microtissue formation, since relatively large numbers of cell pellets could be screened in a short time 'in situ', without having to transfer the pellets onto microscopic slides. Moreover in this manner described here this culture system is also suitable for long-term, real-time live-cell measurements and 3D tissue formation.

In addition, Raman microspectroscopy provides a label-free and non-invasive tool for studying a wide spectrum of nutrient, extracellular matrix and cellular components in tissue-engineered samples.

The future goal is to monitor the extracellular matrix formation – preferably in real time - in large and implantable cartilage constructs. In these future studies Raman microspectroscopy can possibly used as a quality control tool and to evaluate proper cartilaginous matrix formation in tissue engineered constructs.

ACKNOWLEDGEMENT

The authors gratefully acknowledge the support of the Dutch Program for Tissue Engineering (DPTE) through the Grant number TGT. 6737

REFERENCES

1. Kazanci, M., et al., *Bone osteonal tissues by Raman spectral mapping: Orientation-composition*. Journal of Structural Biology, 2006. **156**(3): p. 489-496.
2. Krafft, C., et al., *Mapping of single cells by near infrared Raman microspectroscopy*. Vib Spectrosc, 2003. **32**: p. 75-83.
3. Notingher, I., et al., *In situ characterisation of living cells by Raman spectroscopy*. Spectroscopy-an International Journal, 2002. **16**(2): p. 43-51.
4. Puppels, G.J., et al., *Laser irradiation and Raman spectroscopy of single living cells and chromosomes: sample degradation occurs with 514.5 nm but not with 660 nm laser light*. Exp Cell Res, 1991. **195**(2): p. 361-7.
5. Puppels, G.J., et al., *Studying Single Living Cells and Chromosomes by Confocal Raman Microspectroscopy*. Nature, 1990. **347**(6290): p. 301-303.
6. Matthaus, C., et al., *Raman and infrared microspectral imaging of mitotic cells*. Applied Spectroscopy, 2006. **60**(1): p. 1-8.
7. Notingher, I., et al., *Spectroscopic study of human lung epithelial cells (A549) in culture: Living cells versus dead cells*. Biopolymers, 2003. **72**(4): p. 230-240.

8. Verrier, S., et al., *In situ monitoring of cell death using Raman microspectroscopy*. Biopolymers, 2004. **74**(1-2): p. 157-162.
9. Notingher, I., et al., *In situ spectral monitoring of mRNA translation in embryonic stem cells during differentiation in vitro*. Analytical Chemistry, 2004. **76**(11): p. 3185-3193.
10. Notingher, L., et al., *In situ spectroscopic study of nucleic acids in differentiating embryonic stem cells*. Vibrational Spectroscopy, 2004. **35**(1-2): p. 199-203.
11. Jones, J., et al., *In situ monitoring of chondrocyte response to bioactive scaffolds using Raman spectroscopy*. Key Engineering Materials, 2005. **284-286**: p. 623-626.
12. Crow, P., et al., *Fibre-optic raman spectrsocopy: The prospects for in vivo diagnosis of bladder and prostate cancer*. Journal of Urology, 2004. **171**(4): p. 68-68.
13. Shim, M.G., et al., *In vivo near-infrared Raman spectroscopy: Demonstration of feasibility during clinical gastrointestinal endoscopy*. Photochemistry and Photobiology, 2000. **72**(1): p. 146-150.
14. Hata, T.R., et al., *Non-invasive Raman spectroscopic detection of carotenoids in human skin*. Journal of Investigative Dermatology, 2000. **115**(3): p. 441-448.
15. Mahadevan-Jansen, A., et al., *Development of a fiber optic probe to measure NIR Raman spectra of cervical tissue in vivo*. Photochemistry and Photobiology, 1998. **68**(3): p. 427-431.
16. Utzinger, U., et al., *Near-infrared Raman spectroscopy for in vivo detection of cervical precancers*. Applied Spectroscopy, 2001. **55**(8): p. 955-959.

17. Buschman, H.P., et al., *In vivo determination of the molecular composition of artery wall by intravascular Raman spectroscopy*. Analytical Chemistry, 2000. **72**(16): p. 3771-3775.
18. Matousek, P., et al., *Noninvasive Raman spectroscopy of human tissue in vivo*. Appl Spectrosc, 2006. **60**(7): p. 758-63.
19. Stewart, M.C., et al., *Phenotypic stability of articular chondrocytes in vitro: The effects of culture models, bone morphogenetic protein 2, and serum supplementation*. Journal of Bone and Mineral Research, 2000. **15**(1): p. 166-174.
20. Thirion, S. and F. Berenbaum, *Culture and phenotyping of chondrocytes in primary culture*. Methods Mol Med, 2004. **100**: p. 1-14.
21. Zhang, Z.J., et al., *Hyaline cartilage engineered by chondrocytes in pellet culture: histological, immunohistochemical and ultrastructural analysis in comparison with cartilage explants*. Journal of Anatomy, 2004. **205**(3): p. 229-237.
22. Napolitano, A.P., et al., *Dynamics of the self-assembly of complex cellular aggregates on micromolded nonadhesive hydrogels*. Tissue Engineering, 2007. **13**(8): p. 2087-2094.
23. Rivron, N.C., et al., *Tissue assembly and organization: developmental mechanisms in microfabricated tissues*. Biomaterials, 2009. **30**(28): p. 4851-8.
24. Jin, R., et al., *Injectable chitosan-based hydrogels for cartilage tissue engineering*. Biomaterials, 2009. **30**(13): p. 2544-51.
25. van Manen, H.J., A. Lenferink, and C. Otto, *Noninvasive imaging of protein metabolic labeling in single human cells using stable isotopes and Raman microscopy*. Anal Chem, 2008. **80**(24): p. 9576-82.

26. Uzunbajakava, N., et al., *Nonresonant confocal Raman imaging of DNA and protein distribution in apoptotic cells*. Biophys J, 2003. **84**(6): p. 3968-81.
27. van Manen, H.J., et al., *Intracellular chemical imaging of heme-containing enzymes involved in innate immunity using resonance Raman microscopy*. Journal of Physical Chemistry B, 2004. **108**(48): p. 18762-18771.
28. Pully, V.V., et al., *Hybrid Rayleigh-, Raman and TPE fluorescence spectral confocal microscopy of living cells*. Journal of Raman Spectroscopy.
29. Malini, R., et al., *Discrimination of normal, inflammatory, premalignant, and malignant oral tissue: A Raman spectroscopy study*. Biopolymers, 2006. **81**(3): p. 179-193.
30. Stone, N., et al., *Raman spectroscopy for identification of epithelial cancers*. Faraday Discussions, 2004. **126**: p. 141-157.
31. Krafft, C., et al., *Near infrared Raman spectra of human brain lipids*. Spectrochimica Acta Part a-Molecular and Biomolecular Spectroscopy, 2005. **61**(7): p. 1529-1535.
32. Cheng, W.T., et al., *Micro-Raman spectroscopy used to identify and grade human skin pilomatrixoma*. Microscopy Research and Technique, 2005. **68**(2): p. 75-79.
33. Pully, V.V., *From cells to bone: Raman microspectroscopy of the mineralization of stromal cells [PhD thesis]* in *Department of Medical Cell Biophysics*. 2010, University of Twente: Enschede.
34. Sandell, L.J., et al., *Effects of ascorbic acid and aging on collagen mRNA levels in articular chondrocytes*. Journal of Cell Biol, 1985. **101**: p. 94a.

35. Pinnel, S.R., S. Murad, and D. Darr, *Induction of collagen synthesis by ascorbic acid. A possible mechanism.* Arch Dermatol, 1987. **123**(12): p. 1684-6.

Chapter 3

Chapter 4

Chapter 4

Label-free Raman Monitoring of Extracellular Matrix Formation in 3D PEOT/PBT Scaffolds

*Aliz Kunstar^{1,+}, Anne Leferink^{1,+}, Paul I. Okagbare⁴,
Michael D. Morris⁴, Blake J. Roessler⁵, Cees Otto³,
Marcel Karperien^{1,2}, Clemens A. van Blitterswijk¹, Lorenzo Moroni¹,
Aart A. van Apeldoorn^{1,2}*

¹Department of Tissue Regeneration, ²Present address: Department of Developmental Bioengineering, ³Department of Medical Cell Biophysics of MIRA – Institute for Biomedical Technology and Technical Medicine, University of Twente, Drienerlolaan 5, 7522 NB Enschede, The Netherlands

⁴Department of Chemistry, University of Michigan, 930 N. University Avenue, Ann Arbor, MI 48108, USA

⁵Department of Internal Medicine, Division of Rheumatology, University of Michigan Medical School, Medical Science Research Building II, 1150 West Medical Center Drive, Room 3560, Ann Arbor, MI 48109-5688, USA

⁺These authors contributed equally to the research work.

ABSTRACT: Monitoring the production levels of extracellular matrix (ECM) components is one of the key methods used to determine tissue quality in three-dimensional (3D) scaffolds for regenerative medicine and clinical purposes. Raman spectroscopy can be used for non-invasive sensing of cellular activities. We have investigated the use of conventional and fiber optic Raman microspectroscopy for *in vitro* monitoring of ECM formation in 3D poly(ethylene oxide terephthalate)–poly(butylene terephthalate) (PEOT/PBT) scaffolds.

Chondrocyte-seeded PEOT/PBT scaffolds were analyzed for ECM formation by Raman microspectroscopy, biochemical analysis, histology and scanning electron microscopy (SEM).

ECM deposition by the chondrocytes in the scaffolds was successfully detected by conventional destructive analysis and by label-free Raman microspectroscopy. In the spectra collected by the conventional Raman setups the Raman bands at 937 cm^{-1} and at 1062 cm^{-1} which correspond to collagen and sulfated glycosaminoglycans (sGAGs) respectively could be used as Raman markers for ECM formation in the scaffolds. Collagen synthesis found to be different in single chondrocyte-seeded scaffolds when compared to microaggregate-seeded samples. While normalized band-area ratios for collagen content of single cell-seeded samples had gradually been decreasing during the 21 day culture period, collagen content of the microaggregate-seeded samples had significantly been increasing. We think that seeding microaggregates, instead of single chondrocytes, onto scaffolds is perhaps a better approach for cartilage tissue engineering.

Although the spectra of the samples obtained by the fiber optic Raman system suffered from silica background, which originated from the optical fibers, it allowed the collection of Raman spectra from multiple

pores in the scaffold with one single measurement time point, which generated a more representative average of the Raman signal from the ECM.

Our results provide proof-of-principle that Raman microspectroscopy is a promising non-invasive and rapid tool to monitor ECM deposition and rebuilding. Further investigation is needed to validate the potential of the technique, so that evaluation of cartilaginous matrix formation in tissue engineered constructs will be possible. Discrimination of specific collagen type would be the main focus of future studies.

INTRODUCTION

Articular cartilage is a highly specialized connective tissue with the function to provide smooth and low-friction interaction between the bones of a joint and to distribute the load over the surface of joints during movement. In several pathological conditions, such as osteoarthritis and rheumatoid arthritis or trauma, cartilage shows limited capacity for regeneration due to poor cellularity and its avascular character [1-2]. The main features of cartilage are also closely related to its 3D matrix, which mainly consists of collagen type II, proteoglycans and water [3-4]. Therefore monitoring the production levels of these essential ECM components is one of the key methods used to determine tissue quality in tissue engineered constructs. Conventional quality testing methods, such as immunohistochemistry, histology and microscopy techniques are all destructive and require cell fixation, labeling, staining or cell lysis. In contrast Raman microspectroscopy is a label-free technique, which does not require special sample preparation steps and can be used for non-invasive characterization of cellular

activities [5]. Although, lasers are used as excitation sources in Raman spectroscopy, it has been demonstrated that a careful selection of suitable laser wavelength and laser intensity eliminates the possibility of cell damage [6-7]. This vibrational spectroscopic technique employs an inelastic scattering effect (the Raman effect) to generate the molecular fingerprints of the investigated samples and to detect specific wavelength shifts caused by the vibrations of chemical bonds.

Raman spectral studies have already been performed on structural analysis of collagen [8-9], sGAGs and proteoglycans [10-11]. Furthermore this technique has been successfully applied to study collagen containing ECM formation in a medium-throughput culture system [12] and to monitor chondrocyte response to bioactive scaffolds [13]. Fiber optic Raman systems have already been used for monitoring joint tissues *in vivo* [14] and assessing progress of bone graft incorporation in bone reconstruction and repair transcutaneously [15]. Other researchers have reported *in vivo* measurements from the bladder and prostate [16], oesophagus [17], skin [18], cervix [19-20], and arteries [21].

In this study, we have investigated the applicability of label-free Raman microspectroscopy to detect ECM formation and monitor the production level of essential ECM components over time in 3D PEOT/PBT scaffolds using conventional and fiber optic Raman setups. PEOT/PBT copolymers have been extensively studied and proved to be biocompatible both *in vitro* and *in vivo* [22-25] and have reached clinical applications (PolyActive™, IsoTis Orthopaedics S.A.) as dermal substitutes [26] and bone fillers [27-28].

MATERIALS AND METHODS

Casting of agarose microwell arrays. The agarose microwell arrays were prepared with a soft-lithography technique. Polydimethylsiloxane (PDMS) negative molds were used to routinely cast the arrays, with microwells with a diameter of 200 μm , in 3% agarose gel as described earlier [29]. Ultrapure[®] Agarose (Invitrogen, Carlsbad, CA) was dissolved by heating in sterile phosphate-buffered saline (PBS) solution (Gibco, Carlsbad, CA) to 3%. Seven mL of the dissolved agarose was pipetted into each wells of a 6-well tissue culture plate where the molds were previously placed (one mold/well) and centrifuged briefly to remove air bubbles. After setting in 4 °C for 30 minutes, the solidified gels with the microwell arrays were removed from the wells and separated from the mold using a spatula. A cylindrical puncher was used to cut out the microwell arrays to fit in a 12-well plate.

Fabrication of PEOT/PBT scaffolds. 300PEOT55PBT45 (PolyActive™300/55/45, PolyVation, The Netherlands) is a block copolymer with a weight ratio of 55 to 45 for the two components (PEOT and PBT) respectively, and a molecular weight of the starting poly(ethylene glycol) (PEG) segments of 300Da used in the copolymerization process. 3D regular grids were fabricated by fused deposition modeling with a bioscaffolder (SysENG, Germany) with a fiber to fiber distance of 800 μm , a fiber diameter of approximately 200 μm and a layer thickness of 150 μm . Cylindrical porous scaffolds (6 mm in diameter by 4 mm in height for control studies and 4 mm in diameter by 3 mm in height for the main experiments) were punched out of the 3D regular grids. These scaffolds were sterilized in 70% ethanol 2 times for 30 minutes each, washed in PBS first for 5 minutes and additionally for

other 30 minutes two times, and finally incubated in culture medium overnight prior to cell culture.

Isolation of bovine chondrocytes and cell culture. Primary bovine chondrocytes were isolated from articular cartilage derived from the femoral-patellar groove of a 10-month-old calf by digestion with 420 Units/ml collagenase type II (Worthington Biochemical, Lakewood, NJ). The freshly isolated - passage 0 (P0) - chondrocytes were subcultured in chondrocyte medium (CM) consisting of Dulbecco's modified eagle medium (DMEM, Gibco, Carlsbad, CA) containing 10 v/v % fetal bovine serum (FBS, South American Origin; Biowhittaker, Lonza, Verviers, Belgium), 100 Units/mL penicillin G (Invitrogen, Carlsbad, CA), 100 µg/mL streptomycin (Invitrogen), 0.1 mM nonessential amino acids (Sigma, St. Louis, MO), 0.4 mM proline (Sigma, St. Louis, MO), and 0.2 mM L-ascorbic-acid-2-phosphate (Sigma, St. Louis, MO) at 37 °C under a humidified atmosphere of 5% CO₂.

After being cultured on tissue culture plastic (T-flask; Nunc; Thermo Fischer Scientific, Roskilde, Denmark), in the control studies chondrocytes (P1) were seeded on PA scaffolds in CM. In the single cells versus aggregates studies one part of the chondrocytes (P1) were seeded on PA scaffolds, the rest of the chondrocytes (P1) were seeded on the previously prepared agarose microwell arrays in CM (2865 microwells and 1 x 10⁶ cells / agarose microwell array) and spontaneously formed microaggregates (~350 cells / microaggregate) at the bottom of the microwells after 12 hours. After 1 day of culture, the chondrocyte microaggregates were flushed out with CM from the agarose microwell arrays, collected and seeded on PA scaffolds.

Cell seeding of PEOT/PBT scaffolds. Each scaffold was placed with a sterile tweezer into a well of a non-treated 24-well (in the control studies)

or 48-well-plate (in the single cells versus aggregates studies) (both Nunc, Thermo Fisher Scientific, Roskilde, Denmark).

Control studies

In the control studies 300 µg/ml of human fibronectin (BD Biosciences) was applied to the chondrocyte suspension before seeding, which is known to support cell adhesion [30]. The cell-fibronectin suspension – 3 x 10⁶ cells in a final volume of 50 µl for each scaffold – was pipetted onto the scaffolds and drawn into the scaffold by capillary forces. Samples were left in an incubator at 37 °C under a humidified atmosphere of 5% CO₂ for 45 minutes. Subsequently 2 ml of culture medium was provided carefully for the samples adding drop by drop the medium into the wells and holding the tip of the pipette onto the walls of the microwells, and the samples were placed back into the incubator. After 7 days and 21 days of culture the samples were analyzed by Raman microspectroscopy and histology (data are not shown).

Chondrocytes of C-28/I2 human immortalized chondrocyte cell line were also seeded on PEOT/PBT scaffolds. These cells were used as negative control for matrix formation, since they mainly proliferate and show a low expression of genes involved in matrix synthesis and turnover as it was described before [31]. These samples were cultured in CM under a humidified atmosphere of 5% CO₂ at 37 °C and analyzed by Raman microspectroscopy after 21 days of culture period.

Main studies: Single cells versus Microaggregates

In the main studies the diameter and thickness of the PEOT/PBT scaffolds were decreased, so that less number of cells was needed to be seeded onto the scaffolds. Before transferring the scaffolds into the wells of the 48-well multidish, a layer of 3% agarose gel was deposited onto

the bottom of the wells. A hole - with a diameter which was 1 mm more than the diameter of the scaffold – was punched out from the middle of the gel in each well and the scaffolds were placed into these holes (one scaffold per well/hole). These holes served as barriers and to prevent the cell suspension from flowing out from the scaffold, therefore to provide more efficient cell-seeding. The single chondrocyte or microaggregate suspension (both without fibronectin) – 500.000 cells or 500.000 cells in microaggregate format in a final volume of 30 μ l for each scaffold – were seeded onto the scaffolds. Samples were left undisturbed for 45 minutes and then 1 ml of culture medium was provided carefully to the samples adding drop by drop the medium into the wells and holding the tip of the pipette onto the walls of the microwells. These samples were cultured in chondrogenic differentiation medium consisting of DMEM supplemented with 100 Units/mL penicillin G, 100 μ g/mL streptomycin, 40 μ g/mL proline, 0.2 mM L-ascorbic-acid-2-phosphate, 50 mg/ml insulin-transferrin-selenite (ITS) Premix (Becton Dickinson), 100 μ g/mL sodium pyruvate (Sigma), 10 ng/ml transforming growth factor- β 3 (TGF- β 3, Invitrogen) and 0.1 μ M dexamethasone (Sigma), at 37 °C under a humidified atmosphere of 5% CO₂. The samples were analyzed after 7, 14 and 21 days of culture by Raman microspectroscopy, total DNA quantification and GAG detection assay, SEM and histology.

Confocal Raman Microscopy. In the control studies a Nikon E600 epifluorescence microscope (Nikon, Inc., Melville, New York) was modified for near-infrared (NIR) Raman spectroscopy in house which was previously described [32]. A 785-nm Kaiser Invictus laser was line-focused (Kaiser Optical Systems, Inc., Ann Arbor, Michigan) onto the samples using a 20x/0.75 NA S Fluor objective. Raman-scattered light was collected through the same 20x/0.75 NA S Fluor objective and

dispersed through a spectrograph (HoloSpec $f/1.8$, Kaiser Optical Systems, Inc.). Raman signal was collected for 180 sec on a charge-coupled device (CCD) detector optimized for NIR wavelengths (DU401-BR-DD, Andor Technologies, Belfast, Ireland). Raman transects consisted of 126 Raman spectra arranged at equidistant points along a line through the specimen. Three transects were collected at three various locations (in three pores) across the surface of each scaffold-sample and time point (one sample per time point). A total of 378 (3x126) Raman spectra were collected from each scaffold and time point in this study. Bright field micrographs were collected with a stereomicroscope (Nikon, SMZ800) and with a Plan Apo 1x/0.1 NA objective from each scaffold at all time points.

In the main experiments, Raman measurements were performed using a home-built confocal Raman spectrometer as described earlier [33]. Briefly, a Krypton ion laser (Coherent, Innova 90K, Santa Clara, CA) with an emission wavelength of 647.1 nm was used as the excitation source. A 40x/0.75 NA Olympus UIS2 objective (UPlanFLN, Olympus, Hamburg, Europe) was used to illuminate the sample as well as to collect the Raman-scattered photons in epi-detection mode. The scattered light was filtered by a razor-edge filter (Semrock, Rochester, NY, USA) to suppress reflected laser light and Rayleigh-scattered light, and focused onto a pinhole of 15 μm diameter at the entrance of an imaging spectrograph (HR460; Jobin-Yvon, Paris, France), which contained a blazed holographic grating with 600 grooves/mm. The spectrograph dispersed the Raman-scattered photons on an air-cooled electron-multiplying CCD detector (Newton DU-970N, Andor Technology, Belfast, Northern Ireland). The system provided a spectral resolution of 1.85 to 2.85 $\text{cm}^{-1}/\text{pixel}$ over the wavenumber range from -20 to 3670 cm^{-1} . Raman images were acquired from the samples by recording a full

spectrum from each position of the laser beam guided by the displacement of the scanning mirror in the area of interest on the samples. Each Raman scan resulted in 1024 spectra. These measurements were performed in an area of 30 x 30 μm with a spectral resolution of 310 nm per scan, an accumulation time of 1 s/step and an excitation power of 35mW. Three Raman images were collected from three pores of each sample and triplicates of samples were measured each time point. The samples were scanned by using a scanning mirror system (SM, MG325D and G120D, General Scanning, Bedford, USA). Toluene, a Raman calibration standard, which has accurately known peak frequencies (521, 785, 1004, 1624, 2921 and 3054 cm^{-1}), was used for wavenumber calibration of the spectra. Prior to Raman measurements samples were washed with PBS, fixed in 10% formalin for 10 minutes and washed extensively with PBS.

Raman data analysis. In the control experiments, spectra were corrected for curvature, dark current, and variations in the CCD quantum efficiency. A mean spectrum was calculated and baseline-corrected from each transect after correction for the fused silica background.

In the main experiments the preprocessing of the data was performed as described previously [34-36]. The spectra were preprocessed by: (1) removing cosmic ray events; (2) subtracting the camera offset noise (dark current); and (3) calibrating the wave number axis. The well known band-positions were used to relate wavenumbers to pixels. The frequency-dependent optical detection efficiency of the setup was corrected using a tungsten halogen light source (Avalight-HAL; Avantes BV, Eerbeek, The Netherlands) with a known emission spectrum. The detector-induced etaloning effect was compensated by this procedure. After data correction, the spectra of the Raman scans on respective

measurement days were averaged to generate mean spectra for each sample.

Both in the control and main studies semi-quantitative univariate data analysis was performed by selecting specific vibrational bands of collagen or/and sGAGs in the averaged spectra from each time point, and integrating each band after local baseline subtraction. Subsequently, normalized band-area ratios were obtained from the collagen and sGAG bands over the integrated band of the phenylalanine ring breathing mode at 1001 cm^{-1} . The calculations were made using normalized band area ratios, not absolute values, so the system is rather semi-quantitative than quantitative monitoring of the collagen and sGAG formation.

All data manipulations were performed using routines written in MATLAB 7.4 (The Math Works Inc., Natick, MA).

Fiber-optic Raman spectroscopy. Fiber-optic Raman measurement was carried out using a custom designed fiber optic Raman probe. Details of the Raman probe design have been previously described [15, 37]. Briefly, the fiber optic Raman probe consisted of 50-collection fibers that were arranged into 10 branches. Each branch housed 5-fibers and terminated in a stainless steel ferrule with an outer diameter of 1.25 mm. The Raman probe was used with a custom designed aluminum probe holder to facilitate contact of each fiber with the scaffold. The Raman collection probes were bundled at the distal end into a linear array for coupling to the Raman spectrograph (RamanRxn1, Kaiser Optical Systems Inc.). Laser illumination was achieved using a $300\text{ }\mu\text{m}$ core optical fiber, that terminated in a stainless steel ferrule ($\text{OD} = 400\text{ }\mu\text{m}$) and coupled to an 830 nm laser source. Raman data were acquired with the fiber optic Raman probe and processed with MATLAB using in-house written codes to generate ten Raman spectra for all collection

probes. The ten Raman spectra were averaged to generate mean spectra for each sample (scaffold).

GAG detection assay. Following 7, 14 and 21 days of culture, samples were washed with PBS and frozen at 80 °C. After thawing, the constructs were digested for 16 hours at 56 °C with 1mg/mL proteinase K (Sigma-Aldrich) in Tris/EDTA buffer (pH 7.6). This solution contained 185 µg/mL iodoacetamine and 10 µg/mL Pepstatin A (both Sigma Aldrich). Quantification of total DNA was done using the CyQuant DNA assay (MolecularProbes) and a spectrophotometer (excitation 480 nm, emission 520 nm, Victor3, Perkin Elmer). The amount of GAG was determined spectrophotometrically after reaction with dimethylmethylene blue dye (DMMB, Sigma–Aldrich) in PBE buffer containing 14,2g/l Na₂HPO₄ and 3,72g/L Na₂EDTA, pH6.5. A micro plate reader (Multiskan GO, Thermo Fisher) was used to determine the absorbance at 520 nm. The amount of GAG was calculated using a standard of chondroitin sulfate (Sigma–Aldrich).

Histology. After Raman measurements, samples were embedded in glycol methacrylate (GMA) for histological analysis, sectioned at 10-µm intervals, and stained with Picro-sirius Red (Sigma, St. Louis, MO) for visualization of collagen.

Scanning Electron Microscopy (SEM). Cell morphology and attachment was characterized by SEM analysis with a Philips XL 30 ESEM-FEG. The samples were fixated for 30min in 10% formalin. Subsequently the samples were dehydrated in sequential ethanol series and critical point dried from liquid carbon dioxide using a Balzers CPD 030 Critical Point Dryer. The constructs were gold sputter coated (Cressington) prior to SEM analysis.

Statistical analysis. The results are presented as mean \pm standard deviation (SD). Experimental data were analyzed for statistical significance using a student t-test. Statistical significance was set to p-value < 0.05 (*).

RESULTS AND DISCUSSION

The aim of this study is to investigate the use of conventional and fiber optic Raman microspectroscopy for monitoring ECM formation during culture in 3D PEOT/PBT scaffolds. As a proof of concept, chondrocytes have been seeded as single cells and as microaggregates on PEOT/PBT scaffolds, to investigate if there are differences in ECM formation which can be detected with the Raman setups presented here. The rationale of using microaggregates was to achieve increased matrix formation: it is known that aggregation is an essential step in chondrogenesis and sustains matrix production of chondrocytes [38-39].

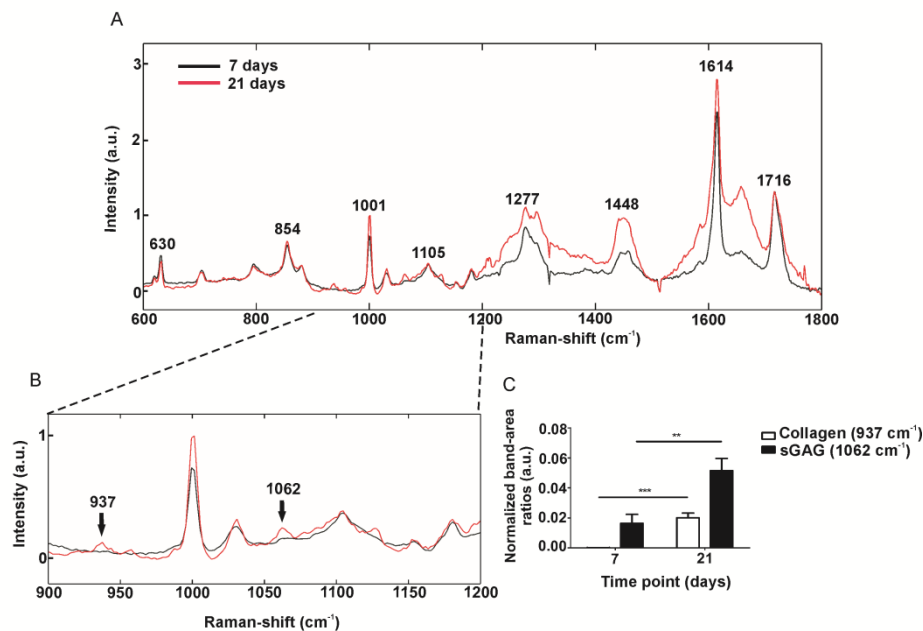


Figure 1. Baseline corrected mean Raman transects from samples of PEOT/PBT scaffolds seeded with bovine chondrocytes from control experiments - acquired after 7 and 21 days of culture period and collected by a conventional Raman setup (785 nm) - in the region **A:** from 600 cm^{-1} to 1800 cm^{-1} **B:** from 900 cm^{-1} to 1300 cm^{-1} . Increased intensities of the Raman bands at 937 cm^{-1} (collagen) and 1062 cm^{-1} (sGAG) were clearly visible from day 7 to day 21 of the culture period. **C:** Semi-quantitative univariate data analysis showed normalized integrated band area ratios of the collagen (white bar) and sGAG (black bar) bands after 7 and 21 days of culture period. The normalized band-area ratios were obtained from the ratio of the collagen or sGAG band over the band of phenylalanine (1001 cm^{-1}). All bands were integrated after baseline subtraction. The normalized band area ratio for both collagen and sGAG content were significantly increased from day 7 to day 21 of culture period (collagen: $p=0.0003$; sGAG: $p=0.0065$).

In the control studies, Raman transects from PEOT/PBT scaffolds seeded with bovine chondrocytes were acquired after 7 and 21 days of culture period using a conventional Raman setup. Mean Raman transects of these samples showed increased intensities of the bands at 937 cm^{-1} and 1062 cm^{-1} from day 7 to day 21 of the culture period (**Fig. 1A and B** - truncated). These bands correspond to collagen (proline, hydroxyproline, C-C skeletal of collagen backbone) [40] and sGAGs [10] respectively, which are essential components of the ECM in cartilage. It was previously described that the band of collagen found at 937 cm^{-1} can be used as a Raman marker for collagen-containing extracellular matrix formation over time in chondrocyte pellet cultures [12]. Furthermore chondrocyte response to bioactive scaffolds has already been monitored by obtaining Raman signal from the extracellular matrix deposited onto the scaffold and by assessing Raman bands indicative for collagen and amide I in the spectral region between 1200 cm^{-1} and 1800 cm^{-1} [13]. To quantify changes in intensities of bands at 937 cm^{-1} and 1062 cm^{-1} , a semi-quantitative univariate data analysis was

performed. The results of the univariate data analysis are shown in **Figure 1C** with the normalized band area ratios for the band signifying collagen and sGAGs. Subsequently, band-area ratios were obtained from the collagen and sGAG bands over the integrated band of the phenylalanine ring breathing mode at 1001 cm^{-1} [41]. Phenylalanine was the best-resolved band and is not sensitive to local chemical environments. The normalized band-area ratio for both collagen and sGAG content increased from day 7 to day 21 of culture period. Mean Raman transects were also obtained – as a negative control - from PEOT/PBT scaffolds without cells (**Fig. 2A and B - truncated**).

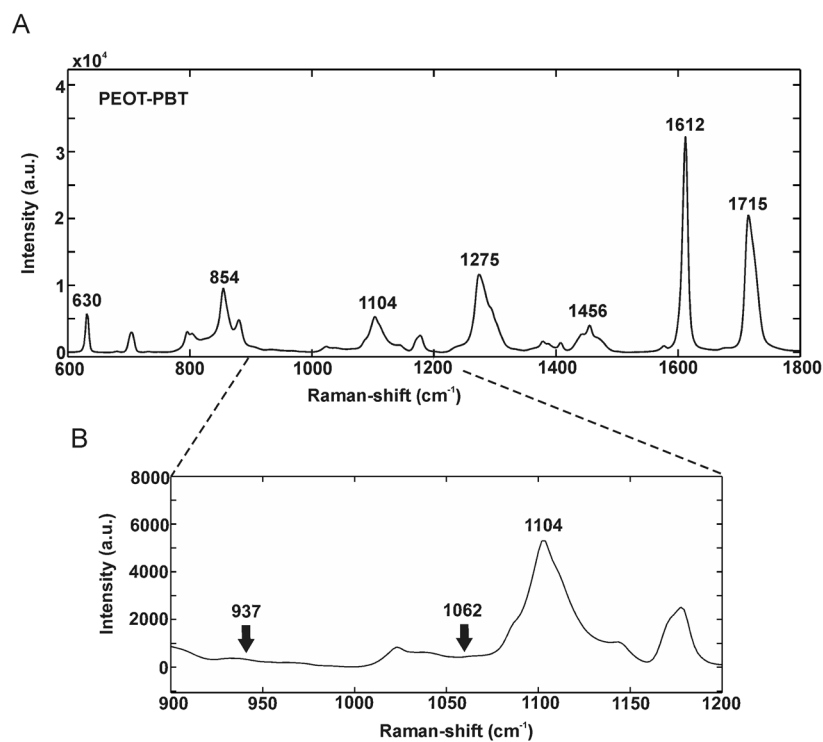


Figure 2. Mean Raman transects from a PEOT/PBT scaffold without cells in the region **A:** from 600 cm^{-1} to 1800 cm^{-1} and **B:** from 900 cm^{-1} to 1300 cm^{-1} . The Raman spectrum mainly had Raman bands in the same region as the Raman spectra of the cell-seeded

scaffolds in Figure 1. In contrast, the spectrum did not have interfering bands in the region between 900 cm^{-1} and 1000 cm^{-1} .

Comparing these spectra with the mean Raman spectra of cell-seeded scaffolds on **Figure 1A and B**, Raman contributions of PEOT/PBT can be distinguished at 630 cm^{-1} , 854 cm^{-1} and between 1100 cm^{-1} and 1800 cm^{-1} in Raman spectra from cell-seeded scaffolds. However these PEOT/PBT specific bands can be easily recognized and do not interfere with ECM specific bands at 937 and 1062 cm^{-1} . In this case the area of measurement overlaps with a part of the polymeric scaffold during Raman imaging, leading to Raman contributions from the polymer in the total spectra.

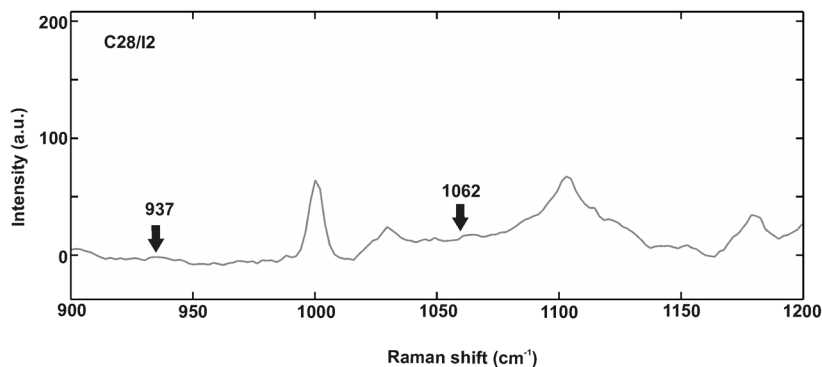


Figure 3. Mean Raman transect from PEOT/PBT scaffold seeded with human C28/I2 chondrocytes (negative control for extracellular matrix formation) in the region from 900 cm^{-1} to 1200 cm^{-1} at day 21 of culture period. Mean Raman transect of this sample did not show bands at 937 cm^{-1} (collagen) and at 1062 cm^{-1} (sGAG).

Raman transects from PEOT/PBT scaffolds seeded with human chondrocytes from C-28/I2 immortalized chondrocyte cell line – which were used as negative control for ECM formation - were also collected after 21 days of culture period. Indeed it was observed that mean Raman transects of these samples did not show bands at 937 cm^{-1} (collagen) and at 1062 cm^{-1} (sGAG), even after 21 days of culture (**Fig. 3**). Furthermore in the bright field micrographs of the same samples hardly any ECM formation was observed (**Fig. 4A**) confirming the Raman data. In contrast in the bright field micrographs of bovine chondrocyte-seeded samples from the control studies (**Fig. 4B**) extracellular matrix-like fiber formation could be detected at day 7 of the culture period. Moreover, the amount of these extracellular matrix-like structures further increased in time and completely covered the scaffold when comparing samples from day 7 to day 21 (**Fig. 4B**).

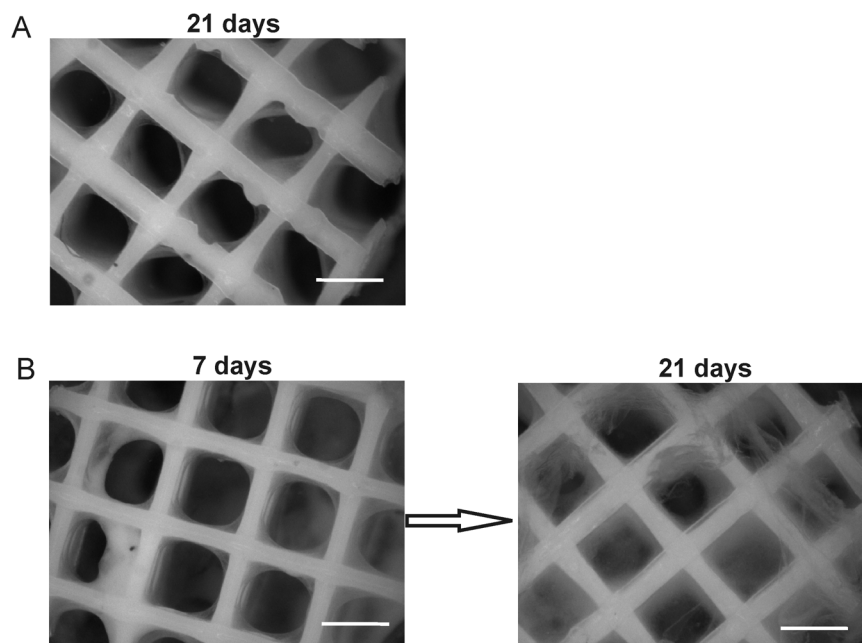


Figure 4. Bright field micrographs of **A:** PEOT/PBT scaffold seeded with human C28/I2 chondrocytes at day 21 of culture period and **B:** PEOT/PBT scaffold seeded with bovine chondrocytes at day 7 and 21 of culture period. Abundant ECM-like structure formation was only observed in the scaffolds seeded with bovine chondrocytes. The image was made with a 10x objective and scale bars are equal to 1000 μm .

In our main study, label-free monitoring of ECM formation was carried out using a conventional and a fiber-optic Raman setup. In a previous study 3D polymer scaffolds were seeded with bovine articular chondrocytes in spinner flasks, so that stirred cell culture promoted the formation of cell aggregates [42]. Cell aggregation enhanced the kinetics of cell attachment without compromising the uniformity of cell distribution on the scaffolds. In the study presented here the seeding of single chondrocytes was compared to the seeding of chondrocyte microaggregates on 3D PEOT/PBT scaffolds. Chondrogenic differentiation medium was used, to stimulate proteoglycan synthesis from chondrocytes in 3D culture [43]. Both the mean Raman spectra from the single chondrocyte – **[Fig. 5A(a) – day 7, (b) – day 14, (c) – day 21]** and chondrocyte microaggregate-seeded **[Fig. 5A(d) – day 7, (e) – day 14, (f) – day 21]** scaffolds showed bands corresponding to phenylalanine (C-C aromatic ring) at 1001 cm^{-1} [41], lipids/proteins (CH_2 bending mode) at 1448 cm^{-1} [44] and amide I at 1657 cm^{-1} [45]. Additionally, Raman bands at 937 cm^{-1} (collagen) and at 1062 cm^{-1} (sGAG) were also detected indicative for ECM deposition by the chondrocytes. Although normalized band-area ratios for sGAG content did not change over time, but collagen synthesis found to be different in single chondrocyte-seeded scaffolds when compared to microaggregate-seeded samples (**Fig. 5B and C**). While normalized band-area ratios for collagen content of single cell-seeded samples

gradually decreased during the 21 day culture period (**Fig. 5B**), that of the microaggregate-seeded samples significantly increased (**Fig. 5C**). Several studies with chondrocytes showed a correlation between aggregation and enhanced cartilaginous tissue formation [46-49]. Therefore, we think that seeding microaggregates, instead of single chondrocytes, onto scaffolds will be an improved approach for cartilage tissue engineering.

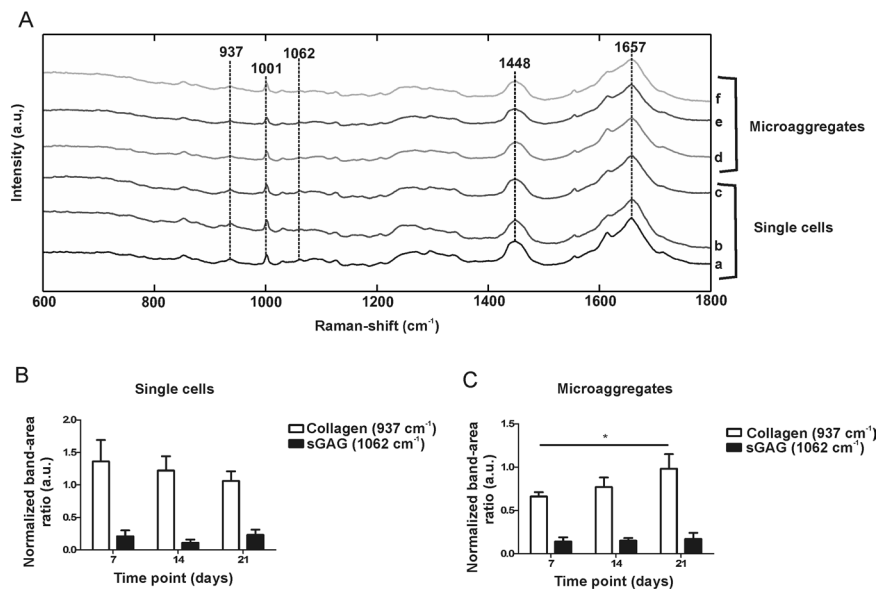
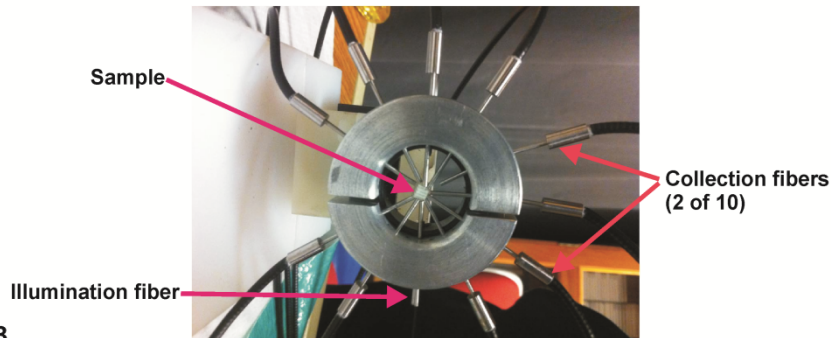


Figure 5. Mean Raman spectra and corresponding normalized band-area ratios from samples of PEOT/PBT scaffolds seeded with bovine single chondrocytes or chondrocyte microaggregates from main experiments. **A:** Mean Raman spectra acquired after 7, 14 and 21 days of culture period and collected by a conventional Raman setup (645 nm) in the region from 600 cm⁻¹ to 1800 cm⁻¹. The spectra were vertically displaced for clarity: (a) 7 days, (b) 14 days, (c) 21 days cultured scaffolds seeded with single chondrocytes, and (d) 7 days, (e) 14 days and (f) 21 days cultured scaffolds seeded with chondrocyte microaggregates. **B, C:** Semi-quantitative univariate data analysis showed normalized

integrated band-area ratios of collagen (white bar) and sGAG (black bar) bands for the Raman spectra of single cell-seeded and microaggregate-seeded scaffolds at day 7, 14 and 21 of culture period. The normalized band-area ratio acquired from the ratio of the collagen or sGAG band to the band of phenylalanine (1001 cm^{-1}). All bands were integrated after baseline subtraction. Although normalized band-area ratios for sGAG content had not been not changing over time, but collagen synthesis found to be different in single chondrocyte-seeded scaffolds when compared to microaggregate-seeded samples. While normalized band-area ratios for collagen content of single cell-seeded samples had gradually been decreasing during the 21 day culture period, that of the microaggregate-seeded samples had significantly been increasing ($p=0.0353$).

A photo-image of the experimental setup of the fiber optic Raman measurements can be seen in **Figure 6A**. Mean Raman spectra from single chondrocyte-seeded scaffolds cultured for 14 days and 21 days and from a scaffold without cells (**Fig. 6B** truncated) that was collected by the fiber optic Raman setup, mainly showed Raman contributions from the optical fibers (i.e. silica Raman) and scaffold material. However, Raman spectra of the cell-seeded scaffolds showed Raman bands at 920 and 972 cm^{-1} corresponding to components of collagen, such as aminoacid proline, these were not found in the spectra of the scaffold without cells. We show in **Figure 2** that PEOT/PBT does not have Raman bands in the spectral region between 900 and 1100 cm^{-1} , so it is likely that bands arising in this region in spectra of bare scaffolds, as can be seen in **Figure 6B**, originated from Raman scattering generated from silica in the optical fibers. A suitable algorithm in MATLAB for accurate silica background subtraction and/or further data processing using multivariate statistical technique such as Band target entropy minimization (BTEM) will greatly reduce the background bands and maximize the Raman bands from the ECM.

A



B

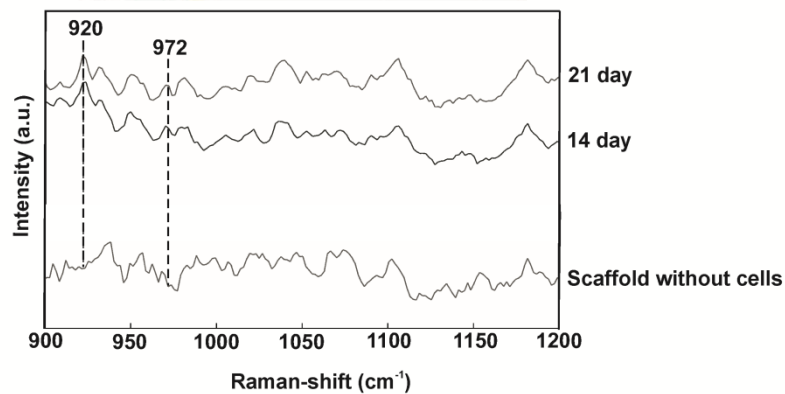


Figure 6. Setup of fiber-optic Raman probe for measurement on single chondrocyte-seeded scaffolds. **A:** The illumination and collection fibers were spread around the scaffold using a custom design aluminium probe holder to facilitate contact of each fiber with the scaffold. **B:** Mean Raman spectra from scaffolds seeded with single bovine chondrocytes - at day 14 and 21 of culture period - and from scaffolds without cells in the region from 900 cm^{-1} to 1200 cm^{-1} . Although, the Raman spectra from the fiber-optic set-up generated silica background from the fiber, the bands at 920 cm^{-1} and 972 cm^{-1} (attributes of ECM) were recoverable.

Additionally we investigated ECM deposition by more conventional methods. GAG formation was successfully detected by biochemical analysis (GAG-assay, **Fig. 7A**) both in the single cell-seeded and microaggregate-seeded samples at day 7, 14 and 21 of culture period.

As an example collagen synthesis of single cell-seeded scaffolds was also shown at day 7 of culture period (**Fig. 7B**).

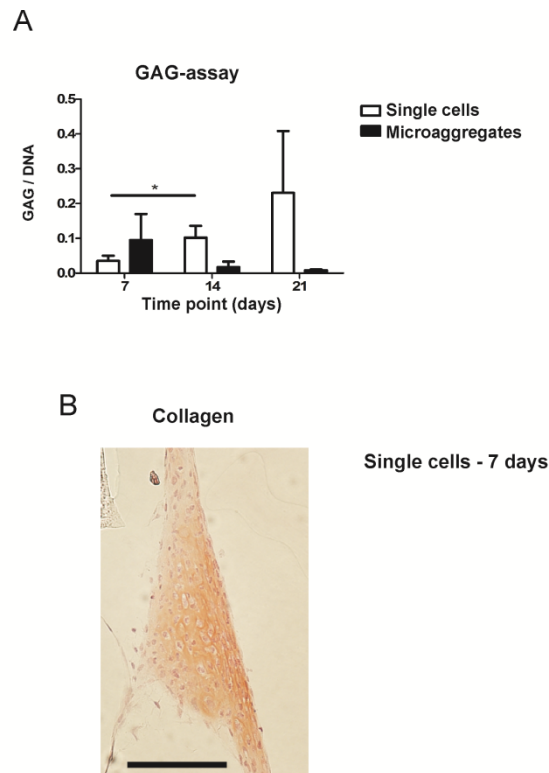


Figure 7. Matrix production. **A:** Results of GAG-assay normalized with DNA content of single chondrocyte- or microaggregate-seeded PEOT/PBT scaffolds. GAG production was detected in all the samples, although significant changes were only observed in the GAG content of the single cell seeded scaffolds from day 7 to day 14 of culture period ($p=0.0303$). **B:** Result of Picro-sirius Red staining visualizing collagen in single chondrocytes-seeded scaffold at day 7 of culture period. The image was made with a 20x objective and scale bar equals to 100 μm .

Furthermore both in the SEM micrographs of the single cell-seeded (**Fig. 8A**) and microaggregate-seeded samples (**Fig. 8B**) matrix-like structure

formation could be observed. Chondrocyte microaggregates adhered to the scaffolds could be also seen in the SEM micrographs of the microaggregate-seeded samples at day 7 of culture period with higher magnifications (1000x and 2500x). After 21 days of culture period the majority of the microaggregates were flattened and fiber-like (matrix-like) structures were excreted by the cells covering the surface of the scaffold.

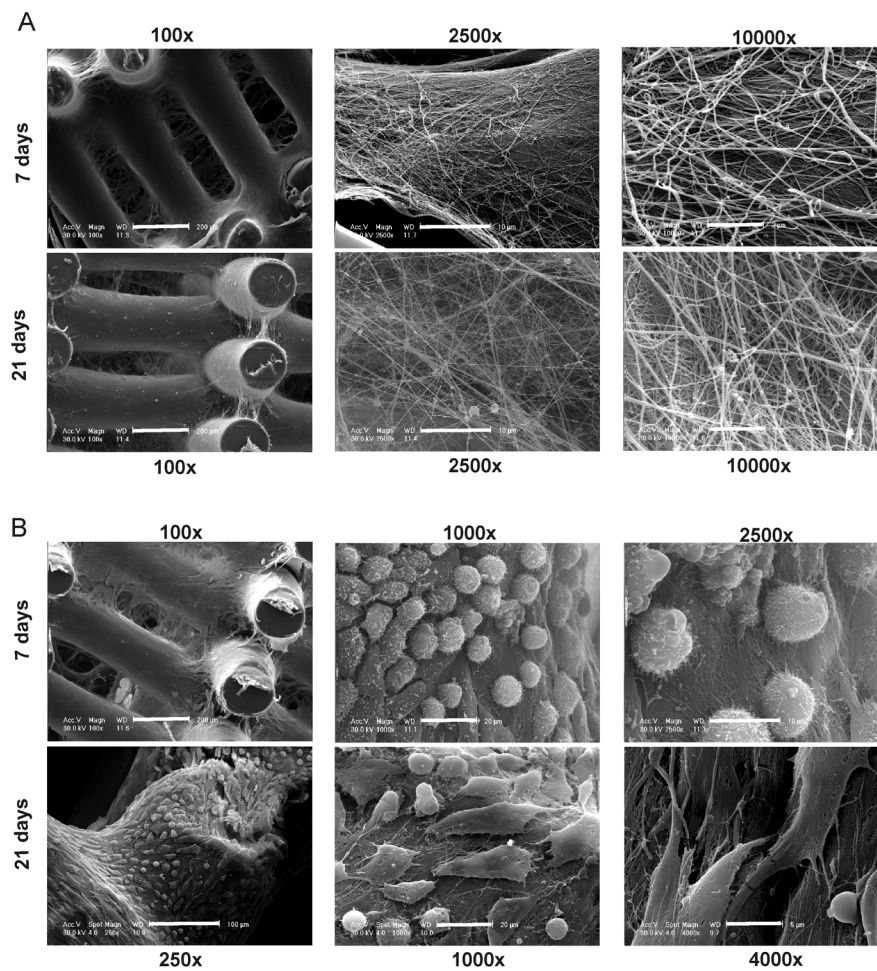


Figure 8. SEM micrographs of **A:** single chondrocyte-seeded and **B:** microaggregate-seeded scaffolds at day 7 and day 21 of culture period. ECM-like structure formation was

observed in all the samples. Chondrocyte-microaggregates adhered to the scaffolds was seen in the images of the microaggregate-seeded samples at day 7 of culture period with higher magnifications (1000x and 2500x). After 21 days of culture period the majority of the microaggregates were flattened and fiber-like (matrix-like) structures were excreted by the cells covering the surface of the scaffold. Magnifications and scale bars: 100x – scale bars equal to 200 μm ; 250x – scale bars equal to 100 μm ; 1000x – scale bars equal to 20 μm ; 2500x – scale bars equal to 10 μm ; 4000x – scale bars equal to 5 μm ; 10000x – scale bars equal to 2 μm .

CONCLUSIONS

In this study, the applicability of confocal Raman microspectroscopy has been demonstrated to detect formation of essential cartilage ECM compounds in 3D PEOT/PBT scaffolds based on the Raman bands at 937 and 1062 cm^{-1} corresponding to collagen and sGAGs respectively. Although normalized band-area ratios for sGAG content did not change over time, collagen synthesis was found to be different in single chondrocyte-seeded scaffolds when compared to microaggregate-seeded samples. While normalized band-area ratios for collagen content of single cell-seeded samples gradually decreased during the 21 day culture period, collagen content of the microaggregate-seeded samples significantly increased. Therefore we think that seeding microaggregates, instead of single chondrocytes, onto scaffolds is an improved approach for cartilage tissue engineering.

The use of fiber-optic set-up for Raman measurement was also demonstrated. Although, the Raman spectra from the fiber-optic set-up generated silica background from the fiber, the bands at 920 cm^{-1} and 972 cm^{-1} (attributes of ECM) were recoverable. The use of a new generation of fluorocarbon fiber-optic Raman probes, which generate a

reference Raman band, for quantitative Raman spectroscopy will eliminate silica background and generate well-resolved Raman spectra of ECM [37]. The fiber optic Raman measurements also allows the collection of Raman spectra from multiple pores in the scaffold with one single measurement time point, which generates a more representative average of the Raman signal from the ECM.

Our results provide proof-of-principle that Raman microspectroscopy is a promising non-invasive and rapid tool to quantitatively monitor ECM deposition and rebuilding. Further investigation is needed to validate the potential of the technique, so that evaluation of cartilaginous matrix formation in tissue engineered constructs will be possible. Discrimination of specific collagen type would be the main focus of future studies.

ACKNOWLEDGEMENT

The authors gratefully acknowledge the funding from the Dutch Program for Tissue Engineering (DPTE) through the grant number TGT. 6737, from the Nederland Institute for Regenerative Medicine (NIRM) through the grant number FES0908 and from the National Institute of Health (NIH) through the grant number R01AR055222 and R01AR056646.

REFERENCES

1. Mankin, H.J., *The response of articular cartilage to mechanical injury*. J Bone Joint Surg Am, 1982. **64**(3): p. 460-6.
2. Dudics, V., et al., *Chondrogenic potential of mesenchymal stem cells from patients with rheumatoid arthritis and osteoarthritis: measurements in a microculture system*. Cells Tissues Organs, 2009. **189**(5): p. 307-16.
3. Zhang, Z., et al., *Hyaline cartilage engineered by chondrocytes in pellet culture: histological, immunohistochemical and ultrastructural analysis in comparison with cartilage explants*. J Anat, 2004. **205**(3): p. 229-37.
4. Kuettner, K.E., *Biochemistry of articular cartilage in health and disease*. Clin Biochem, 1992. **25**(3): p. 155-63.
5. Krafft, C., et al., *Mapping of single cells by near infrared Raman microspectroscopy*. Vib Spectrosc, 2003. **32**: p. 75-83.
6. Notingher, I., et al., *In situ characterisation of living cells by Raman spectroscopy*. Spectroscopy-an International Journal, 2002. **16**(2): p. 43-51.
7. Puppels, G.J., et al., *Laser irradiation and Raman spectroscopy of single living cells and chromosomes: sample degradation occurs with 514.5 nm but not with 660 nm laser light*. Exp Cell Res, 1991. **195**(2): p. 361-7.
8. Frushour, B.G. and J.L. Koenig, *Raman scattering of collagen, gelatin, and elastin*. Biopolymers, 1975. **14**(2): p. 379-91.
9. Leikin, S., et al., *Raman spectral evidence for hydration forces between collagen triple helices*. Proceedings of the National Academy of Sciences of the United States of America, 1997. **94**(21): p. 11312-11317.
10. Ellis, R., E. Green, and C.P. Winlove, *Structural Analysis of Glycosaminoglycans and Proteoglycans by Means of Raman Microspectrometry*. Connective Tissue Research, 2009. **50**(1): p. 29-36.
11. Bansil, R., I.V. Yannas, and H.E. Stanley, *Raman spectroscopy: a structural probe of glycosaminoglycans*. Biochim Biophys Acta, 1978. **541**(4): p. 535-42.
12. Kunstar, A., et al., *Raman Microspectroscopy: A Noninvasive Analysis Tool for Monitoring of Collagen-Containing Extracellular Matrix Formation in a Medium-Throughput Culture System*. Tissue Engineering Part C-Methods, 2011. **17**(7): p. 737-744.

13. Jones, J.R., et al., *In situ monitoring of chondrocyte response to bioactive scaffolds using Raman spectroscopy*. Bioceramics, Vol 17, 2005. **284-286**: p. 623-626.
14. Matousek, P., et al., *Noninvasive Raman Spectroscopy of human tissue in vivo*. Applied Spectroscopy, 2006. **60**(7): p. 758-763.
15. Okagbare, P.I., et al., *Transcutaneous Raman spectroscopy for assessing progress of bone graft incorporation in bone reconstruction and repair*. Photonic Therapeutics and Diagnostics VII, 2011. **7883**.
16. Crow, P., et al., *Fibre-optic raman spectroscopy: The prospects for in vivo diagnosis of bladder and prostate cancer*. Journal of Urology, 2004. **171**(4): p. 68-68.
17. Shim, M.G., et al., *In vivo near-infrared Raman spectroscopy: Demonstration of feasibility during clinical gastrointestinal endoscopy*. Photochemistry and Photobiology, 2000. **72**(1): p. 146-150.
18. Hata, T.R., et al., *Non-invasive Raman spectroscopic detection of carotenoids in human skin*. Journal of Investigative Dermatology, 2000. **115**(3): p. 441-448.
19. Mahadevan-Jansen, A., et al., *Development of a fiber optic probe to measure NIR Raman spectra of cervical tissue in vivo*. Photochemistry and Photobiology, 1998. **68**(3): p. 427-431.
20. Utzinger, U., et al., *Near-infrared Raman spectroscopy for in vivo detection of cervical precancers*. Applied Spectroscopy, 2001. **55**(8): p. 955-959.
21. Buschman, H.P., et al., *In vivo determination of the molecular composition of artery wall by intravascular Raman spectroscopy*. Analytical Chemistry, 2000. **72**(16): p. 3771-3775.
22. Beumer, G.J., C.A. van Blitterswijk, and M. Ponec, *Biocompatibility of a biodegradable matrix used as a skin substitute: an in vivo evaluation*. J Biomed Mater Res, 1994. **28**(5): p. 545-52.
23. Bakker, D., et al., *Effect of implantation site on phagocyte/polymer interaction and fibrous capsule formation*. Biomaterials, 1988. **9**(1): p. 14-23.
24. Beumer, G.J., C.A. van Blitterswijk, and M. Ponec, *Degradative behaviour of polymeric matrices in (sub)dermal and muscle tissue of the rat: a quantitative study*. Biomaterials, 1994. **15**(7): p. 551-9.
25. Moroni, L., et al., *Design of biphasic polymeric 3-dimensional fiber deposited scaffolds for cartilage tissue engineering applications*. Tissue Eng, 2007. **13**(2): p. 361-71.
26. Mensik, I., et al., *Effectiveness and Safety of the PEGT/PBT Copolymer Scaffold as Dermal Substitute in Scar Reconstruction Wounds (Feasibility Trial)*. Cell Tissue Bank, 2002. **3**(4): p. 245-53.

27. Meijer, G.J., et al., *Polyactive as a bone-filler in a beagle dog model*. Int J Oral Maxillofac Surg, 1996. **25**(3): p. 210-16.
28. Du, C., et al., *Bone growth in biomimetic apatite coated porous Polyactive((R)) 1000PEGT70PBT30 implants*. Biomaterials, 2002. **23**(23): p. 4649-4656.
29. Napolitano, A.P., et al., *Dynamics of the self-assembly of complex cellular aggregates on micromolded nonadhesive hydrogels*. Tissue Engineering, 2007. **13**(8): p. 2087-2094.
30. Nikolovski, J. and D.J. Mooney, *Smooth muscle cell adhesion to tissue engineering scaffolds*. Biomaterials, 2000. **21**(20): p. 2025-2032.
31. Finger, F., et al., *Molecular phenotyping of human chondrocyte cell lines T/C-28a2, T/C-28a4, and C-28/I2*. Arthritis and Rheumatism, 2003. **48**(12): p. 3395-3403.
32. Esmonde-White, K.A., et al., *Raman spectroscopy of synovial fluid as a tool for diagnosing osteoarthritis*. J Biomed Opt, 2009. **14**(3): p. 034013.
33. van Manen, H.J., A. Lenferink, and C. Otto, *Noninvasive imaging of protein metabolic labeling in single human cells using stable isotopes and Raman microscopy*. Anal Chem, 2008. **80**(24): p. 9576-82.
34. Uzunbajakava, N., et al., *Nonresonant confocal Raman imaging of DNA and protein distribution in apoptotic cells*. Biophys J, 2003. **84**(6): p. 3968-81.
35. van Manen, H.J., et al., *Intracellular chemical imaging of heme-containing enzymes involved in innate immunity using resonance Raman microscopy*. Journal of Physical Chemistry B, 2004. **108**(48): p. 18762-18771.
36. Pully, V.V., et al., *Hybrid Rayleigh-, Raman and TPE fluorescence spectral confocal microscopy of living cells*. Journal of Raman Spectroscopy.
37. Okagbare, P.I. and M.D. Morris, *Polymer-capped fiber-optic Raman probe for non-invasive Raman spectroscopy*. Analyst, 2012. **137**(1): p. 77-81.
38. Pizette, S. and L. Niswander, *BMPs are required at two steps of limb chondrogenesis: Formation of prechondrogenic condensations and their differentiation into chondrocytes*. Developmental Biology, 2000. **219**(2): p. 237-249.
39. Tacchetti, C., et al., *In vitro morphogenesis of chick embryo hypertrophic cartilage*. J Cell Biol, 1987. **105**(2): p. 999-1006.
40. Cheng, W.T., et al., *Micro-Raman spectroscopy used to identify and grade human skin pilomatrixoma*. Microscopy Research and Technique, 2005. **68**(2): p. 75-79.

41. O Faolain, E., et al., *A study examining the effects of tissue processing on human tissue sections using vibrational spectroscopy*. *Vibrational Spectroscopy*, 2005. **38**(1-2): p. 121-127.
42. Vunjak-Novakovic, G., et al., *Dynamic cell seeding of polymer scaffolds for cartilage tissue engineering*. *Biotechnology Progress*, 1998. **14**(2): p. 193-202.
43. Mauck, R.L., et al., *Regulation of cartilaginous ECM gene transcription by chondrocytes and MSCs in 3D culture in response to dynamic loading*. *Biomech Model Mechanobiol*, 2007. **6**(1-2): p. 113-25.
44. Frank, C.J., R.L. McCreery, and D.C.B. Redd, *Raman-Spectroscopy of Normal and Diseased Human Breast Tissues*. *Analytical Chemistry*, 1995. **67**(5): p. 777-783.
45. Krafft, C., et al., *Near infrared Raman spectra of human brain lipids*. *Spectrochimica Acta Part a-Molecular and Biomolecular Spectroscopy*, 2005. **61**(7): p. 1529-1535.
46. Duke, P.J., E.L. Daane, and D. Montufar-Solis, *Studies of chondrogenesis in rotating systems*. *J Cell Biochem*, 1993. **51**(3): p. 274-82.
47. Naumann, A., et al., *Tissue engineering of autologous cartilage grafts in three-dimensional in vitro macroaggregate culture system*. *Tissue Eng*, 2004. **10**(11-12): p. 1695-706.
48. Moreira Teixeira, L.S., et al., *High throughput generated micro-aggregates of chondrocytes stimulate cartilage formation in vitro and in vivo*. *Eur Cell Mater*, 2012. **23**: p. 387-99.
49. Wolf, F., et al., *Cartilage tissue engineering using pre-aggregated human articular chondrocytes*. *Eur Cell Mater*, 2008. **16**: p. 92-9.

Chapter 4

Chapter 5

Recognizing different tissues in human fetal femur cartilage by label-free Raman microspectroscopy

*Aliz Kunstar¹, Jeroen Leijten^{1,2}, Stefan van Leuveren¹,
Janneke Hilderink^{1,2}, Cees Otto³, Clemens A. van Blitterswijk¹,
Marcel Karperien^{1,2}, Aart A. van Apeldoorn^{1,2}*

¹Department of Tissue Regeneration, ²Present address: Department of Developmental Bioengineering, ³Department of Medical Cell Biophysics of MIRA – Institute for Biomedical Technology and Technical Medicine, University of Twente, Drienerlolaan 5, 7522 NB Enschede, The Netherlands

ABSTRACT: Traditionally the composition of bone and cartilage is determined by standard histological methods. In this study we used Raman microscopy which provides information on the molecular composition, a molecular “fingerprint”, to detect differences between the zones in human fetal femur cartilage without the need for additional staining or labeling. Raman area scans were made from the (pre)articular cartilage, resting, proliferative and hypertrophic zones of growth plate and endochondral bone within human fetal femora. Multivariate data analysis was performed on Raman spectral datasets to construct cluster images with corresponding cluster averages. Cluster analysis resulted in detection of individual chondrocyte spectra that could be separated from cartilage extracellular matrix (ECM) spectra, and was verified by comparing cluster images with intensity based Raman images for DNA/RNA band. Specific dendrograms were created, using Wards clustering method, and principal component analysis (PCA) was performed with the separated and averaged Raman spectra of cells and ECM of all measured zones. Overall (dis)similarities between measured zones were effectively visualized on the dendrograms and main spectral differences were revealed by PCA allowing for label-free detection of individual cartilaginous zones and for label-free evaluation of proper cartilaginous matrix formation for future tissue engineering and clinical purposes.

INTRODUCTION

Fetal long bones consist of (pre)articular cartilage, growth plate cartilage and bone tissue. (Pre)articular cartilage, which will eventually become the articular cartilage and also called as proximal resting zone, is located several cell layers below the surface of the joint. Together, they regulate longitudinal bone growth and long bone development. Fetal long bones differ from postnatal long bones in that they do not possess a secondary center of ossification. Moreover, their growth plates are much thicker and the chondrocytes are more compactly located [1]. In general, the growth plate can be subdivided into four distinct zones: the resting zone, the proliferative zone, the prehypertrophic zone and the hypertrophic zone. Resting zone chondrocytes are small, uniform and compactly positioned and are characterized by low rates of proliferation and synthesis of proteoglycans and collagen type IIB [2-3]. In the proliferative zone the chondrocytes have an increased proliferation rate that results in the formation of longitudinal columns. In addition, this zone has increased collagen type II and XI synthesis [1]. Following this zone is the prehypertrophic zone where chondrocytes lose their ability to proliferate and gradually increase in size due to swelling. In the hypertrophic zone a cascade of events is triggered including ECM mineralization, angiogenesis and apoptosis of chondrocytes [1].

Current knowledge regarding the composition of the different zones is mainly based on histology [4], immunohistochemistry [5], in situ hybridization [6-7] and electron microscopy [8]. However, these methods do not yield direct information on the molecular composition of the investigated samples. Therefore, elucidating the molecular compositions

of the different cartilage zones can result in a deeper understanding of the changes underlying terminal differentiation of chondrocytes, which drives the development of long bones. Raman spectroscopy is an analytical technique able to measure the molecular composition by providing a spectrum that contains information regarding all the chemical bonds present within the sample. As opposed to histology and immunohistochemistry, which only provides information regarding the presence of specific compounds, Raman spectroscopy creates a “fingerprint” representing the entire molecular composition of the sample. Raman spectroscopy is based on the inelastic light scattering effect [9-11], in which one in a million photons is scattered with a different wavelength after interaction with the sample than the incident photons [12]. The wavelength shift of these scattered photons is specific for the chemical bond where the photon is scattered. By detecting all the photons with a shifted wavelength a Raman spectrum can be constructed. Raman spectroscopy induces no cell damage if suitable laser wavelengths and powers are used [13-14]. Since the first application of Raman spectroscopy on cells [15], this technique has been widely used for biological applications.

In this study, different zones of human fetal femoral tissue were studied with Raman microspectroscopy. In order to be able to compare Raman results to histological data, all experiments were performed on cryosections. The aim of this study was to determine whether confocal Raman microspectroscopy is able to effectively discriminate between different cartilaginous zones of a developing diarthrodial joint and to identify the molecular differences between the (pre)articular cartilage and the different zones of the growth plate cartilage. Together, this

knowledge contributes to our understanding on how to generate a specific sort of cartilage for future tissue engineering and clinical purposes.

EXPERIMENTAL SECTION

Sample preparation. Bovine articular cartilage pieces were obtained from the femoral-patellar groove of a 10 months old calf, fixed in 10% formalin for 10 minutes and washed in phosphate buffered saline (PBS, Gibco) solution. After informed consent and medical ethical committee approval for the use of human donor material had been obtained, fetal femurs were isolated from three human fetuses undergoing elective termination of pregnancy with 20 weeks of gestation. Femurs were snap-frozen in liquid nitrogen and stored at -80 °C till processing. The samples were embedded in cryomatrix (Cryomatrix, Shandon), frozen to -49 °C, sectioned at 20- μ m intervals at -19 °C using a cryotome (Shandon 77210160, Shandon) and placed on UV grade calcium fluoride (CaF₂) slides (Crystran Ltd., UK). Before Raman measurements, the cryosections of the human fetal femur were fixed in 10% formalin for 10 minutes and extensively washed with PBS; and the cryosections of bovine articular cartilage were extensively washed with PBS.

Histology. The embedded samples of the fetal femora were sectioned at 8- μ m intervals using the cryomicrotome and stained with Safranin-O (Sigma, St. Louis, MO) for visualization of sulfated glycosaminoglycans (sGAGs), haematoxylin and eosin (H&E, Sigma, St. Louis, MO) for

visualization of the nuclei and cytoplasm and Alizarin Red S (Sigma, St. Louis, MO) for visualization of calcification.

Confocal Raman Microspectroscopy. Raman measurements were performed using a home-built confocal Raman spectrometer as described earlier [16]. Briefly, a Krypton ion laser (Coherent, Innova 90K, Santa Clara, CA) with an emission wavelength of 647.1 nm was used as the excitation source. An air objective (Olympus UIS2, UPlanFLN, Olympus, Hamburg, Europe; 40x, 0.75 NA) was used to illuminate the sample as well as to collect the Raman-scattered photons in the epi-detection mode. The scattered light was filtered by a razor-edge filter (Semrock, Rochester, NY, USA) to suppress reflected laser light and Rayleigh-scattered light, and focused onto a pinhole of 15 μm diameter at the entrance of an imaging spectrograph/monochromator (HR460; Jobin-Yvon, Paris, France), which contains a blazed holographic grating with 600 grooves/mm. The spectrograph disperses the Raman-scattered photons on an air-cooled electron-multiplying charge-coupled device (EMCCD, Newton DU-970N, Andor Technology, Belfast, Northern Ireland). The system provided a spectral resolution of 1.85 to 2.85 cm^{-1} /pixel over the wavenumber range from -20 to 3670 cm^{-1} . The samples were scanned by using a scanning mirror system (SM, MG325D and G120D, General Scanning, Bedford, USA). Raman spectra were acquired in the so called “spectral scanning mode” of: 1. washed cryosection with bovine articular cartilage, 2. unwashed cryosection without cartilage and 3. washed cryosection without cartilage. In this measurement mode, a single full spectrum is obtained by raster

scanning the laser beam with a laser power of 35mW over an area of 30 $\mu\text{m} \times 30 \mu\text{m}$ in 30s. Raman images were acquired from cryosections of human fetal femurs by recording a full spectrum from each position of the laser beam guided by the displacement of the scanning mirror in the area of interest on the samples. These measurements were performed in an area of 30 x 30 μm with an accumulation time of 1 s/step and an excitation power of 35mW. The laser spot size used in this study was 310 nm. The 30 x 30 μm area scans were made with 30 μm distances adjacent from each other by using a Kleindiek substage LT6820 controlled by a Kleindiek NanoControl (Kleindiek Nanotechnik, Reutlingen, Germany), in such a way that a total area of 120 x 120 μm could be constructed from these initial scans. After data correction, the scans of 30 x 30 μm areas of the fetal femur samples resulted in 256 spectra each, which were subsequently combined into areas of 120 x 120 μm consisting of 4096 spectra from each zone in the human fetal femur.

Toluene, a Raman calibration standard - with accurately known peak frequencies (521, 785, 1004, 1624, 2921 and 3054 cm^{-1}) - was used for wavenumber calibration of the spectra.

Raman data analysis. Preprocessing of the data was performed as described in literature [17-19]. Briefly, the spectra were preprocessed by: (1) removing cosmic ray events; (2) subtracting the camera-offset noise (dark current); and (3) calibrating the wave number axis. The well-known band-positions were used to relate wavenumbers to pixels. The frequency-dependent optical detection efficiency of the setup was

corrected using a tungsten halogen light source (Avalight-HAL; Avantes BV, Eerbeek, The Netherlands) with a known emission spectrum. Also the detector-induced etaloning effect was compensated by this procedure.

Singular value decomposition (SVD) was applied to the hyperspectral data cubes to reduce the uncorrelated noise resulting in the raw three-dimensional (3D) data matrix after converting them to 2D matrix [20]. The SVD-treated data was analyzed by multivariate data analysis procedures. In multivariate analysis, both principal component analysis (PCA) and hierarchical cluster analysis (HCA) were performed on the datasets resulting in cluster images and corresponding cluster averages. HCA made use of the scores obtained from the PCA to visualize the regions containing high spectral similarities, and which allowed for separation of cell spectra from ECM spectra.

Cell-clusters and ECM-clusters were arranged in separate databases and dendrograms were made using Ward's clustering method (HCA) based on Euclidean inter-point distances [21]. Squared Euclidean distances as distance measure and Ward's algorithm to separate Raman spectra into clusters were used. The influence of small variations in the baseline was minimized by preprocessing data with a first derivative Savitsky-Golay algorithm, which was implemented as a seven point smoothing and a quadratic polynomial fit [22-23]. The data was further autoscaled to the mean of the spectra along the frequency axis [22-23]. Additionaly PCA analysis was performed on the separated cell and ECM cluster average spectra. PCA is a mathematical reduction of the dimensionality of the measurement matrix into fewer variables

(principal components), which describe the most significant variance between the data [23-24].

All data manipulations were performed using routines written in MATLAB 7.4 (The Math Works Inc., Natick, MA). Ward's clustering and PCA analysis on the separated cell- and ECM- cluster average spectra were performed using PLS toolbox (Eigenvectors Research Inc., Wenatchee, WA) in MATLAB 7.8.

RESULTS AND DISCUSSION

The aim of this study was to determine whether confocal label-free Raman microspectroscopy is able to effectively discriminate between various tissues, particularly between (pre)articular cartilage and growth plate cartilage of human fetal femur. Detailed understanding of the molecular composition might prove essential in the quest to generate a specific (sub)type of cartilage and to identify molecular markers to distinguish between these two types of cartilage for future tissue engineering and clinical purposes.

Histology. In order to demonstrate the healthy and unaffected nature of the fetal femur, we subjected 8 μm thick cryosections to histological analysis using Alizarin Red S, Safranin-O and H&E stainings. The results of the histological staining were demonstrated in **Figure 1**. Alizarin Red S staining confirmed that (pre)articular cartilage, resting and proliferative zone cartilage did not contain any detectable levels of calcification. As expected, the terminal areas of the hypertrophic zone showed mild levels of calcification. Moreover, the entire matrix of the

endochondral bone was intensely stained for calcification. Safranin- O staining visualized sGAGs, one of the major components of the ECM. In the (pre)articular cartilage and resting zone of the growth plate abundant sGAG deposition was observed. Light microscopy confirmed that in the proliferative zone the ECM-to-cell ratio decreased. In the hypertrophic zone the ratio of ECM to cell further decreased. In the endochondral bone no detectable amounts of sGAGs were present. With the H&E staining, it was demonstrated that the cells in the (pre)articular cartilage and resting zone were very small and compactly located, in the proliferative zone they have increased in size and the column-like structure of the cells were clearly visible. In the hypertrophic zone the cells have greatly increased in size and only a small amount of ECM formation was observed. The endochondral bone appeared quite similar to the hypertrophic zone. The combined histological analysis demonstrated the healthy nature of the specimen and allowed for distinct localization of the various zones.

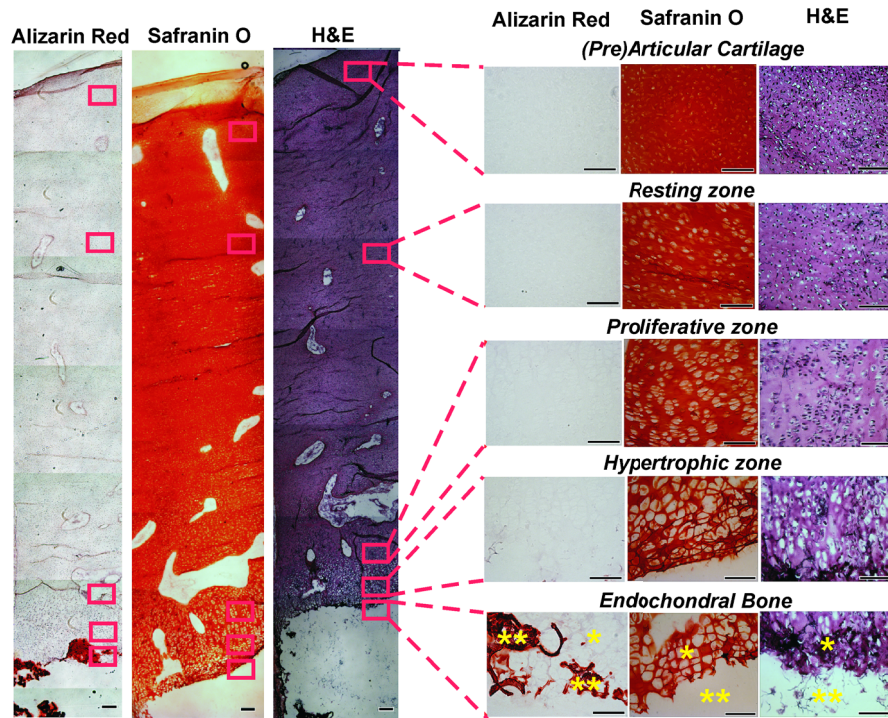


Figure 1. Histological analysis of human fetal femurs: Alizarin Red S staining visualized calcification, Safranin O staining visualized sGAGs and H&E staining visualized nuclei and cytoplasm. In the detailed images of the endochondral bone some parts of the terminal hypertrophic zone can also be observed (the terminal hypertrophic zone is labeled with a star and the endochondral bone with two stars). The boundary between the terminal hypertrophic and endochondral bone part is irregular. The overview scans were made with a 4x objective and scale bars equal 200 μm . The detailed scans were made with a 20x objective and scale bars equal 100 μm .

Confocal Raman Microspectroscopy. It has previously been reported that the use of paraffin prohibits the acquisition of useful Raman-measurements [25]. In contrast, it has been shown that the use of cryomatrix – after washing the tissue cryosections with PBS - does not interfere with Raman measurements [26]. Therefore, in this study cryomatrix was used to embed tissue samples and cryosections were prepared for Raman measurements. In addition, CaF_2 - slides were used as a substrate of the tissue sections for all the Raman measurement to avoid non-relevant Raman background signal.

Compared with the Raman spectrum of washed cartilage section (**Fig. 2A**), both the spectrum of the unwashed (**Fig. 2B**) and washed (**Fig. 2C**) cryomatrix (without cartilage) showed Raman bands in the same regions, except the Raman bands at 630 cm^{-1} and 1732 cm^{-1} . These peaks could be assigned to glycerol [27] and Poly(Vinyl Alcohol) (PVA) [28] respectively, which are the major compounds of the cryomatrix. The lack of these two peaks - in the Raman spectrum of washed cartilage section - guaranteed the absence of cryomatrix and therefore it did not interfere with the cartilage measurements.

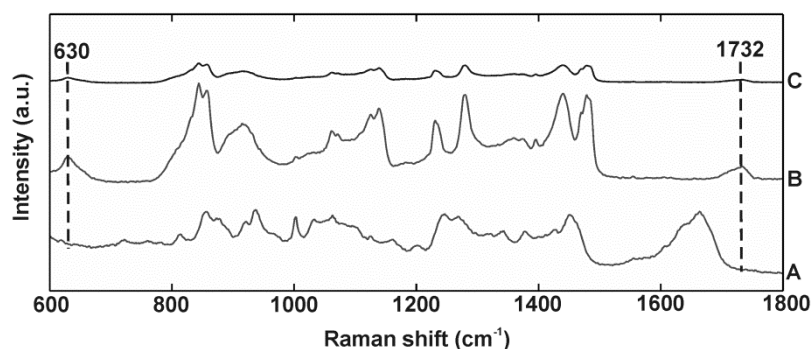


Figure 2. Raman spectra of cryosections with and without cartilage sample. **A:** washed cryosection with bovine articular cartilage, **B:** unwashed cryosection without cartilage, **C:** washed cryosection without cartilage - in the range of 500-1800 cm^{-1} - acquired in the so called "spectral scanning mode". The spectra are equally scaled and vertically displaced for clarity.

Raman spectroscopic studies of native cartilage have mainly focused on direct analysis of ECM components. Raman analysis has been performed for the analysis of collagen in the sclera, articular cartilage and subchondral bone of wild-type and transgenic mice harboring structural truncations in the introduced collagen type II transgene [29]. Moreover, Raman microspectroscopic mapping studies have already been carried out on human bronchial tissue [30]. FTIR spectroscopy is usually a more common tool to study articular cartilage. For example, It has been demonstrated in literature that FTIR imaging is useful in quantitatively assessing pathology-related changes in composition and distribution of primary macromolecular extracellular matrix components of human osteoarthritic cartilage [31].

In this study, Raman measurements on human fetal femur samples were performed on the areas highlighted in **Figure 1** and on sections consecutive to the sections used for histological analysis. Bright field images (**Fig. 3**) were obtained - in the bright field mode of the Raman-setup - from (pre)articular cartilage, resting, proliferative and hypertrophic zone of growth plate and endochondral bone from human fetal femora corresponded with the respective zones demonstrated with conventional histological analysis (**Fig. 1**). Raman-scans representative of 120 x 120 μm were made in the same zones as the observed ones in the depicted bright field images. Cluster images with the corresponding

cluster averages were obtained from each area (**Fig. 3**). Hierarchical clustering separated Raman spectra of cells from Raman spectra of ECM. This was verified by comparing hierarchical cluster images with intensity based Raman images for DNA/RNA bands (**Fig. 3**) at 1576 cm^{-1} . The intensity based Raman images showed a high DNA/RNA concentration at the same locations as the purple clusters in the cluster images and could be shown as separate clusters in each hierarchical cluster image, which confirms that cells and ECM can be effectively separated based on their respective Raman spectra.

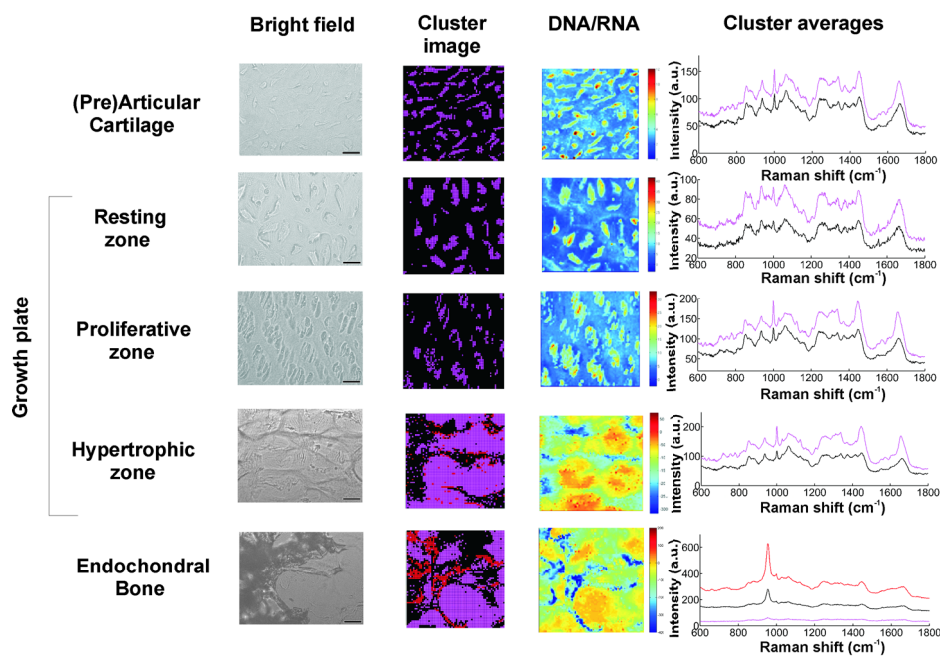


Figure 3. Bright field images, cluster images with corresponding Raman cluster averages from cells and ECM and Raman images from the (pre)articular cartilage, the resting, proliferative and hypertrophic zone of the growth plate and the endochondral bone from the human fetal femur. Raman images were focused on the intensity of the DNA/RNA band at 1576 cm^{-1} . Each cluster average spectrum is corresponding to the

cluster with the same color in the cluster images (e.g.: the purple spectrum of the cluster averages is corresponding to the purple clusters in the cluster image). In addition, purple clusters correspond to cell clusters and black clusters to ECM in all zones of the fetal femur. In endochondral bone, 2 clusters, black and red are representing the ECM, which can be explained by the heterogenous character of ECM in this region. In the hypertrophic zone, the red clusters represent unspecific fluorescent background noise, therefore they were not included in further data analysis. The truncated and separated (for cells and ECM) cluster averages are also demonstrated in Figure 4 (cells) and Figure 5 (ECM) in more detail for a more elaborate depiction. Scale bars on the bright field images equal 20 μm .

For further data analysis, cluster averages corresponding to cells and/or ECM were combined in separate databases, thus creating one database specific for all cell-cluster averages and one database specific for all ECM-cluster averages of each zone. All cell-cluster averages showed well-described bands corresponding to collagen [32], phenylalanine [33], lipids/proteins (CH_2 bending mode [34] and amide I [35-36]), DNA/RNA [37-38] (**Table 1** - see band assignments and wavelengths).

ASSIGNMENT	WAVELENGTH in cm^{-1} (References)
Collagen (proline/hydroxyproline/ C-C skeletal of collagen backbone)	937 (32)
Phosphate (PO_4^{3-})	954 (39)
Phenylalanine (C-C aromatic ring)	1001 (33)
Lipids/proteins (CH_2 and amide I)	1448 (34) and 1656 (35-36)
DNA/RNA (Guanine - N_3)	1576 (37-38)

Table 1. Band assignments and wavelengths for Raman peaks.

Comparing the cell-cluster averages (**Fig. 4A**) with the ECM-cluster averages (**Fig. 5**), the Raman peak of the DNA/RNA at 1576 cm^{-1} was clearly visible in all the cell-spectra, while it was absent in all the ECM-spectra. This supported our assumption that the cells and ECM could be separated based on their Raman spectra for further analysis. Raman image from (pre)articular cartilage focused on the intensity of the

DNA/RNA peak at 1576 cm^{-1} was also demonstrated in **Figure 4B**. As it was expected, the highest intensity (red) of the DNA/RNA peak was observed inside the cells. Except the DNA/RNA band and small differences in band intensities, cell and ECM spectra had identical peaks. All the cluster averages from the cells (**Fig. 4A**) showed relatively identical Raman peaks, except for the peak in the spectrum of the endochondral bone cell presented at 954 cm^{-1} . As expected, this peak was undetectable in cell spectra from other zones, but appeared as a very intense peak in the spectra of endochondral bone ECM spectrum and as a less intense one in the hypertrophic zone ECM spectrum (**Fig. 5**). This peak is representative for $\text{PO}_4^{3-} \nu_1$ symmetric vibration [39], which is a marker for calcification of the ECM. As expected, these results indicate milder levels of mineralization in the hypertrophic zone ECM than in the endochondral bone ECM, which was also shown by Alizarin Red S staining in Figure 1 and can be correlated with well-known biochemical differences between these zones of the fetal femur.

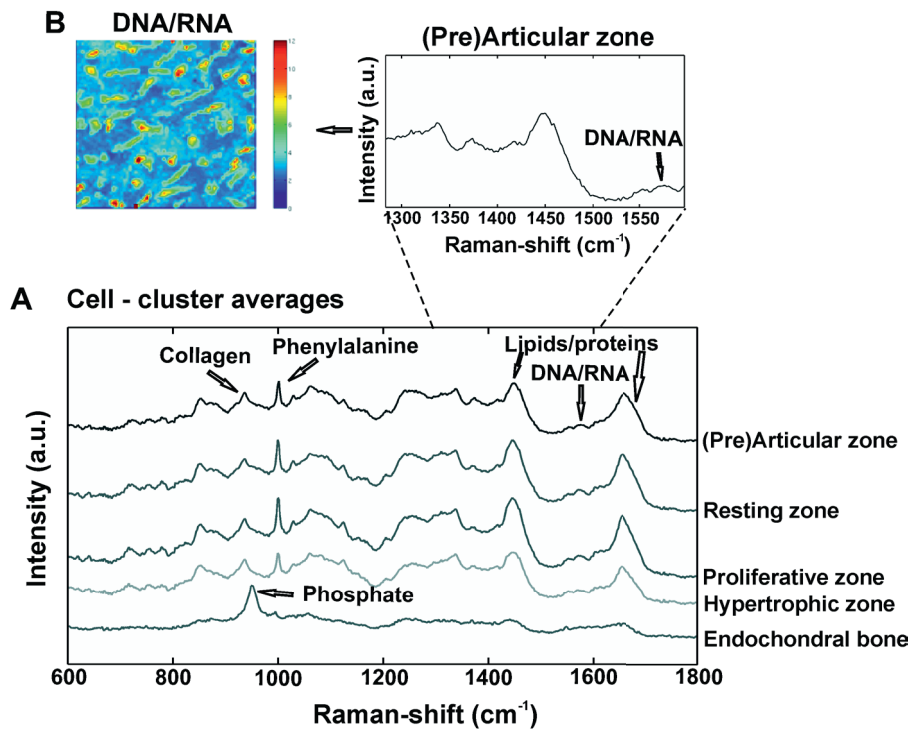


Figure 4. Raman cluster averages of cells. **A:** Average Raman spectra of cells from the (pre)articular cartilage, the resting, proliferative and hypertrophic zone and the endochondral bone in the region from 600 cm^{-1} to 1800 cm^{-1} . The spectra were vertically displaced for clarity. Truncated Raman spectrum from the (pre)articular zone represented in the region from 1300 cm^{-1} to 1600 cm^{-1} . **B:** Raman image from (pre)articular cartilage (prearticular zone) focused on the intensity of the DNA/RNA peak at 1576 cm^{-1} .

In addition Wards clustering method (HCA) based on Euclidean inter-point distances - on cell and ECM cluster averages from all the 3 donors - was used to create dendrograms (**Fig. 6**). The dendrogram in **Figure 6A** shows the clustering of Raman average spectra of the cells from the different zones of the fetal femora. Before HCA, cell spectra from all 3

donors were averaged, the smaller the variance-weighted distance between the cluster centers was, the more they resembled each other. Starting from the right hand side of the dendrogram the first 2 clusters resulted in grouping of spectra corresponding to: 1. (pre)articular cartilage and resting zone cells, 2. hypertrophic zone, proliferative zone and endochondral bone cells.

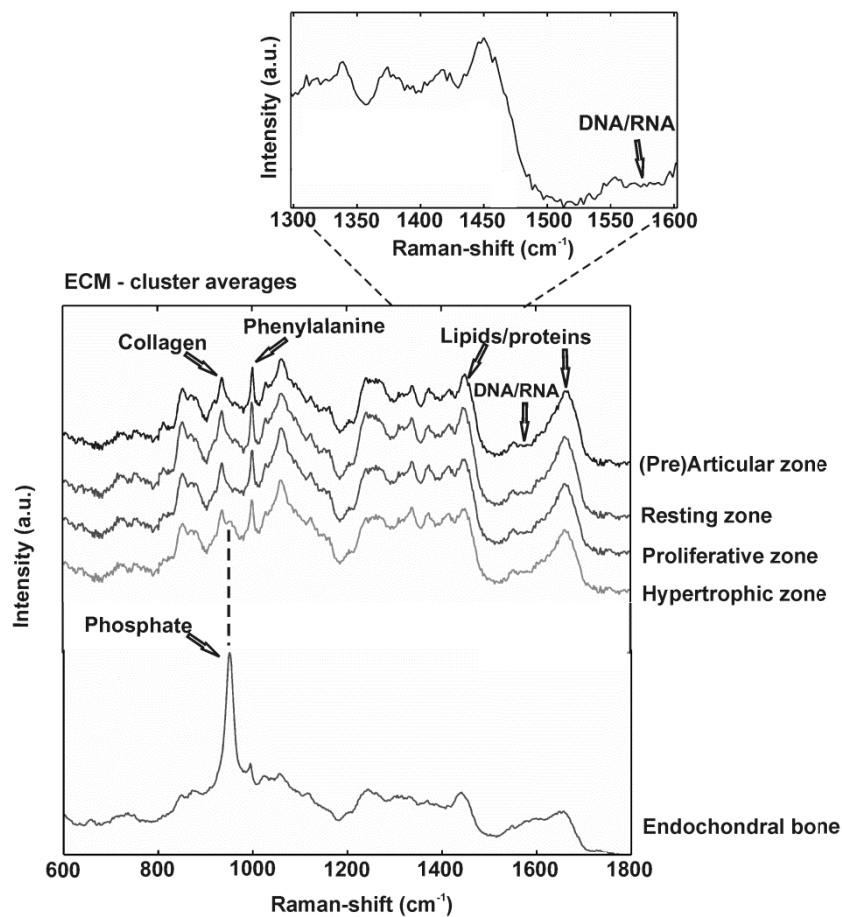


Figure 5. Raman cluster averages of ECM. Average Raman spectra of ECM from the (pre)articular cartilage, the resting, proliferative and hypertrophic zone and the endochondral bone in the region from 600 cm^{-1} to 1800 cm^{-1} . The spectra were vertically displaced for clarity. Truncated Raman spectrum from the (pre)articular zone represented in the region from 1300 cm^{-1} to 1600 cm^{-1} .

The first node separated the spectra corresponding to endochondral bone cells from the cluster of the hypertrophic zone and proliferative zone cells. Since cells in the hypertrophic zone grew rapidly and the cells in the proliferative zone proliferated rapidly [1] one might expect these cells to have a different chemical composition than the (pre)articular cartilage and resting zone cells, which were in a relatively quiescent state. The difference between chondrocytes and bone cells would obviously be the expression of different genes and therefore different RNAs and intracellular proteins. Some of the DNA and RNA Raman band positions are unique for certain nucleotides [36, 40], and could therefore help to discriminate between different cell types. The second node separated the spectra corresponding to the (pre)articular cartilage from the resting zone cells. The third cluster involved all the spectra from the hypertrophic zone and proliferative zone cells. The dendrogram in **Figure 6B** shows the clustering of the Raman average spectra of the ECM from the measured zones of the fetal femur. Before HCA, the ECM spectra from all 3 donors were averaged. As expected, endochondral bone ECM with calcium deposition resembled the least with ECM of all other cartilaginous zones. Moreover, proliferative zone ECM resembled rather hypertrophic zone ECM than (pre)articular cartilage and resting zone ECM.

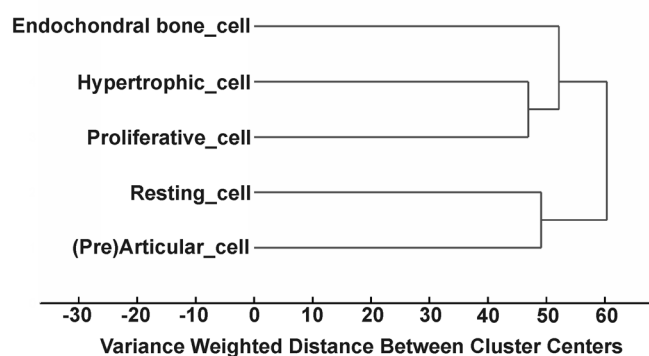
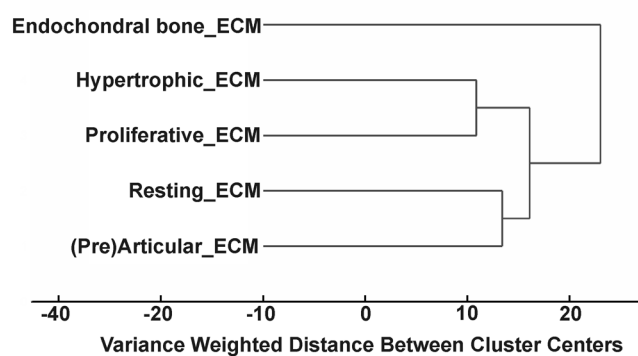
A Dendrogram of Data with Preprocessing: 1st Derivative (order:4, window: 7pt) + Autoscale**B** Dendrogram of Data with Preprocessing: 1st Derivative (order:4, window: 7pt) + Autoscale

Figure 6. HCA by Wards clustering method of Raman average spectra from **A:** cells and **B:** ECM acquired from the measured zones of the human fetal femur. Each cluster shows grouping of spectral information based on the different zones of the human fetal femur: (pre)articular cartilage, the resting, proliferative and hypertrophic zone and the endochondral bone.

After performing HCA, a more elaborate investigation was done to explore where the established dissimilarities originate from in order to find Raman markers identifying the molecular differences between the (pre)articular cartilage and growth plate cartilage. In order to find these markers a PCA was performed on the separated cell- and ECM-cluster average spectra. This method has already been successfully applied for monitoring of spectral differences in mRNA translation of embryonic stem cells during differentiation [23]. This type of analysis allows for the interpretation of similarities and differences between the clusters of the samples by analyzing the PCA scores and loadings [23]. In Raman spectroscopy, the PCA loadings are combinations between Raman spectra of components that describe the biggest difference between spectra [23].

By analyzing the cell-cluster averages by PCA (**Figure 7A and B**) – utilizing mean-centering on all the spectra as preprocessing - the first principal component gave 72.44% of the variance and described the difference between the (pre)articular cartilage cells and cells from the zones of the growth plate. (Pre)articular cartilage cells were characterized by high positive values of PC1 scores (endochondral bone cells had low positive values) while cells from the resting, proliferative and hypertrophic zones had negative scores (**Figure 7A**). The PC1 loading spectrum resembled the spectrum of intracellular proteins and lipids with characteristic peaks for collagen at 937 cm^{-1} , phenylalanine at 1001 cm^{-1} , CH_2 bending mode (lipids/proteins) at 1448 cm^{-1} and amide I (lipids/proteins) at 1656 cm^{-1} (**Figure 7B**). The spectrum of the PC1 loading showed – since it allows interpretation of biochemical differences between groups – that the main differences between the (pre)articular

cartilage cells and cells from the zones of the growth plate originated from difference in intracellular protein levels. By analyzing the ECM-cluster averages by PCA (**Figure 7C and D**) – utilizing mean-centering on all the spectra as preprocessing - the first principal component gave 97,10% of the variance and described the difference between the endochondral bone ECM and ECM from the rest of the zones of fetal femur. (Pre)articular cartilage, resting zone and proliferative zone ECM were characterized by negative values of PC1 scores while endochondral bone ECM had high positive scores (**Figure 7C**). The PC1 loading spectrum showed the strongest peak at 954 cm^{-1} corresponding to phosphate (**Figure 7D**). This result showed that the phosphate content of the endochondral bone ECM was the major contributor for biochemical difference between endochondral bone and the rest of the zones. The hypertrophic zone ECM was found to have low positive scores, which indicated a mild level of phosphate production (onset of mineralization) in the ECM of this zone.

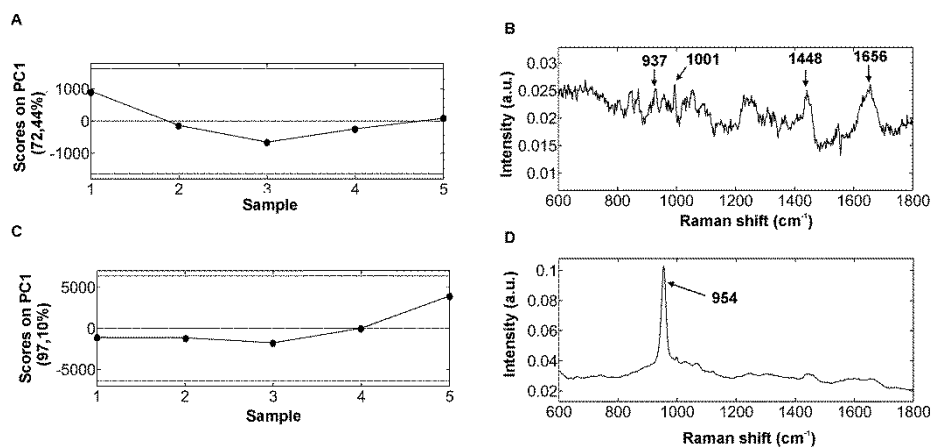


Figure 7. PCA analysis. **A:** PC1 scores of cells from different zones of the fetal femur (sample 1= (pre)articular cartilage cells, sample 2= resting zone cells, sample 3=

proliferative zone cells, sample 4=hypertrophic zone cells, sample 5= endochondral bone cells). **B:** PC1 loading from PCA analysis of cell cluster averages. The PC1 loading spectrum resembles the spectrum of intracellular proteins. **C:** PC1 scores of ECM from different zones of the fetal femur (sample 1= (pre)articular cartilage ECM, sample 2= resting zone ECM, sample 3= proliferative zone ECM, sample 4=hypertrophic zone ECM, sample 5= endochondral bone ECM). **D:** PC1 loading from PCA analysis of ECM cluster averages. The PC1 loading spectrum shows the strongest peak at 954 cm^{-1} corresponding to phosphate.

CONCLUSIONS

Unlike histology and immunohistochemistry, which only give information on the presence of specific compounds, Raman microspectroscopy provides a “fingerprint” representing the entire molecular composition of the zones in human fetal femur. We were able to distinguish bands specific for collagen, phosphate, phenylalanine, DNA/RNA and amide I. Although unique single difference Raman markers could not be detected in the cartilaginous zones of the femora, but the overall (dis)similarities between measured zones were effectively visualized using dendrograms created by Wards clustering method. Hierarchical clustering of spectra from different zones in the dendrograms could be related to well-known biochemical differences between cells and ECM from different zones. Furthermore, the main spectral differences could be determined by analyzing the PCA scores and loadings obtained after PCA analysis of separate cell and ECM cluster average spectra of the different zones. Therefore, these results show the applicability of label-free Raman microspectroscopy to distinguish between the various cartilage tissues in the human fetal femur cartilage. In addition, it shows its potential to

study proper cartilaginous matrix formation for future tissue engineering and clinical purposes. In cartilage tissue engineering hypertrophy occurrence in tissue engineered constructs during in vitro generation of hyaline cartilage is a well-described problem. Identifying label-free Raman markers for hypertrophy, and distinguishing between (pre)articular and growth plate (more specifically cartilage of the hypertrophic zone) cartilage by cluster analysis of Raman spectra from these zones provides an excellent method for monitoring the quality of cartilage transplants.

ACKNOWLEDGEMENT

The authors gratefully acknowledge the support of the Dutch Program for Tissue Engineering (DPTE) through the Grant number TGT. 6737, the TeRM Smart Mix Program of the Netherlands Ministry of Economic Affairs and the Netherlands Ministry of Education, Culture and Science.

REFERENCES

1. Ballock, R.T. and R.J. O'Keefe, *Current concepts review: The biology of the growth plate*. Journal of Bone and Joint Surgery - Series A, 2003. **85**(4): p. 715-726.
2. Melrose, J., et al., *The use of Histochoice™ for histological examination of articular and growth plate cartilages, intervertebral disc and meniscus*. Biotechnic and Histochemistry, 2008. **83**(1): p. 47-53.
3. Eames, B.F., L. De la Fuente, and J.A. Helms, *Molecular ontogeny of the skeleton*. Birth Defects Research Part C - Embryo Today: Reviews, 2003. **69**(2): p. 93-101.
4. Abad, V., et al., *The role of the resting zone in growth plate chondrogenesis*. Endocrinology, 2002. **143**(5): p. 1851-1857.

5. Mau, E., et al., *PTHrP regulates growth plate chondrocyte differentiation and proliferation in a Gli3 dependent manner utilizing hedgehog ligand dependent and independent mechanisms*. *Developmental Biology*, 2007. **305**(1): p. 28-39.
6. Sandberg, M. and E. Vuorio, *Localization of types I, II, and III collagen mRNAs in developing human skeletal tissues by in situ hybridization*. *J Cell Biol*, 1987. **104**(4): p. 1077-84.
7. Vu, T.H., et al., *MMP-9/gelatinase B is a key regulator of growth plate angiogenesis and apoptosis of hypertrophic chondrocytes*. *Cell*, 1998. **93**(3): p. 411-422.
8. Burdan, F., et al., *Morphology and physiology of the epiphyseal growth plate*. *Folia Histochemica et Cytobiologica*, 2009. **47**(1): p. 5-16.
9. Colthup, N.B., L.H. Daly, and S.E. Wiberly, *Introduction to Infrared and Raman Spectroscopy*. Academic Press, New York, 1990.
10. Hendra, P., C. Jones, and G. Warnes, *Fourier Transform Raman Spectroscopy*. Ellis Horwood, Chichester, 1991.
11. Schrader, B., *Infrared and Raman Spectroscopy: Methods and Applications*. Verlag Chemie, Weinheim, 1995.
12. Ellis, D.I. and R. Goodacre, *Metabolic fingerprinting in disease diagnosis: Biomedical applications of infrared and Raman spectroscopy*. *Analyst*, 2006. **131**(8): p. 875.
13. Notingher, I., et al., *In situ characterisation of living cells by Raman spectroscopy*. *Spectroscopy*, 2002. **16**(2): p. 43-51.
14. Puppels, G.J., et al., *Laser irradiation and Raman spectroscopy of single living cells and chromosomes: Sample degradation occurs with 514.5 nm but not with 660 nm laser light*. *Experimental Cell Research*, 1991. **195**(2): p. 361-367.
15. Puppels, G.J., et al., *Studying Single Living Cells and Chromosomes by Confocal Raman Microspectroscopy*. *Nature*, 1990. **347**(6290): p. 301-303.
16. Van Manen, H.J., A. Lenferink, and C. Otto, *Noninvasive imaging of protein metabolic labeling in single human cells using stable isotopes and Raman microscopy*. *Analytical Chemistry*, 2008. **80**(24): p. 9576-9582.
17. Uzunbajakava, N., et al., *Nonresonant confocal Raman imaging of DNA and protein distribution in apoptotic cells*. *Biophysical Journal*, 2003. **84**(6): p. 3968-3981.

18. Van Manen, H.J., et al., *Intracellular chemical imaging of heme-containing enzymes involved in innate immunity using resonance Raman microscopy*. Journal of Physical Chemistry B, 2004. **108**(48): p. 18762-18771.
19. Pully, V.V., et al., *Hybrid Rayleigh-, Raman and TPE fluorescence spectral confocal microscopy of living cells*. Journal of Raman Spectroscopy, 2010.
20. Uzunbajakava, N., J. Greve, and C. Otto, *Raman microscopy of cells: chemical imaging of apoptosis*. Multiphoton Microscopy in the Biomedical Sciences Iii, 2003. **4963**: p. 223-230.
21. Hervada-Sala, C. and E. Jarauta-Bragulat, *A program to perform Ward's clustering method on several regionalized variables*. Computers & Geosciences, 2004. **30**(8): p. 881-886.
22. Pully, V.V., *From cells to bone: Raman microspectroscopy of the mineralization of stromal cells [PhD thesis]* 2010, University of Twente: Enschede, The Netherlands. p. 90.
23. Notingher, I., et al., *In situ spectral monitoring of mRNA translation in embryonic stem cells during differentiation in vitro*. Analytical Chemistry, 2004. **76**(11): p. 3185-3193.
24. Wold, S., K. Esbensen, and P. Geladi, *Principal Component Analysis*. Chemometrics and Intelligent Laboratory Systems, 1987. **2**(1-3): p. 37-52.
25. Faolà, ~~Rimario~~ *Raman spectroscopic evaluation of efficacy of current paraffin wax section dewaxing agents*. Journal of Histochemistry and Cytochemistry, 2005. **53**(1): p. 121.
26. Wang, C.Y., et al., *Diagnosis of oral cancer by light-induced autofluorescence spectroscopy using double excitation wavelengths*. Oral Oncology, 1999. **35**(2): p. 144-150.
27. Krafft, C., et al., *Near infrared Raman spectra of human brain lipids*. Spectrochimica Acta Part a-Molecular and Biomolecular Spectroscopy, 2005. **61**(7): p. 1529-1535.
28. Hergeth, W.D., *Raman Scattering on Polymeric Dispersions*. Chemical Engineering and Technology, 1998. **21**(8): p. 647-651.
29. Dehring, K.A., et al., *Correlating changes in collagen secondary structure with aging and defective type II collagen by Raman spectroscopy*. Appl Spectrosc, 2006. **60**(4): p. 366-72.

30. Koljenovic, S., et al., *Raman microspectroscopic mapping studies of human bronchial tissue*. Journal of Biomedical Optics, 2004. **9**(6): p. 1187-1197.
31. David-Vaudey, E., et al., *Fourier Transform Infrared Imaging of focal lesions in human osteoarthritic cartilage*. Eur Cell Mater, 2005. **10**: p. 51-60; discussion 60.
32. Cheng, W.T., et al., *Micro-Raman spectroscopy used to identify and grade human skin pilomatrixoma*. Microscopy Research and Technique, 2005. **68**(2): p. 75-79.
33. Ó Faoláin, E., et al., *A study examining the effects of tissue processing on human tissue sections using vibrational spectroscopy*. Vibrational Spectroscopy, 2005. **38**(1-2): p. 121-127.
34. Frank, C.J., R.L. McCreery, and D.C.B. Redd, *Raman-Spectroscopy of Normal and Diseased Human Breast Tissues*. Analytical Chemistry, 1995. **67**(5): p. 777-783.
35. Lakshmi, R.J., et al., *Tissue Raman spectroscopy for the study of radiation damage: Brain irradiation of mice*. Radiation Research, 2002. **157**(2): p. 175-182.
36. Notingher, I., et al., *Discrimination between ricin and sulphur mustard toxicity in vitro using Raman spectroscopy*. Journal of the Royal Society Interface, 2004. **1**(1): p. 79-90.
37. Ruiz-Chica, A.J., et al., *Characterization by Raman spectroscopy of conformational changes on guanine-cytosine and adenine-thymine oligonucleotides induced by aminoxy analogues of spermidine*. Journal of Raman Spectroscopy, 2004. **35**(2): p. 93-100.
38. Fung, M.F.K., et al., *Pressure-tuning Fourier transform infrared spectroscopic study of carcinogenesis in human endometrium*. Biospectroscopy, 1996. **2**(3): p. 155-165.
39. Tarnowski, C.P., M.A. Ignelzi, and M.D. Morris, *Mineralization of developing mouse calvaria as revealed by Raman microspectroscopy*. Journal of Bone and Mineral Research, 2002. **17**(6): p. 1118-1126.
40. Chan, J.W., et al., *Micro-Raman spectroscopy detects individual neoplastic and normal hematopoietic cells*. Biophysical Journal, 2006. **90**(2): p. 648-656.

Chapter 6

Conclusion and future perspectives

Raman microspectroscopy provides a label-free and non-invasive tool for studying a wide spectrum of nutrient, extracellular matrix and cellular components in tissue-engineered samples. Unlike conventional methods, such as histology, immunohistochemistry, immunocytochemistry, which only give information on the presence of specific compounds, Raman spectroscopy provides a spectroscopic “fingerprint” representing the entire molecular composition of samples of interest. Results presented in this thesis demonstrate the potential of confocal label-free Raman spectroscopy as a tool to study behaviour of chondrocytes, which are widely used cell sources for cartilage tissue engineering.

In **Chapter 2** chondrocyte dedifferentiation in a 2D monolayer culture system has been successfully studied by using non-invasive confocal non-resonant Raman and coherent anti-Stokes Raman scattering (CARS) microspectroscopy to assess the quality of culture expanded chondrocytes. We describe that a Raman band at 2924 cm^{-1} representing lipids is associated with chondrocyte dedifferentiation. Interestingly, several studies on articular cartilage have indicated the possible role for extensive lipid accumulation in the onset of chondrocyte degeneration [1-3]. Therefore label-free monitoring of lipid content of chondrocytes within cartilage tissue using non-resonant Raman and CARS microscopy can be a valuable future, investigative and diagnostic tool, for studying degenerative cartilage diseases.

In Chapter 3 the feasibility of Raman microspectroscopy to detect the formation of collagen-containing extracellular matrix formation over time was demonstrated. Microaggregates, formed from a defined number of single chondrocytes, were created in agarose microwell arrays and used to evaluate extracellular matrix formation. These microwells arrays can be used as a medium-throughput platform for Raman applications and screening of microtissue formation. The abovementioned system allows for the generation of relatively large numbers of cell aggregates of well-defined size and cell numbers which can be screened in a short time 'in situ', without having to transfer these pellets onto microscope slides. Moreover the microwell systems described here is also suitable for long-term, live-cell measurements and can be used to observe 3D tissue formation.

Obviously the ultimate future goal is to monitor cartilage extracellular matrix formation – preferably in real time - in large and implantable cartilage constructs. In **Chapter 4** the feasibility of confocal Raman microspectroscopy to detect formation of essential cartilage ECM compounds in 3D PEOT/PBT scaffolds has been investigated. *In vitro* generated cartilage ECM was studied based on Raman bands at 937 and 1062 cm^{-1} , which correspond to collagen and sGAGs respectively. Collagen synthesis was found to be different in single chondrocyte-seeded scaffolds when compared to microaggregate-seeded samples. While normalized band-area ratios for collagen content of single cell-seeded samples had gradually been decreasing over time, the collagen content of microaggregate-seeded samples had significantly been increasing. Several studies with chondrocytes showed a correlation

between aggregation and enhanced cartilagenous tissue formation [4-5]. We think that seeding microaggregates, instead of single chondrocytes, onto scaffolds is perhaps a better approach for cartilage tissue engineering. In addition, the use of a fiber-optic set-up for Raman measurements of ECM formation inside scaffolds was also studied. Although, measurements using the fiber-optic set-up were limited by the silica background signal generated from the optical fibers used, the bands at 920 cm^{-1} and 972 cm^{-1} , attributes of ECM, were still distinguishable. The use of a new generation of fiber-optic Raman probes, which is currently being developed for quantitative Raman spectroscopy will lead to better optical probes with lower silica background contribution and can lead to well-resolved Raman spectra of ECM. The improved Raman probes also allow collection of Raman spectra from multiple pores in the scaffold within one single measurement time point. Such an improved setup ultimately would not only lead to a better representation of the total Raman signature of such tissue engineered constructs, but could decrease measurement time as well. If these specialized probes allow for an aseptic configuration, measurements of live cells and tissue formation would become possible. This setup would literally allow for a new look into tissue formation and cell behavior inside porous scaffolds, during culture period, in static and dynamic culture systems. However in most conventional macro-scale bioreactors, real-time optical monitoring of tissue formation during the culture period is more than a challenging task. This is due to the practical problem of coupling large and complex bioreactors to non-invasive optical microscopes [6]. Microfabrication technology in the field of tissue engineering can provide an alternative solution for this problem.

It has already been shown that Raman optical analysis of cells and cellular differentiation in microfluidic bioreactors is feasible down to the level of subcellular organelles during tissue development [6].

In order to gain more knowledge on the Raman “fingerprint” of cartilage as a biological system, **Chapter 5** describes the different zones of the human fetal femur monitored by confocal Raman microspectroscopy. The ultimate goal was to find label-free markers which can distinguish between (pre)articular cartilage and growth plate cartilage for future tissue engineering and clinical applications. Overall (dis)similarities between measured zones were effectively visualized on the dendrograms created by Ward’s clustering and main spectral differences were revealed by principal component analysis allowing for label-free detection of individual cartilaginous zones and for label-free evaluation of proper cartilaginous matrix formation for future tissue engineering and clinical purposes. In cartilage tissue engineering, occurrence of hypertrophy in tissue engineered constructs during in vitro generation of hyaline cartilage is a well-described problem. Identifying label-free Raman markers for hypertrophy and distinguishing between (pre)articular and growth plate (more specifically cartilage of the hypertrophic zone) cartilage by cluster analysis of Raman spectra from these zones provide an excellent method for monitoring the quality of cartilage transplants.

Overall the results of this thesis provide a new insight into chondrocytes and cartilage for which Raman microspectroscopy can be a promising non-invasive tool to quantitatively and qualitatively monitor formation of cartilage ECM and study the behaviour of primary chondrocytes in different cell culture systems.

This thesis provides the first glance into the use of Raman microscopy for studying cartilage and chondrocytes. Since the first discovery of the Raman effect, technological advances have boosted the development of faster, better, cheaper and user-friendlier Raman spectroscopic systems. Based on current literature, and perhaps a small part of this thesis, it is safe to say that Raman spectroscopy is not just another spectroscopic technique, but also can be used for microscopic observations, like used in fluorescence microscopy. If the appropriate scientific questions are asked it can be used as a valuable tool for biologists to study cells and tissues at the sub-micrometer level.

A further investigation is needed to validate the potential of the technique for tissue engineering applications, so that better evaluation of cartilaginous matrix formation in tissue engineered constructs will be possible and Raman microscopy becomes more mainstream.

REFERENCES

1. Bonucci, E., M. Cuicchio, and L.C. Dearden, *Investigations of Aging in Costal and Tracheal Cartilage of Rats*. Zeitschrift Fur Zellforschung Und Mikroskopische Anatomie, 1974. **147**(4): p. 505-527.
2. Carlson, C.S., et al., *The ultrastructure of osteochondrosis of the articular-epiphyseal cartilage complex in growing swine*. Calcif Tissue Int, 1986. **38**(1): p. 44-51.
3. Lippiello, L., T. Walsh, and M. Fienhold, *The Association of Lipid Abnormalities with Tissue Pathology in Human Osteoarthritic Articular-Cartilage*. Metabolism-Clinical and Experimental, 1991. **40**(6): p. 571-576.
4. Duke, P.J., E.L. Daane, and D. Montufar-Solis, *Studies of chondrogenesis in rotating systems*. J Cell Biochem, 1993. **51**(3): p. 274-82.

Chapter 6

5. Naumann, A., et al., *Tissue engineering of autologous cartilage grafts in three-dimensional in vitro macroaggregate culture system*. *Tissue Eng*, 2004. **10**(11-12): p. 1695-706.
6. Pully, V.V., et al., *Microbioreactors for Raman microscopy of stromal cell differentiation*. *Anal Chem*, 2010. **82**(5): p. 1844-50.

Summary

Cartilage tissue engineering generally includes the use of three dimensional scaffolds in combination with primary chondrocytes or differentiated mesenchymal stem cells in order to create a bioartificial cartilage construct for future clinical use. Usually polymeric scaffolds are used because of their beneficial biomechanical properties, which are designed to support the proliferation and differentiation of chondrocytes or so-called progenitor cells in order to assist extracellular matrix formation and aid cartilage repair when applied *in vivo*. Studies performed to investigate the composition and quality of tissue engineered cartilage are usually done by destructive methods like immunohistology, biochemistry or electron microscopy. Non invasive methods allowing for real time or non destructive monitoring of cell behavior in combination with biomaterials could potentially give novel insight into a wide spectrum of nutrient, extracellular matrix and cellular components as well intracellular changes all important parameters when creating bioartificial cartilage constructs. This thesis aims therefore to study relevant parameters in cartilage tissue engineering by using a non destructive biochemical high resolution microscopy tool called confocal Raman microspectroscopy. Confocal Raman microspectroscopy is a label-free microscopy tool for the analysis and visualization of biochemical composition of individual cell and their surrounding extracellular matrix, in native tissues, cell cultures and tissue engineered constructs.

In **Chapter 1**, a general introduction is given on cartilage tissue engineering, the Raman theory, Raman microspectroscopy and Raman microspectroscopy applied in tissue engineering in general, and cartilage tissue engineering in particular. Commonly, the use of

Summary and Samenvatting

autologous chondrocytes for clinical applications requires a culture expansion step of chondrocytes to obtain a sufficient number of cells for cell therapy or tissue engineering applications. Culture expansion of chondrocytes is known to be associated with chondrocyte dedifferentiation causing primary cells to lose the appropriate phenotype. In **Chapter 2**, use of label-free Raman microspectroscopy to monitor chondrocyte dedifferentiation has been explored with the ultimate goal to develop a non-invasive assay for assessing the quality of expanded chondrocytes which can potentially be used for cartilage repair. In **Chapter 3 and 4** the chondrocyte behavior in three dimensional culture systems was investigated by *in vitro* monitoring of extracellular matrix formation in a medium-throughput cell aggregate culture system, in which soft-lithography was used for the creation of agarose microwell arrays (Chapter 3) for creating size controlled aggregates. In chapter 4 these aggregates were used for the manufacturing of tissue engineered constructs using poly-(ethyleneglycol terephthalate)-poly(butylene terephthalate) block copolymers. An additional aim of this chapter was, besides the analysis of tissue quality in large tissue engineered constructs, to detect possible differences in matrix formation of single cell- and microaggregate-seeded scaffolds using Raman microspectroscopy. In **Chapter 5** the main focus was to determine whether confocal Raman microspectroscopy is able to effectively discriminate between different cartilaginous zones of a developing diarthrodial joint and to identify the molecular differences between the (pre)articular cartilage and the different zones of the growth plate cartilage. The results of all these chapters combined lead to more insight into understanding of chondrocytes, cartilage and its extra cellular matrix and how Raman microspectroscopy could assist in unravelling cell and tissue properties

during cell culture and tissue engineering. The Raman spectroscopic and imaging data obtained during these studies can be used to create tissue engineered cartilage for future cell therapy, where Raman microspectroscopy can be used as a quality control tool to assess the biochemical composition of cells and the extra cellular matrix produced by these cells.

The overall results presented in this thesis demonstrate the potential of confocal label-free Raman spectroscopy in combination with dedicated data analysis to quantitatively and qualitatively determine the formation of cartilage and study the behavior of chondrocytes in different cell culture systems used for tissue engineering in a non-destructive manner.

Samenvatting

Weefseltechniek, ofwel 'tissue engineering', van kraakbeen behelst het gebruik van driedimensionale dragermaterialen ('scaffolds') in combinatie met primaire chondrocyten of gedifferentieerde mesenchymale stamcellen om een bio-artificieel construct te creëren voor klinische toepassing. Over het algemeen worden hiervoor, omwille van hun gunstige biomechanische eigenschappen, polymeer 'scaffolds' gebruikt die zodanig zijn ontworpen dat zij de proliferatie en differentiatie van chondrocyten en/of progenitorcellen ondersteunen, de productie van extracellulaire matrix stimuleren en – wanneer ze *in vivo* worden toegepast – kraakbeenherstel bevorderen. Studies naar de compositie en kwaliteit van 'tissue-engineered' kraakbeen maken over het algemeen gebruik van destructieve methoden als immunohistochemie, biochemie en elektronenmicroscopie. Niet-invasieve methoden die het mogelijk maken om op een niet-destructieve manier het gedrag van cellen in combinatie met biomaterialen in de tijd te volgen kunnen nieuwe inzichten geven in een breed spectrum van nutriënten, extracellulaire matrix en cellulaire componenten, alsmede intracellulaire veranderingen: stuk voor stuk belangrijke parameters voor het creëren van een bio-artificieel kraakbeen construct. Deze thesis heeft als doel relevante parameters in kraakbeen 'tissue engineering' te bestuderen met behulp van niet-destructieve biochemische hoge resolutie microscopie: confocale Raman microspectroscopie. Dit is een label-vrije microscopische techniek voor de analyse en visualisatie van de biochemische compositie van individuele cellen en de omliggende extracellulaire matrix in weefsels, celkweken en 'tissue-engineered' constructen.

In **hoofdstuk 1** wordt een algemene introductie gegeven over (1) kraakbeen 'tissue engineering', (2) Raman theorie, (3) Raman microspectroscopie en (4) de toepassing van Raman microspectroscopie binnen het gebied van 'tissue engineering', in het bijzonder 'tissue engineering' van kraakbeen. Het gebruik van autologe chondrocyten voor klinische toepassingen vereist over het algemeen het expanderen van de chondrocyten om voldoende cellen te verkrijgen voor celtherapie of 'tissue engineering'. Het *in vitro* expanderen van chondrocyten gaat gepaard met dedifferentiatie waardoor deze primaire cellen hun karakteristieke fenotype verliezen. In **hoofdstuk 2** wordt het gebruik van Raman spectroscopie voor het bestuderen van dedifferentiatie van chondrocyten onderzocht met als doel om een niet-invasieve assay te ontwikkelen voor het bestuderen van de kwaliteit van geëxpandeerde chondrocyten die mogelijk gebruikt worden voor kraakbeenherstel. In **hoofdstuk 3 en 4** wordt het gedrag van chondrocyten in drie-dimensionale constructen bestudeerd. Een techniek genaamd 'soft-lithography' is gebruikt voor het maken van agarose microwells, waarmee op gecontroleerde wijze cel aggregaten kunnen worden gecreëerd. In dit 'medium-throughput' kweekstelsel is vervolgens *in vitro* de aanmaak van extracellulaire matrix in de tijd gevolgd (hoofdstuk 3). In hoofdstuk 4 worden deze microaggregaten gecombineerd met poly-(ethyleenglycol terephthalate)-poly(butylene terephthalate) block copolymeren voor het produceren van 'tissue engineered' constructen. Naast het analyseren van de weefselkwaliteit in grote 'tissue engineered' constructen, wordt in dit hoofdstuk de aanmaak van extracellulaire matrix in 'scaffolds' gezaaid met individuele cellen en 'scaffolds' gezaaid met microaggregaten onderling vergeleken met behulp van Raman microspectroscopie. **Hoofdstuk 5** bestudeert de mogelijkheden om met confocale Raman microspectroscopie effectief

Summary and Samenvatting

onderscheid te maken tussen de verschillende kraakbeen zones in een gewricht en om de moleculaire verschillen tussen (pre)articulair kraakbeen en de verschillende zones van kraakbeen in de groeiplaat te identificeren. De resultaten van deze hoofdstukken samen geven meer inzicht in chondrocyten, kraakbeen, de extracellulaire matrix en de rol van Raman microspectroscopie bij het bestuderen van cel en weefseigenschappen tijdens celweek en 'tissue engineering'. De verkregen Raman spectroscopische en beeldvormingsdata kunnen bijdragen aan het creëren van 'tissue engineered' kraakbeen voor toekomstige cel therapie, waarin Raman microspectroscopie kan dienen als kwaliteitscontrole door de biochemische compositie van de cellen en de geproduceerde extracellulaire matrix in kaart te brengen.

De resultaten in dit proefschrift demonstreren de potentie van confocale label-vrije Raman spectroscopie gecombineerd met specifieke data analyse om op een kwalitatieve en kwantitatieve wijze in verschillende celweek systemen voor 'tissue engineering' het gedrag van chondrocyten en de vorming van kraakbeen op een niet-destructieve wijze te bestuderen.

List of Publications

A. Kunstar, C. Otto, M. Karperien, C.A. van Blitterswijk, A.A. van Apeldoorn: *Raman Microspectroscopy – A Non-Invasive Analysis Tool for Monitoring of Collagen-Containing Extracellular Matrix Formation in a Medium-Throughput Culture System*. Tissue Engineering Part C Methods, 2011; 17(7):737-44.

M.A. Lopez-Heredia, K. Sariibrahimoglu, W. Yang, M. Bohner, D. Yamashita, **A. Kunstar**, A.A. van Apeldoorn, E.M. Bronkhorst, R.P. Felix Lanao, S.C.G. Leeuwenburgh, K. Itatani, F. Yang, P. Salmon, J.G.C. Wolke, and J.A. Jansen: *Influence of the pore generator on the evolution of the mechanical properties and the porosity and interconnectivity of a calcium phosphate cement*. Acta Biomaterialia, 2012; 8(1):404-14.

Manuscript submitted for publication:

A. Kunstar, J. Leijten, S. van Leuveren, J. Hilderink, C. Otto, C.A. van Blitterswijk, M. Karperien, A.A. van Apeldoorn: *Recognizing different tissues in human fetal femur cartilage by label-free Raman microspectroscopy*.

Manuscripts in preparation:

A. Kunstar, A. Leferink, P.I. Okagbare, M.D. Morris, B.J. Roessler, C. Otto, M. Karperien, C.A. van Blitterswijk, L. Moroni, A.A. van Apeldoorn: *Label-free Raman monitoring of extracellular matrix formation in 3D PEOT/PBT scaffolds*.

List of Publications

A. Kunstar, E.T. Garbacik, T.W.G.M. Spitters, H.L. Offerhaus, C. Otto, C.A. van Blitterswijk, M. Karperien, A.A. van Apeldoorn: *Raman microspectroscopy: A label-free tool for monitoring chondrocyte dedifferentiation.*

Curriculum Vitae

Aliz was born on the 15th of September in 1982 in Békéscsaba, Hungary.

In 2000, she moved to the capital city, Budapest to start her MSc studies in the Eötvös Loránd University, Faculty of Science, Institute of Biology. She performed her Master thesis research in the Department of Stem Cell Biology, National Medical Center, which resulted in a Master thesis and two publications entitled *Chondrogenic potential of mesenchymal stem cells from patients with rheumatoid arthritis and osteoarthritis – measurements in a microculture system* (Published in Cells Tissues Organs) and *A novel anti-inflammatory function of human galectin-1: inhibition of hematopoietic progenitor cell mobilization* (Published in Exp. Hematology). She was graduated as a biologist in 2005.

Between 2005 and 2007, she worked as a guest research fellow in the Center of Tumorbiology and Microbiology, Karolinska Institute, Stockholm, Sweden and as a research fellow in the Department of Pathogenetics, National Institute of Oncology, Budapest, Hungary.

In 2007, she started to work as a pre-doctoral fellow in the Department of Tissue Regeneration, MIRA- Institute of Biomedical Technology and Technical Medicine, University of Twente, The Netherlands. We can read now this PhD dissertation as an outcome of her PhD research.

Curriculum Vitae

Acknowledgements

This chapter is dedicated to all the people I have met during my PhD, without whom I would not have made it and the work presented in here would never be completed.

I wish to express my gratitude to my promoter Clemens van Blitterswijk and co-promoter Aart van Apeldoorn, who invited me to become a PhD student and gave me the opportunity to do my PhD research in the Tissue Regeneration Group. Clemens, Aart, Marcel, Cees, Janine and Lorenzo, thank you for all guidelines and support you offered me during my PhD research. Jan, Pamela, Roman and Bernke, you are great scientists and I am grateful for having worked together in the same research group. Anouk and Jacqueline, thank you for your assistance and help in the lab during the 4 years of my research. Audrey, thank you for all your help during my PhD and your help in handling thesis administration.

I would like to thank my graduation committee members Prof. Dr. G. van der Steenhoven, Dr. G. van Osch, Prof. Dr. J.L. Herek, Prof. Dr. M. Karperien, Prof. Dr. J.F.J Engbersen, Prof. Dr. F.P.J.G. Lafeber, Prof. Dr. P.J. Dijkstra for their time and effort reviewing this thesis.

To my paranympths, Mijke and Janneke, both of you were always there when I needed help and advice during my PhD life, I cannot thank enough for that. Mijke, I got to know you when you were still a Master student and we bacame office mates. It was a great and fun time we shared, you were one of the most hard-working and enthusiastic Master student (and later PhD student) I have ever met in TR, it was also motivating for me. You are also a great friend. Janneke, it was a fun time sharing the girls' office together with Anindita and Ana, you are my

Acknowledgements

favourite office mates. Beside we also had it common and shared all the beauty and hurdles of working on a Raman-project. Your precisity in work is leading by example. Hartelijk bedankt voor de hulp met de samenvatting. Thank both of you for your friendship and support!

I would also like to thank Vishnu Pully for his help and for teaching all the ins and outs of handling the Raman setup.

To Erik Garbacik and Herman L. Offerhaus for the CARS measurements and their help and suggestions for Chapter 2.

I would like to thank Prof. Morris and Prof. Roessler for giving me the great opportunity to work and perform experiments in their laboratories in the University of Michigan in US. Special thanks Paul and Karen for helping me with the Raman measurements there and Paul for the additional fiber-optic measurements. Without this collaboration, I could not have Chapter 4 in my thesis.

I would like to acknowledge to the Dutch Program for Tissue Engineering (DPTE, TGT.6737) for the generous financial support, which made it possible to pursue my PhD research and attend to numerous conferences.

To all the members of the TR and DBE Group, it was a unique experience to work in an inspiring and stimulating international atmosphere. The Portuguese spirit – Ana, Hugo, Andre, Lili, Emilie, Sandra, Filipe, Jorge, Ines and Andreia - in the Group is unforgettable! I have to tell at that time I was even considering to learn Portuguese instead of Dutch. I enjoyed a lot our trips, especially the one to Gerês in Portugal - thanks to Jun giving me the support being the only other non-portuguese on that trip and introducing the Chinese spirit to me. Here I would like to mention and thank Fede, the always joyful Italian girl, for

Acknowledgements

her company, who also accompanied us on some of those trips. Petra, thank you for your friendship and for all the great time we shared, I missed you a lot after you had left to Wageningen. Bjorn, thank you for the amazing Christmas time that I could spend with you and your family in Zwolle, when I could not be with mine in Hungary and stucked in Enschede alone because of the snow storms. Beside you organized the best parties and BBQs ever. Dr. Hemant special thanks to you for all your help and support! Jeroen and Anne, thank you for your help and guidelines in growth plate- and scaffold-topic, without you I could not have Chapter 4 and 5 in my thesis. Stefan, your assignment was as much a learning experience for me as it was for you! Tim, thanks a lot for your help with the histology for Chapter 2. Anindita, Anand, Joyce, Eelco, Jun, Nico, Gustavo, Charlene, Karolina, Erik, Bin, Ling, Wim, Nathalie, Ellie, Nicole, Jetse, Parthi, Giulia, Febry, Andrea, Nilo, Jingwei, Bach: you all contributed to the supportive and fun atmosphere in TR and thanks for everyone for all the lunches, dinners, parties and BBQs during my PhD life!

To my great friends, Zsuzsi, Nori, Bea, Vishi, Lamia, Giovane, Merly, Dennis and Alicia, you were always next to me to give support if I needed in hard times and shared happiness in good times since we got to know each other.

Végül, de nem utolsósorban, köszönöm Anyu, Apu és az egész család a támogatásokat, ti mindig mellettem álltok a bajban és boldogságban is.

Alíz, Budapest, 2012

Acknowledgements
